Microbead-based Raman/Surface Enhanced Raman Scattering Immunoassays for Multiplex Detection

A THESIS SUBMITTED

BY

Lijuan Wei

FOR THE DEGREE OF DOCTOR OF PHILOSOPHY

School of Chemical Engineering

The University of Adelaide, Australia

October 2013

I dedicate this whole thesis to my beloved husband,

for his support, encouragement and love.

DECLARATION

I certify that this work contains no material which has been accepted for the award of any other degree or diploma in any university or other tertiary institution and, to the best of my knowledge and belief, contains no material previously published or written by another person, except where due reference has been made in the text. In addition, I certify that no part of this work will, in the future, be used in a submission for any other degree or diploma in any university or other tertiary institution without the prior approval of the University of Adelaide and where applicable, any partner institution responsible for the joint-award of this degree.

I give consent to this copy of my thesis when deposited in the University Library, being made available for loan and photocopying, subject to the provisions of the Copyright Act 1968.

The author acknowledges that copyright of published works contained within this thesis resides with the copyright holder(s) of those works.

I also give permission for the digital version of my thesis to be made available on the web, via the University's digital research repository, the Library catalogue and also through web search engines, unless permission has been granted by the University to restrict access for a period of time.

Lijuan Wei

Signed date

ACKNOWLEDGEMENTS

I would like to take this opportunity to thank everyone who assisted me to complete this research project. I must say without their help and support this thesis would never have been possible.

First and foremost I extremely appreciate my supervisors Associate Professor Sheng Dai and Associate Professor Bo Jin for their guidance, encouragement and help during my PhD journey. Their valuable discussion, helpful advice and kindly suggestions are vitally important to me. I must say, this work would be far from over without their support.

I acknowledge Dr Jingxiu Bi and Dr Hu Zhang at School of Chemical Engineering, the University of Adelaide for their suggestions and advice in our group meeting, Ms Lyn Waterhouse and Dr Benjamin Wade from Adelaide Microscopy for their excellent technical assistance with TEM, SEM, and fluorescence microscope instruments, and Dr Anthony Quinn from Lastek Pty Ltd for his kindly support and help with Raman equipments.

As a recipient of a CSC-UoA joint postgraduate scholarship, I am greatly thankful the China Scholarship Council (CSC), the University of Adelaide, and my supervisors for financial support to this project, my tuition fee and my living expense.

Meanwhile, I would like to thank the group members at Bionanotechnology Laboratory at the University of Adelaide, both past and present. These include Dr Hongjie An, Dr Giuseppe Laera, Vipasiri Vimonses, Manjot Kaur Toor, Guiqin Cai, Frank Song, Tze Haw Sia, Xing Xu, Guanran Zhang, Leiyuan Guo, Ming Dai, Bingyang Shi, Guangan Jia and Masoumeh Zargar. Thank them for providing me introduction at the very beginning of my

study and valuable discussion and suggestions on my whole research project, as well as offering valuable friendships.

I would also like to thank my friends, Hong Yi, Chang Chen, Lifang Zhong and Tongzhi Wu, for all kinds of supports and friendships, which helped me through my stressful and demanding times.

Last but not least, my greatest gratitude must go to my family and my husband, who provided me with selfless love, support and encouragement throughout my study.

ABSTRACT

The aim of this thesis project was to develop polymer microbead-based Raman/surface enhanced Raman scattering (SERS) immunoassay systems for the multiplex, specific and sensitive detection of biological molecules. Immunoglobulin G (IgG) was used as model proteins. In the system, gold nanoparticles (AuNPs) serve as SERS-active substrates. Different Raman-active molecules, such as 4-mercaptobenzoic acid (4MBA), can be easily self-assembled on the AuNPs as SERS tags. Polymer microbeads offer as immune-solid supports and provide Raman signatures. This study focused on the fabrication of different SERS tags, SERS-active microbeads and Raman spectroscopic-encoded microbeads for microbead-based Raman/SERS immunoassay development.

Polymer microbead-based Raman/SERS immunoassay system was first developed using 50 nm AuNPs and 130-600 μm carboxylated polystyrene (PS) microbeads synthesised by suspension polymerisation. Antibodies (FITC-labelled donkey anti-goat IgG) were conjugated to polymer microbeads by EDC/NHS coupling chemistry. The SERS tags were comprised of Raman-active molecules (4MBA) and AuNPs. Antigens (DyLight^{TM}649-labelled goat anti-human IgG) were successfully conjugated on SERS tags to form SERS reporters. The immunoassay was performed by mixing the protein conjugated polymer microbeads and SERS reporters together. Due to the specific recognition between antibody and antigen, AuNPs can be attached on the surface of polymer microbeads. The results were verified using fluorescence imaging and Raman/SERS analysis.

Since flow cytometry can rapidly sort large number of cells and particles in a short time, our intention was to take the advantages of both flow cytometry and Raman effects to develop Raman flow cytometry for multiplex and rapid detection. Therefore, monodisperse polymer microbeads with unique Raman signatures need to be synthesised. The

preparation of the monodisperse polymer microbeads with specific Raman signatures was carried out by two approaches. Firstly, the SERS-active microbeads were synthesised by the deposition of AuNPs on the surface of polymer microbeads and the addition of the Raman-active molecules prior to silica coating. The preparation of polystyrene microbead/AuNP composite microspheres was achieved through two methods (direct adsorption and in-situ growth). The mechanism for the silica coating of polystyrene/AuNP composite microspheres was discussed in details. 4-mercaptophenol (4MP) was self-assembled on the composite microspheres, followed by silica coating to obtain the SERS-active microbeads.

Secondly, the Raman spectroscopic-encoded copolymer microbeads were fabricated using styrene (Sty), 4-tertbutylstyrene (4tBS), and 4-methylstyrene (4MS) by dispersion polymerisation. Acrylic acid (AA) was used as the co-monomer to generate carboxyl groups on the surface of polymer microbeads. Six kinds of copolymer microbeads with the average diameters between 1.07 and 1.69 μm, including poly(Sty-AA), poly(Sty-4tBS-AA), poly(4tBS-AA), poly(Sty-4MS-AA), poly(4MS-AA), and poly(4tBS-4MS-AA), were synthesised with narrow size distribution and unique Raman fingerprints, which could be employed as spectroscopic-encoded microbeads in microbead-based Raman/SERS immunoassay system.

Monodisperse polystyrene microbeads with 1.6 μm diameter were also used to perform the polymer microbead-based Raman/SERS immunoassays. A similar immunoassay system as previous was applied for IgG recognition based on AuNPs and monodisperse PS microbeads, which were sorted and analysed using flow cytometry and Raman equipment.

In summary, the thesis proposed a new strategy for multiplex detection and reported the preliminary studies on polymer microbead-based Raman/SERS immunoassay. Different SERS-active microbeads and Raman spectroscopic-encoded copolymer microbeads have been successfully synthesised.

TABLE OF CONTENTS

LIST OF FIGURES

LIST OF TABLES

ABBREVIATIONS

In this thesis, the following abbreviations are used.

AA	acrylic acid
Ab.	antibody
Ag.	antigen
AgNPs	silver nanoparticles
AIBN	2,2'-azobis(2-methylpropanitrile)
APTMS	3-aminopropyl-trimethoxysilan
4ATP	4-aminothiophenol
AuNPs	gold nanoparticles
BPO	benzoyl peroxide
BSA	bovine serum albumin
CM	chemical enhancement mechanism
CV	crystal violet
CV	coefficient of variation
DI water	deionised water
D_{n}	number-average diameter
EDC	1-ethyl-3-(3-dimethylaminopropyl) carbodiimide) hydrochloride
EEF	effective enhancement factor
EGDMA	ethylene glycol dimethacrylate
ELISA	enzyme-linked immunosorbent assay
EM	electromagnetic enhancement mechanism
FC	flow cytometry
$HAuCl_4 \cdot 3H_2O$	gold (III) chloride trihydrate
IR	Infrared
LOD	limit of detection
LSPR	localized surface plasmon resonance
4MBA	4-mercaptobenzoic acid
4MP	4-mercaptophenol
4MS	4-methylstyrene
Na_3Ct	trisodium citrate dehydrate

NHS	N-hydroxysuccinimide
PBS	phosphate buffer saline
PS	polystyrene
PVA	polyvinyl alcohol
PVP	polyvinyl pyrrolidone
QDs	quantum dots
R6G	Rhodamine 6G
RT	room temperature
SAMs	self-assembled monolayers
SEM	scanning electron microscope
SERS	surface enhanced Raman scattering
S/N	signal-to-noise
Sty	styrene
4tBS	4-tert-butylstyrene
TEM	transmission electron microscope
TEOS	tetraethyl orthosilicate
THF	tetrahydrofuran
Tris	tris (hydroxymethyl)aminomethane
UV-Vis	ultraviolet-visible

CHAPTER 1 Introduction

1.1 Background

Cancer is a complex disease and poses significant risks to human beings. Millions of patients were and are being taken their lives by these incurable diseases. Histological examination of biopsy specimen and serological tests such as enzyme-linked immunosorbent assays (ELISA) are commonly used technologies for cancer diagnostics. However, these technologies are time-consuming, expensive, and somewhat subjective.[1] In addition, the conventional diagnostic methods are difficult to detect the early lung cancer, such as dysplasia and carcinoma in situ.[2] Moreover, human diseases currently tend to be complicated, which requires the analytes being measured simultaneously in one single sample, namely multiplex detection. Unfortunately, the current techniques and development on the disease detection are hard to achieve the multiplex detection of diseases in a short measurement time. Early and multiplex cancer diagnostics are crucial for the effective treatment of life-threaten diseases and prevention of death. Hence, there is a need to develop more effective and novel disease diagnostic tools for the accurate and effective detection of abnormal cells and for the multiplex detection of diseases.

Raman scattering, a vibrational scattering technique, is well known for its specificity in chemical, biological and biomedical analyses of molecules.[3] It can distinguish the molecules with high similarity due to its narrow vibrational band. There is no photobleaching related to Raman scattering. Another major advantage of Raman scattering is that it can be applied in aqueous environment, which makes Raman scattering an important analytical tool for biological-based measurements. To date, Raman scattering has been popularly employed in the fields of biology, chemistry, environment, pharmaceuticals, forensics, and materials science. Especially, studies have been done to

apply Raman scattering on cancer diagnostics.[4] The broad applications of Raman scattering indicate that it is a competitive technique compared to Infrared (IR) and fluorescence.

However, the limitations of Raman scattering are its small cross-section and weak Raman emission, making it unlikely to achieve measurements with high signal-to-noise (S/N) ratios without any enhancement procedure. Surface enhanced Raman scattering (SERS) is a powerful analytical technique to get strongly enhanced Raman signals of molecules by the formation of self-assembled monolayer (SAMs) onto metal surface. The localized surface plasmon resonance (LSPR) of metal nanoparticles can make the Raman signals of those self-assembled organic molecules enhance by many orders of magnitude. Up to 10^{14} Raman enhancement factors have been reported through the formation of aggregates, which enable the detection of single molecules.[5] After its first recognition in 1974, SERS has been extensively applied in analytical chemistry.[6] Great attentions have been paid on SERS-based biological diagnostics and bioimaging in recent years.[7-10]

SERS-based immunoassays have been developed for disease detection. The abnormal cancer cells always contain overexpressed antigens, which can be considered as the signals of diseases and targeted for cancer detection. Different labels, including enzyme, fluorescence, isotopes, and luminescence, are normally employed to assist the detection of specific antibody and antigen interaction during the immunoassays. Notably, SERS labels have many advantages over these traditional labels, such as no photobleaching, harmless to environment, high sensitive and high throughput, which enable SERS labels to replace the conventional labels for immunoassays. Capture substrates, SERS reporters and capture antigens are three main parts for a typical SERS-based immunoassay. In practice, solid surfaces are used as capture substrates. But the application of solid substrates on immunoassays is limited by the extended incubation time and repeated washing process.[11]

Alternatively, living cells or particles can also be used as the solid supports, which build flow-based immunoassays. When directly using cell as substrate, the complex biological environment of cell may cover the Raman signals of analytes.[12] The antigen concentration at the early-stage of disease is relatively low and hard to be measured directly using cell-based immunoassay. However, particle-based SERS immunoassays can overcome those problems. Different antigens are present in the solution, which can be directly detected using particle-based SERS immunoassays. Magnetic nanoparticles, silver/gold nanoparticles, and silica nanoparticles can be employed in particle-based SERS immunoassays.[13-15]

Polymer microbeads are fascinating materials and play an important role in biosciences. They have been considered as protein carriers and applied on biodetection based on immunoassays.[16] Moreover, polymer microbeads contain many repeat units and each repeat unit can operate as one individual bioanalytical tag. The development of different polymers will result in a large pool of barcoded library, which can be applied in the multiplex detection system. The synthesis of 630 copolymers has been reported using 15 spectroscopically active styrene monomers.[17] Each of copolymers has specific Raman and Infrared (IR) fingerprint and can be used to build up the barcoded library. Furthermore, different barcoded polymers have been used in the antigen detection.[18]

Therefore, the combination of polymer science and SERS allows the development of a large pool of vibrational spectroscopic information and might provide a novel multiplex direction for complex disease diagnosis. The development of polymer microbeads will not only significantly improve the detection sensitivity but also make the detection to be more multiplexed during particle-based SERS immunoassay. To date, there are insufficient reports on the development of particle-based SERS immunoassays using the vibrational

spectroscopic information of polymer microbeads. This project aims at developing a rapid, but reproducible, sensitive and specific multiplex detection technique for human disease diagnosis based on polymer microbeads and SERS immunoassays, so-called the microbead-based Raman/SERS immunoassays. Different Raman spectroscopic-encoded microbeads, including polystyrene microbeads and copolymer microbeads, and SERS-active microbeads are going to be prepared. The microbeads can serve as immune-solid supports and provide unique Raman signatures during the immunoassays. It is expected that this research project can develop a new technique for ultrasensitive detection of human cancers as well as improving the feasibility and efficiency of polymer and nanomaterials on biomedical applications.

1.2 Aims and Objectives

In terms of the properties and applications of SERS and polymer microbeads, the overall aim of this research project is to prepare different kinds of SERS-active microbeads or Raman barcoded microbeads, and to develop polymer microbead-based Raman/SERS immunoassay systems for multiplex detection. The specific objectives of the project are:

(1) to synthesise gold nanoparticles (AuNPs) with different sizes,
(2) to understand the SAMs of Raman-active molecules, such as 4-mercaptobenzoic acid (4MBA), on different AuNPs and their SERS signatures,
(3) to prepare polystyrene (PS) microbeads by suspension polymerisation or dispersion polymerisation,
(4) to prepare SERS-active polymer microbeads by the adsorption of AuNPs on the surface of monodisperse PS microbeads and the addition of Raman-active molecules prior to silica coating,

(5) to prepare various monodisperse copolymer microbeads with unique Raman signatures using dispersion polymerisation, and

(6) to evaluate the efficiency and feasibility of microbead-based Raman/SERS immunoassays for Immunoglobulin (IgG) detection.

1.3 Thesis Outline

This thesis contains 9 chapters.

In Chapter 1, a general introduction of cancer detection, the choice of surface enhanced Raman scattering and polymer microbeads for multiplex detection, the aims and objectives of this project, and the structures of the thesis are outlined.

Chapter 2 reports a comprehensive literature review related to the project. The introduction of Raman scattering, surface enhanced Raman scattering, SERS-active substrates, AuNPs, SERS-based immunoassays, polymerisation techniques and microbead-based immunoassay for multiplex detection are involved in the literature review section.

Chapter 3 describes the general experimental methods and various characterisation techniques employed in this study, such as UV-Vis spectrophotometer, TEM, SEM, Raman spectrometer, Raman microscope, Fluorescence microscope, and Flow cytometry.

In Chapter 4, a polymer microbead-based SERS immunoassay system was developed for IgG detection using gold nanospheres and polystyrene microbeads, where the large polystyrene microbeads were prepared using suspension polymerisation. The AuNPs can be attached to the surface of PS microbeads because of the specific recognition between matched antibodies and antigens. The Raman signatures of both polystyrene and SERS molecules (4MBA) are detected on the matched pairs.

Chapter 5 focuses on the fabrication of polystyrene/AuNP composite microspheres by the Hybridisation of AuNPs on microbead surface. Two methods, direct adsorption and in-situ growth, were used for the fabrication of composite microspheres. The polystyrene/AuNP composite microspheres can be formed by both methods. There is no surface modification or surfactants applied and the whole process is driven by thermal dynamic effect, where small AuNPs act as stabilisers of metastable polymer microbeads.

In Chapter 6, the silica coating of polystyrene/AuNP composite microspheres has been investigated. The influences of deposition time, ammonia concentration, water concentration and TEOS concentration on the silica coating have been investigated in details. Raman-active molecule (4MP) has been introduced to fabricate monodisperse SERS-active microbeads.

In Chapter 7, different kinds of copolymer microbeads with narrow size distribution and unique Raman signatures are synthesised using dispersion polymerisation.

In Chapter 8, the research focuses on the microbead-based flow cytometric/SERS immunoassays for IgG detection using gold nanosphere-based SERS reporters and monodisperse PS microbeads, prepared by dispersion polymerisation.

Finally, Chapter 9 draws the conclusions and discusses the possible future perspectives.

CHAPTER 2 Literature Review

This chapter provides a comprehensive review of Raman scattering, the theory and enhancement mechanisms of SERS, and SERS-active substrates. AuNPs as SERS-active substrates, including the synthesis, formation mechanisms, unique properties, and self-assembled monolayers of gold nanoparticles/nanostructures are described. The applications of SERS-based immunoassays are also reported. Moreover, a brief review on the preparation of polymer microbeads and the applications of microbead-based immunoassays are included in this Chapter.

2.1 Surface Enhanced Raman Scattering (SERS)

2.1.1 Raman Scattering

When a beam of light illuminates the substance, the incident light might directly pass through, be absorbed, or be scattered by the molecules according to the interaction between incident photons and molecules. If there is no interaction between incident light photons and molecules, the incident light directly pass through the material and transmission occurs. When the incident light photon energy equals to the energy gap between the ground state and the electronically excited state of the molecules, the incident light can be absorbed by the molecules and absorption occurs. When the electromagnetic waves of incident light cause the oscillation of electron cloud distribution in intramolecular, the light will be re-radiate in all directions, which means the incident light is scattered by the substance.

Scattering can be divided into Rayleigh scattering and Raman scattering. When light of a certain wavelength interacts with a molecule, most photons are elastically scattered and therefore have the same energy as the incident photons. That is called Rayleigh scattering. However, there is a small amount of photons (approximately 1 in 10^6 photons), which are inelastically scattered, where the energy of the scattered photon is different from the

energy of incident photons. This scattering is called Raman scattering, in which a vibrational quantum is excited (Stokes Raman scattering) or annihilated (Anti-Stokes Raman scattering). It was first discovered in 1928 by C. V. Raman.[19] Because of the discovery of Raman effect, he won the Nobel Prise in 1930.

A comparison of Rayleigh scattering and Raman scattering is shown in Figure 2.1. Δ_V is the difference between the excitation frequency (v_0) and scattering frequency (v_1), which corresponds to the vibrational level of the molecule.[20] In terms of Rayleigh scattering, the scattering frequency (v_1) is identical to the excitation frequency (v_0) and there is no energy loss or gain ($\Delta_V = 0$). Meanwhile, Raman scattering is an inelastic scattering including stokes scattering and anti-stokes scattering. For stokes scattering, the scattering energy is transferred to the vibrational mode of the molecule, so the scattering frequency (v_1) is smaller than the excitation frequency (v_0). Otherwise, v_1 is larger than v_0 when the molecule losses energy for anti-stokes scattering. Since the anti-stokes scattering is much less intense than stokes scattering, stokes scattering is normally measured in Raman scattering.

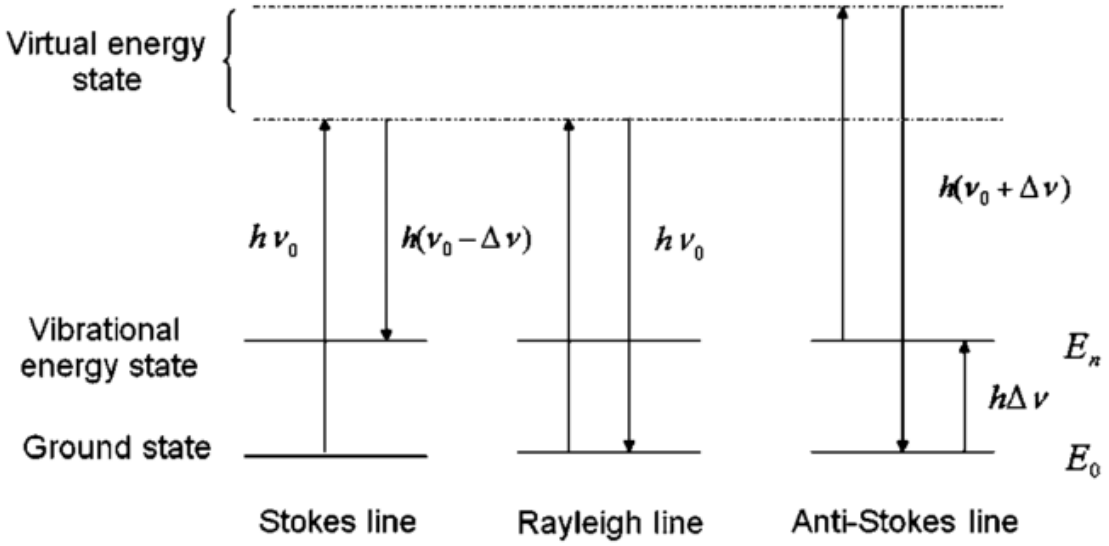

Figure 2.1 Energy level diagram for Raman scattering and Rayleigh scattering.[20]

Raman scattering can provide more detailed vibrational information of molecules and distinguish the molecules with great structural similarity. The contribution of water to Raman signals is low, so it is well-suited for analysing the samples in aqueous environment. The Raman spectra of different inorganic materials, such as graphite, graphene, carbon nanotubes, crystals, and silicon, have been extensively investigated.[21-26] Raman scattering can be used to monitor the number of layers of graphene, quality of layers and doping levels.[27] Graphene with less than five layers can be clearly distinguished by Raman fingerprints.[26] Moreover, it is also an effective way to analyse polymers and biological macromolecules.[28-30]

2.1.2 Surface Enhanced Raman Scattering

Although Raman scattering has many advantages, the limitation is its low intensity, which leads to the weak Raman signals. The reason is that the number of photons for Raman scattering is quite small. It shows low sensitivity that means long data acquisition times and high laser powers needed to gain reliable Raman signals.[8] The samples also normally

require being highly concentrated during the measurement. Therefore, unlike the Infrared (IR) and fluorescence spectra, the Raman scattering has received less attention on its development and applications, especially in material and molecular detection. Hence, it is of great importance to enhance the Raman signals during measurements.

In 1974, an enhancement of Raman intensities of pyridine was first observed by the adsorption of pyridine on roughened silver electrode by Fleishmann and co-workers.[6] In 1977, Albrecht *et al.* and Van Duyne *et al.* independently verified the sensitivity of Raman spectroscopy and this phenomenon was defined as the surface enhanced Raman scattering (SERS).[31, 32] Since then, plenty of studies have been carried out to investigate the effect of SERS between various organic molecules and metals, such as silver, gold, copper, lithium, sodium, potassium, indium, aluminium, platinum, and rhodium.[33]

SERS can provide the high agreement of structural information about the organic molecules, which is identical to the normal Raman scattering. Compared with normal Raman scattering, SERS can obtain obviously enhanced signals of analytes using low power lasers and low magnification optics, and can enhance the Raman signals with high magnitudes. It is a technique that links Raman spectroscopy and the exciting optical properties metal nanoparticles/structures together.[34] When the molecule adsorbed on or close to the rough surface of precious metal particles/nanostructures, the Raman signal can be enhanced significantly. Precious metal nanoparticles, such as silver, gold and copper, can be applied to enhance the Raman signals of molecules. The single molecule detection has been achieved using this technique, where up to 10^{14} to 10^{15} magnitudes can be obtained when adsorbing Rhodamine 6G (R6G) or crystal violet (CV) onto the surface of silver nanoparticles (AgNPs).[5, 35]

There is no doubt that SERS has become a significant laser spectroscopic characterisation technique for the investigation of vibrational properties and structural information of adsorbed molecules on metal substrates. Many scientists devoted themselves to study the applications of SERS on biosciences and have gained great achievements during last few decades.[9, 10, 36-43] Until now, SERS has been applied on different areas, including single molecule detection, DNA sensor, glucose sensing, and *in vivo* cancer imaging, etc.[44-47]

2.1.3 Enhancement Mechanisms and Effective Enhancement Factors

2.1.3.1 Enhancement Mechanisms

Since the first discovery of enhanced Raman signals, extensive investigation efforts have given to identify possible mechanisms to explain the enhancement effect. Currently, two enhancement mechanisms are commonly accepted to describe the effect of surface enhanced Raman scattering: electromagnetic enhancement mechanism (EM) and chemical enhancement mechanism (CM).[33, 48]

The EM rises from the enhanced local electric fields of metallic structures around the adsorbed molecule due to the excitation of electro-magnetic resonances in the metallic structures.[49, 50] The electromagnetic effect depends on the localized surface plasmon resonance (LSPR) of metallic structure and the surface of which responses to the incoming waves, resulting in the enhancement of the electric field. EM is a long-range enhancement mechanism. The enhancement can vary by several orders of magnitude, depending on the metallic materials and the coupling between different surfaces.[51]

A simple physical model has been used to understand the interparticle coupling effect and is illustrated in Figure 2.2. When the light is polarised parallelly to the interparticle axis

(Figure 2.2 down) and the nanoparticles are getting closer, the proximity of these charges to the molecule can be made arbitrarily small and the capacitive field sensed by the molecule becomes correspondingly large. The interaction of the two particles also results in a magnitude increase of the dipole, which arises from the combined field of incident light and the field of the other particles, resulting in the polarisation amplification. On the other hand, when the light is polarised orthogonally to the interparticle axis (Figure 2.2 top), the capability is unavailable.[52]

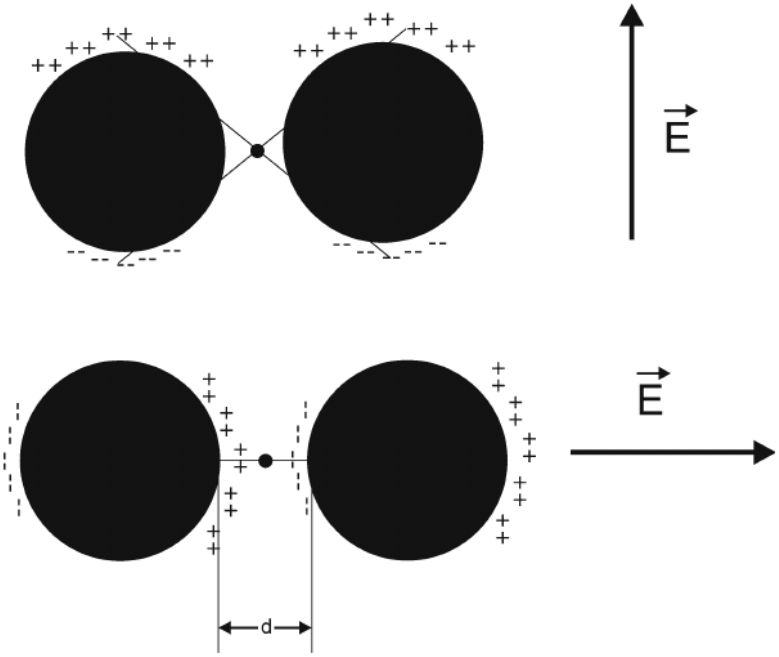

Figure 2.2 Simple graphical illustration of the reason that light polarised with the *E*-vector along the interparticle axis can result in huge enhancements in the gap between the two nanoparticles while the orthogonal polarisation cannot. For light polarised along the interparticle axis the proximity of the charges (induced by the optical fields) to the molecule can be made arbitrarily small and hence the field sensed by the molecule commensurately large as the nanoparticles are brought closer together. That capability is not available for light polarised orthogonally to the interparticle axis.[52]

The CM is original from the relationship between molecules and metals. The molecules electronically couple with metal surface and give rise to the enhancement effect.[53] Unlike the EM mechanism, CM is a short-range enhancement mechanism.[54] It involves charge transfer intermediate state between the adsorbed molecules and the metal surfaces.[55] The charge transfer includes the processes either from the metals to the adsorbed molecules or from the molecules to the metals. A dynamical charge transfer model has been proposed and can be illustrated by four main steps:[34, 56]

(1) Excitation of an electron into a hot-electron state and formation of electron-hole pair,
(2) Transfer of the hot electron into the lowest unoccupied molecular orbital (LUMO) of the adsorbed molecule,
(3) Transfer of the hot electron from the LUMO back to the metal, and
(4) Recombination of electron-hole pair and emission of Raman photon.

Obviously, the enhancement mechanism of the CM is based on the chemical interaction between the molecules and the metals.

However, neither EM nor CM can fully explain the entire phenomenon. It is commonly recognised that EM and CM coexist in the SERS systems. But their contributions to Raman signal are variable in different systems. Theoretically, EM contributes to 8-10 orders of magnitude to the Raman enhanced signals, while CM can enhance 1-2 orders of magnitude.

Kneipp and co-workers compared the signals of normal Raman scattering (I_{NRS}) with SERS (I_{SERS}).[57] The equations are as below.

$$I_{NRS}(v_s) = N \cdot I(v_L) \cdot \sigma^R_{free} \tag{2.1}$$

$$I_{SERS}(v_s) = N' \cdot I(v_L) \cdot | A(v_L) |^2 \cdot | A(v_S) |^2 \cdot \sigma_{ads}^R \quad (2.2)$$

In a normal Raman scattering, the total Raman signal (I_{NRS}) is proportional to the number of molecules (N), the intensity of laser ($I(v_L)$) and the Raman cross-section (σ_{free}^R). In SERS, $A(v_L)$ *and* $A(v_S)$ represent the field enhancement factors of the laser and Stokes fields, respectively. This is based on electromagnetic field enhancement. σ_{ads}^R is an increased Raman cross-section as chemical enhancement. N' is the number of molecules adsorbed on the metal particles and is involved in SERS.

2.1.3.2 Effective Enhancement Factors

The effective enhancement factor (EEF) can be used to evaluate the performance of SERS-active substrates. Therefore, the calculation of EEF is necessary and vital important for the development and practical applications of the SERS-active substrates. Briefly speaking, EEF is a value that compares the enhanced intensity of Raman signals obtained under SERS conditions to that under normal Raman conditions.[58] The EEF can normally reach 10^7-10^8 and some of SERS substrates can even reach 10^{12}, which are sufficient for single molecule detection.[21]

Typically, EEF can be calculated using the following equation:

$$EEF = \frac{I_{\mathrm{SERS}} N_{\mathrm{bulk}}}{I_{\mathrm{bulk}} N_{\mathrm{SERS}}} \quad (2.3)$$

where I_{SERS} and I_{bulk} are the intensities of the same band for the SERS and bulk spectra; where N_{bulk} is the number of molecules for a bulk samples and N_{SERS} is the number of molecules in SERS excited by the laser beam. This is a general EEF calculation used by

most authors.[59-62] It can be used to compare the average SERS enhancements across different substrates.

There are also a few more complicated definitions on the calculation of EEF, including single molecule enhancement factor (SMEF), SERS substrate enhancement factor (SSEF), analytical enhancement factor (AEF), and hot spot enhancement factor (HSEF), etc.

(1). Single molecule enhancement factor (SMEF) is for a given molecule at a specific position. The following definition of SMEF is given:[61]

$$SMEF = \frac{I_{\mathrm{SERS}}^{\mathrm{SM}}}{\langle I_{\mathrm{RS}}^{\mathrm{SM}} \rangle} \tag{2.4}$$

where $I_{\mathrm{SERS}}^{\mathrm{SM}}$ is the SERS intensity of the single molecule under consideration, whereas $\langle I_{\mathrm{RS}}^{\mathrm{SM}} \rangle$ is the average Raman intensity per molecule for the same probe. This definition depends on the Raman tensor of the probe, the solvent and the refractive index of the solvent. It is independent on the position or orientation of the molecule.

(2) SERS substrate enhancement factor (SSEF) was proposed by Le Ru *et al*. and by calculating the average surface area of a nanocapsule.[61] The definition is as follow.

$$SSEF = \frac{I_{\mathrm{SERS}}/(\mu_{\mathrm{M}}\mu_{\mathrm{S}}A_{\mathrm{M}})}{I_{\mathrm{RS}}/(c_{\mathrm{RS}}H_{\mathrm{eff}})} \tag{2.5}$$

where A_{M} is the surface area of the metallic substrate, μ_{M} [m^{-2}] is the surface density of the individual nanostructures producing the enhancement, μ_{S} [m^{-2}] is the surface density of molecules on the metal, c_{RS} represents the concentration of the solution used for the non-SERS measurement, and H_{eff} is the effective height of the scattering volume. This expression modifies the commonly used average EEF in equation 2.3.

(3) Analytical enhancement factor (AEF) is extremely suitable for the case of SERS active liquids.[61]

$$AEF = \frac{I_{\mathrm{SERS}}/c_{\mathrm{SERS}}}{I_{\mathrm{RS}}/c_{\mathrm{RS}}} \tag{2.6}$$

where c_{RS} represents the concentratioan of an analyte solution and I_{RS} is Raman signal produced under non-SERS conditions. The SERS signal (I_{SERS}) is produced from the same analyte on a SERS substrate with different concentration (c_{SERS}) under the identical experimental conditions and preparation conditions.

(4) Hot spot enhancement factor (HSEF) is to calculate the average enhancement over all molecules resident in the hotspot of a single nanocapsule. Hot spot areas as the contact areas between nanoparticles are estimated during the calculation.[63]

$$HSEF = \frac{f_{\mathrm{SERS}}S_{\mathrm{SERS}}}{f_{\mathrm{Raman}}S_{\mathrm{Raman}}}\frac{I_{\mathrm{Raman}}}{I_{\mathrm{SERS}}}\frac{N_{\mathrm{Raman}}}{N_{\mathrm{SERS}}} \tag{2.7}$$

where f_{Raman} is for the fraction detected in Raman measurements and f_{SERS} is for the fraction detected in SERS measurements. I_{SERS} and I_{Raman} represents the intensities of laser excitation for the Raman and SERS experiments, respectively. N_{Raman} is the molecules present in the detection volume with the total intensity of this solution measured (S_{Raman}). N_{SERS} is the average value of molecules per hot spot with the intensity S_{SERS}.

2.2 Specific SERS-active Systems

One of the most important criteria for the practical applications of SERS is how to select and prepare the SERS substrates with excellent SERS performance. The substrates should have high SERS effective enhancement factors. They also should be stable, reproducible, and can be easily fabricated with low-cost. Covering the SERS substrates with molecules

can form the SERS probes or reporters which can be easily detected using Raman equipments. Table 2.1 lists various materials developed as SERS substrates. More substrates can be found in the literature.[20]

The shape, size and composition of the metallic nanostructures are important factors influencing the performance of SERS substrates. As we can see in Table 2.1, roughed electrodes, metallic nanoparticles, nanocomposite structures, and nanostructured metal island films are commonly used as SERS-active substrates. Electrodes are the earliest SERS substrates, but the effect enhancement factors are relatively lower than that of metal nanoparticles, which limits the applications of electrodes.

Precious metal nanoparticles exhibit strong absorption bands in visible region, which are closed to the excitation laser lines for SERS. Moreover, high intensity of SERS signals can be observed through the formation of nanoparticle aggregates. That can promote the electromagnetic field enhancement between nanoparticles, which may be increased by several orders of magnitude.[64] Besides that, the metal nanoparticles are easily prepared and dispersed in solution. Therefore, nanoparticles are well suited for molecule sensing. AgNPs and AuNPs are the most commonly used metal nanoparticles for SERS substrates. The Raman signals enhanced by AgNPs are normally higher than that using AuNPs, but AgNP colloidal solutions are relatively unstable.[65] The effect enhancement factor of AuNPs can reach up to 10^9 times, which enable the ultrasensitive detection at single molecule level.

Table 2.1 SERS substrates and analytes.

Substrates	Analytes	LOD	EEF	Ref.
Ag electrode	pyridine	N.A.	N.A.	6
	pyridine	N.A.	~10^5	32
	benzoic acid	N.A.	N.A.	66
	4-(methylthio)benzoic acid	N.A.	N.A.	67
	L- and D- cysteine	N.A.	N.A.	68
	6-mercaptopurine	N.A.	N.A.	69
	4-aminopyridine	N.A.	N.A.	70
Au electrode	pyridine	N.A.	N.A.	71
	iron phthalocyanine	N.A.	N.A.	72
	benzenethiol	N.A.	N.A.	73
	benzenemethanethiol			
	p-cyanobenzenemethanethiol			
	diphenyl disulfide			
	dibenzyl disulfide			
	1,10-phenanthroline	N.A.	N.A.	74
	poly(neutral red)	N.A.	N.A.	75
Cu electrode	pyridine	N.A.	N.A.	71
	iron phthalocyanine	N.A.	N.A.	72
	1,3,5-benzenetricarboxylic acid	N.A.	N.A.	76
Pt electrode	benzene	N.A.	N.A.	77
	benzonitrile	N.A.	N.A.	78
Rh electrode	acetylene	N.A.	N.A.	79
Co electrode	4-aminopyridine	N.A.	N.A.	70
AgNPs	4-(methylthio)benzoic acid	N.A.	N.A.	67
	crystal violet	Single molecule	N.A.	35
	R6G	Single molecule	10^{14}-10^{15}	5

	lysophosphatidic acid	4×10^{-10} M	N.A.	80
	yeast cytochrome c	Single molecule	N.A.	81
	cholinesterase inhibitors	1.8×10^{-8} M	N.A.	82
AuNPs	DNA nucleosides	N.A.	N.A.	83
	single living cells	single cell	N.A.	37
	R6G	N.A.	10^9	84
	alkaline phosphatase	$\sim4\times10^{-15}$ M	N.A.	85
	thrombin	10^{-13} M	N.A.	86
	trinitrotoluene	2×10^{-12} M	10^9	87
Copper colloids	pyridine	N.A.	N.A.	88
Nanoporous Copper	R6G	N.A.	$\sim1.85\times10^5$	89
	crystal violet 10B			
TiO_2 nanoparticles	4-mercaptobenzoic acid	10^{-4}–10^{-3} M	N.A.	90
Ag Nanosphere Dimers	distyrylbenzene	N.A.	3×10^6	91
Ag/Au coreshell	thiophenol	N.A.	N.A.	92
	p-aminothiophenol			
SiO_2/Au coreshell	*p*-mercaptoaniline	N.A.	N.A.	93
TiO_2/Au coreshell	meso-tetra(4-carboxylphenyl)	N.A.	N.A.	94
	porphine (TCPP)			
	tris(2,2′- bipyridyl) ruthenium(II)			
	chloride (Ru(bpy))			
	R6G			
Fe_2O_3/Au coreshell	pyridine	N.A.	N.A.	95
Fe_3O_4/SiO_2/Ag	R6G	10^{-14} M	$>1.28\times10^6$	96
Ag nanorod on glass	*trans*-1,2-bis(4-pyridyl)ethene	N.A.	$\sim5\times10^8$	97
AuNPs on glass	*p*-aminothiophenol	N.A.	10^7	98
AgNPs decorated-silicon nanocones	label-free DNA	10^{-8} M	N.A.	99
Wrinkled nanoporous	R6G	10^{-12} M	$\geq10^9$	100

$Au_{79}Ag_{21}$ films	DNA nucleobase adenine			
Porous Al_2O_3 substrate sputter-coated with gold	R6G	$10^{13}/cm^{-2}$	N.A.	101
Fiber optic probe integrated with AgNRs	trans-Bis(4-pyridyl)ethane (BPE) and adenine	10^{-7} M	N.A.	102
Thiol-modified Fe_3O_4/Ag	polycyclic aromatic hydrocarbons	at μg/L level	N.A.	103
Hollow-core photonic crystal fiber	R6G	10^{-10} M	N.A.	104
Ag Nanodesert Rose	*trans*-1,2-bis(4-pyridyl)ethylene	10^{-7} M	$3 \times 10^{4.}$	105
	4-mercaptopyridine	10^{-10} M	2×10^{5}	
	R6G	10^{-15} M	2×10^{10}	

2.3 Gold Nanoparticle-based SERS Substrates

2.3.1 Preparation of Gold Nanoparticles

'Top-down' and 'bottom-up' approaches are commonly used for the synthesis of AuNPs. The top-down approach involves cutting the bulk metals into nanoparticles. The bottom-up approach involves building up the nanoparticles from atomic level. The bottom-up approach is the most popular method, since the size and morphology of nanoparticles can be easily controlled under solution-based reaction. Gold halides, for example chloroauric acid ($HAuCl_4$), are used as precursor to prepare AuNPs. There are a variety of methods developed for the preparation of AuNPs with different shapes and sizes using the 'bottom-up approach'. The most commonly used method for the spherical AuNP synthesis is chemical reduction method. Different reducing agents, such as sodium citrate, sodium borohydride and white phosphorus, can be used to reduce chloroauric acid to AuNPs.

Sodium borohydride, which is a strong reducing agent, can produce nanoparticles with diameters of 1-5 nm in the presence of thiol capping agents, like dodecanethiol and p-mercaptophenol.[106-108] Large particles can be produced using sodium citrate (Figure 2.3), which is a relatively weak reducing regent and acts as both reducing agent and capping agent in the citrate reduction method. The reduction of gold chloride by sodium citrate was first developed by Turkevish *et al*. in 1951 and modified by Frens in 1973.[109, 110] It is the most commonly used and simplest method for AuNP fabrication. The particle size is dependent on the feed molar ratios of sodium citrate and gold chloride. The lower molar ratio of sodium citrate and gold chloride is, the larger particle size is. Generally, monodisperse particles with 10-20 nm diameters can be obtained using the citrate reduction method. Larger particles can also be produced using this method but with non-spherical and irregular shapes.[110]

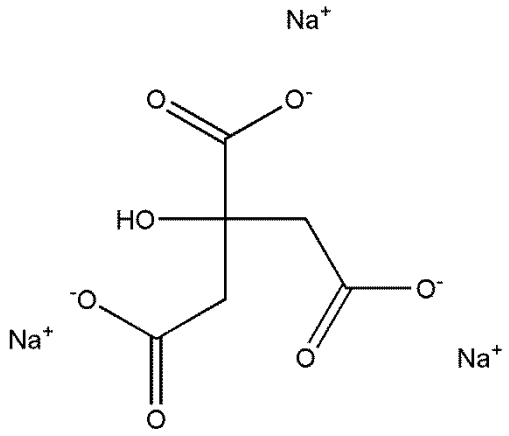

Figure 2.3 Chemical structure of trisodium citrate.

The seed-growth method was developed as a promising tool for controlling the size and shape of nanoparticles. In this procedure, small metal particles are first fabricated using sodium borohydride as a reducing agent, and then they are used as seed solution to further grow metal particles. As a result, different sizes and shapes of nanoparticles can be easily

produced by varying the ratios of metal salt and seed solution. The AuNPs with uniform particle size between 5 and 40 nm were synthesised.[111] The gold particle seeds with 3.5 nm were synthesised using sodium borohydride as a reducing agent and trisodium citrate as a capping agent. The surfactant cetyltrimethylammonium bromide (CTAB) was applied to inhibit the secondary nucleation and stabilised the formed nanoparticles in growth media, where metal salt ($HAuCl_4$), a weak reducing agent (ascorbic acid) and seeds were present. After that, AuNPs with 5-40 nm diameters were formed using step by step seeding. AuNPs with narrow size distributions up to 180 nm were also synthesised by replacing sodium borohydride with trisodium citrate.[112] Recently, larger uniform AuNPs with up to 300 nm were reported using the mixture of ascorbic acid and sodium citrate as both reducing and stabilising agents.[113] The results also indicated that the slow and separated addition of reducing and precursor solutions is essential for the formation of good shape and uniform particles using this method.

2.3.2 Mechanisms of Gold Nanoparticle Growth

Since the citrate reduction method is a particularly popular approach for the preparation of AuNPs, it is used as a model reaction to investigate the formation mechanism of AuNPs. Turkevich *et al*. conducted many studies to investigate the formation mechanism of AuNPs on nucleation, growth, and aggregation.[109, 114, 115] In 1994, Chow and Zukoski demonstrated that the formation of large particles occured in the early stage of reaction and the size decreased to form small particles through the course of the reaction.[116] There were a few other studies reported on the formation mechanism of AuNPs via citrate reduction method.[117-119] However, it is still not fully understood due to the shortage of dynamic information. Ultraviolet-Visible (UV-Vis) spectrophotometer and transmission electron microscopy (TEM) have been used to measure the localized surface plasmon resonance

(LSPR) bands and the morphologies of AuNPs. Since the nucleation and particle formation normally occur in a short time of period, it is hard to be monitored using UV-Vis spectrophotometer and TEM.

Polte *et al*. presented a new method by monitoring particle formation via the small-angle X-ray scattering and X-ray absorption near-edge spectroscopy using synchrotron radiation, which enables time-resolved in-situ investigation of size and composition of the formed nanoparticles.[120] The mechanism of nanoparticle formation can be divided into four steps (Figure 2.4): (a). Fast nucleation; (b). Aggregation of nuclei into big particles; (c). Slow growth by further reduction of gold precursor; and (d). Rapid growth with completely consumption of precursor. The second step on the coalescence of nuclei was considered as the key procedure to control nanoparticle size distribution. However, the formation mechanism of nanoparticles is still under discussion till now.[121, 122]

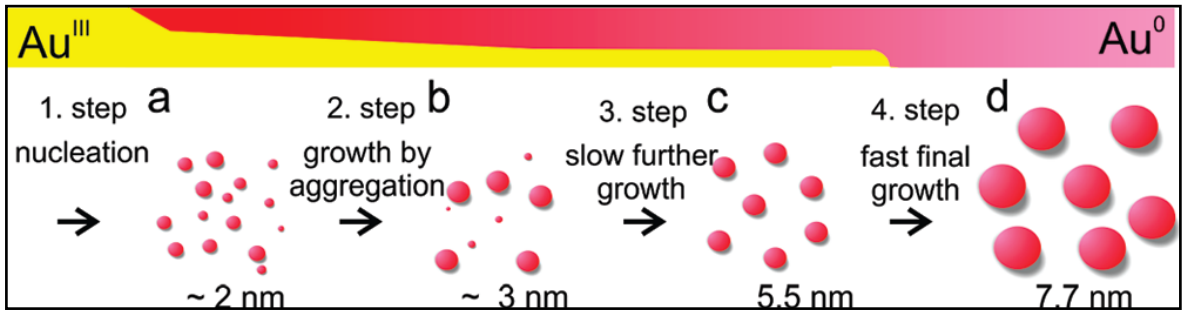

Figure 2.4 Schematic illustration for the deduced process of gold nanoparticle formation.[120]

2.3.3 Surface Plasmon Resonance of Gold Nanoparticles

Metal nanoparticles in the nanometer regime show different plasmon absorption characteristics due to their size-dependent and shape-dependent properties. When a nanoparticle is much smaller than the wavelength of incident light and the frequency of

incident photon is resonant with the coherent oscillation of the conduction band electrons, the absorption band is generated, which is called the surface plasmon resonance (SPR).[123] The plasmon oscillation of a nanoparticle is demonstrated in Figure 2.5. When the conduction electron charge cloud is displaced relative to the nuclei, the oscillation of the electron cloud relative to the nuclear framework occurs, which is caused by a restoring force arising from Coulomb attraction between electrons and nuclei. Four factors, electron density, effective electron mass, and the shape and size of the charge distribution, can determine the oscillation frequency.[124]

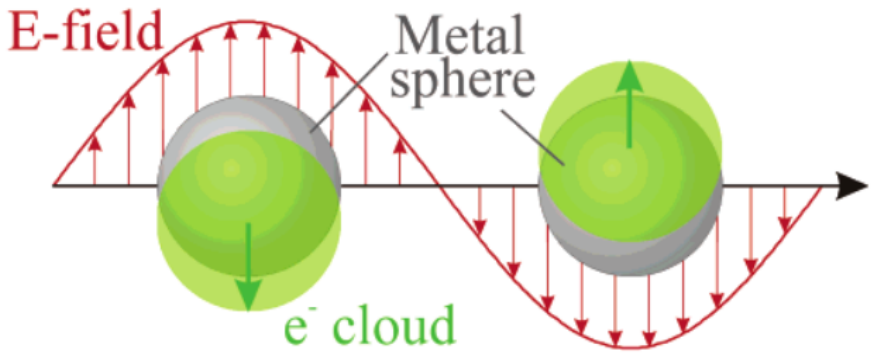

Figure 2.5 Schematic of plasmon oscillation for a sphere nanoparticles, showing the displacement of the conduction electron charge cloud relative to the nuclei.[124]

The frequency and intensity of the SPR are also related to the size, shape, composition and environment of AuNPs and can be calculated using Mie theory.[125-127] Therefore, the unique SPR properties of metal nanoparticles can be used to evaluate the particle size, concentration and aggregation property of colloidal solutions. The size effect of AuNPs on the SPR is demonstrated in Figure 2.6. The maximum surface plasmon resonance of gold colloidal solutions occurs within visible region and red-shifts with increasing particle size from 10 nm to 100 nm. It was reported that the synthesised AuNP colloidal solutions show the SPR peaks at 517, 521, 533, and 575 nm for the nanoparticles with the size of 9, 22, 48,

and 99 nm.[128] The SPR peak of 520 nm for 22 nm diameter AuNPs has also been reported and confirmed by the modelling data using Mie theory.[129] Because of the unique surface plasmon resonance, AuNPs can absorb different lights, and then show different colours depending on the sizes and shapes, which make AuNPs more attractive for further applications. The solution appears red when the maximum SPR is around 520 nm, and it turns to purple at higher maximum SPR.

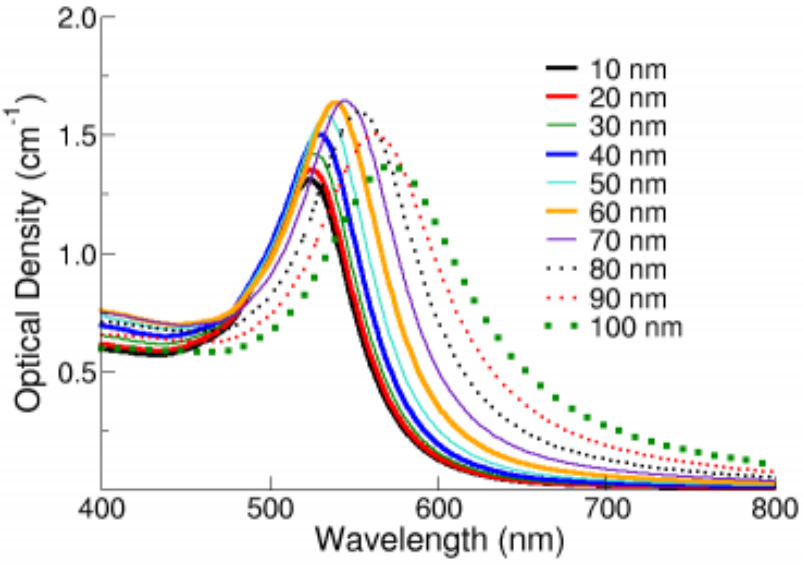

Figure 2.6 The surface plasmon resonance of gold colloidal solutions with different diameters ranging from 10 -100 nm.[130]

Furthermore, the SPRs and colours of gold colloidal solutions will also change when nanoparticles aggregate. The formation of a second absorption peak at longer wavelengths around 650-750 mm is evident, which is associated with the electric dipole-dipole interaction and the coupling between the plasmons of interparticles. When the interparticle distance is substantially greater than the average particle diameter, nanoparticle solution shows red or purple colour. However, the colour of the aggregates turns blue when the interparticle distance decreases to less than the approximately average diameter of particle.[131, 132] Figure 2.7 shows the effect of aggregation on the optical absorption spectra.

With the amount of AuNP aggregation increases, seen from Figure 2.7a-f, the second absorption peak becomes more noticeable and extends to longer wavelength. Meanwhile, the intensity of original SPR peak decreases.

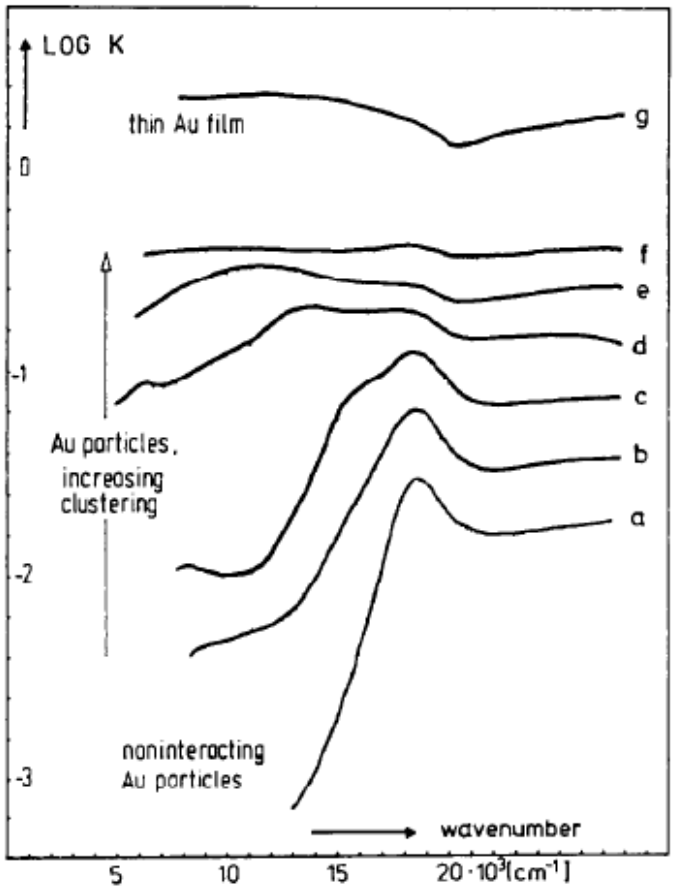

Figure 2.7 Sequence of optical absorption spectra of Au particles with the amount of aggregation increasing from a to f. For comparison, curve g shows the absorption $K = 4\pi k/\lambda$ of a thin plane Au film.[131]

2.3.4 Self-assembled Monolayers of Gold Nanoparticles/Structures

Self-assembled monolayers (SAMs) are formed by the adsorption of organic materials on metal surface. SAMs play an important role on the stabilisation of metal nanoparticles and nanostructures. The organic materials adsorbed on the metal surface can serve as an electrostatic or physical barrier against aggregation.[133] Additionally, it is an easy way to

tailor the interfacial properties of metals. Gold nanoparticle/nanostructure-based substrate is a most popular system for studying the SAMs. Love *et al.* listed five reasons for choosing gold as substrate for SAMs: (1) easy to obtain for both colloidal solution and thin film, (2) easy to pattern by lithographic tools and chemical etchants, (3) is an inert metal, (4) are commonly used for analytical techniques, (5) is biocompatible with cells.[133] The SAMs of organic molecules on the gold surface have been widely investigated.[134-137] The most intensively studied group of SAMs on gold surface is derived from the adsorption of thiols since strong Au-S bond can be formed.

A variety of thiol-based AuNPs was synthesised during the last a few years. Brust *et al.* first developed the long chain alkanethiolate-stabilised AuNPs, which are easily dispersible in organic solvent and very stable like simple chemical compounds.[106] They further reported the synthesis of AuNPs derivatised by a bifunctional stabilising thiol ligand p-mercaptophenol.[107] Following their step, a lot of work has been done to modify the properties of nanoparticles through adding the functional groups on the particle surface. Fleming *et al*. reported the formation of SAMs on AuNP-coated silica microspheres using 3-mercaptopropionic acid, 11-mercaptoundecanoic acid and 2-aminoethanethiol. The stability and exchange properties of SAMs were examined and their results showed that the self-assembled microspheres were stable during the biomolecular interaction analysis and carboxylate-terminated monolayers were more stable than amine-terminated monolayers.[138] Different synthesised mercapto anionic surfactants, including mercaptopropane-, mercaptohexane-, mercaptooctane-, and mercaptodecane- sodium sulfonate were investigated to self-assemble onto sodium borohydride-reduced AuNPs by Azzam *et al*.[139] The results indicated that these surfactants (C3-C10) could stabilise the

AuNPs and the stability increased with the decrease of alkyl chain length of these surfactants.

Since the delocalized π-electron in the benzene ring can promote electrical conductivity, there is an increasing interest in SAMs using aromatic thiols in recent years.[137] Sabatani *et al*. reported the formation of SAMs on gold electrodes with aromatic thiols, including thiophenol (TP), p-biphenyl mercaptan (BPM), and p-terphenyl mercaptan (TPM). They found that the formation of SAMs films using BPM and TPM were more stable than that of TP.[140] Barriet *et al*. compared the formation of SAMs derived from the adsorption of 4-mercaptophenylboronic acid (MPBA) with the SAMs of thiophenol (TP), 4-mercaptophenol (MP), and 4-mercaptobenzoic acid (MBA) on gold-coated wafer and concluded that the surface coverage of SAMs was in the following order: TP < MP < MPBA < MBA.[141] Benzylmercaptan (BM) and para-cyanobenzylmercaptan (pCBM) were also self-assembled on the gold substrates and the result indicated that the well-ordered monolayers of BM and pCBM can be vertically formed on substrate surface through the attachment of thiol group.[142] Furthermore, p-mercaptopyridine (p-MPy) was self-assembled on gold substrates and further immobilised with AuNPs to form gold nanoparticulate films, resulting in the strong enhanced Raman signals of p-MPy.[143] This system has been intensively studied for the development of SERS-active substrates.[144-146]

Disulfides (RS-SR´) can form the similar structure as thiols, but they are less soluble than thiols. Porter *et al.* prepared the SAMs from the adsorption of *n*-octadecyl disulfide onto the surfaces of AuNPs and AgNPs.[135] The results revealed that the disulfide-derived 3-D SAMs on the surface of AuNPs were well ordered, highly crystalline, and indistinct from those prepared from the adsorption of *n*-octadecanethiol. Shon *et al.* reported the synthesis of mixed monolayer-protected gold clusters using unsymmetrical disulfides and thiol. It

was found that thiols and disulfides had the similar growth dynamics for monolayer-protected gold clusters.[147] Sulphides (RSR´) are also used for SAMs due to their ability to self assemble into well-ordered monolayers. The molecule n-dioctadecyl sulfide was self-assembled on the Au(111) surface and the investigation using X-ray photoelectron spectroscopy indicated that the SAM was formed through the sulphur was bond on the surface of Au(111).[148]

Moreover, in practical, amino, carboxyl and phosphine groups were used together with thiol or sulphide groups for SAMs, such as aminothiophenol, mercaptobenzoic acid and amino acids.[149, 150] Thiol and sulphide group as head group can attach to the gold surface and form the S-Au band with gold, while the amino, carboxyl and phosphine groups as tail group can connect with other molecules to increase the biocompatibility of SAMs. 4-aminothiophenol (4-ATP) self-assembled AuNPs were used to detect thrombin based on SERS and the detection limit can reach 10^{-13} M.[86]

2.4 Applications of AuNPs and SERS on Immunoassays

2.4.1 Immunoassay and Multiplex Detection

Human immune system can generate various antigens on the surface of abnormal cells. The detection of those antigens can be utilised for disease diagnostics. The investigation of immunoassay focuses on the recognition of antibodies by antigens or antigens by antibodies due to the high specific interaction between antibodies and antigens.[151] Labels are normally used to identify antibodies or antigens. Enzyme,[152] fluorescence,[153] isotopes with or without radioactivity,[154] and chemi- and bioluminescence[155] have been used as labels during the immunoassay.

Enzyme-linked immunosorbent assay (ELISA) is one of the most popular immunoassay formats for the detection of antibody or antigen in a sample. This assay contains unknown antibody or antigen that was immobilised on a solid support substrate (such as 96-well microwell assay plate, or to the walls of plastic tubes, or onto filter membranes). An enzyme or fluorescent probe is needed to attach to the antibody as a reporter system for both direct and indirect measurements.[156] The ELISA technique is very specific and the antigen does not need to be purified. However, the disadvantages are tedious, time-consuming, and less-sensitive at low antigen concentrations. Moreover, multiplex detection is of great importance during disease diagnostics, requiring the detection of various analytes in one sample. Therefore, the development of a high-throughput, highly sensitive, and low-cost approach for early-stage human disease detection is still a challenging topic. More accurate and specific techniques need to be developed for multiplex detection.

Recent years, different immunoassay techniques based on nanoparticles, such as AgNPs, AuNPs, quantum dots (QDs), and magnetic nanoparticles, have been developed due to the development and advantages of nanotechnology.[157-159] Precious metal nanoparticles, AgNPs and AuNPs, have attracted much attention because of their SERS effect. The SERS-based immunoassay combines the properties of SERS and nanoparticle-antibody conjugations together during the detection. The immunoparticles are used to recognise the biomolecules and the SERS signals can be used to distinguish the molecules. It has several advantages compared with other readout methods. SERS technique depends on the chemical structure and properties of Raman-active molecules, so there are fluorescence label-free and no photobleaching. The high enhancement effective factor enables the detection of molecules at low concentration, which can significantly decrease the limits of detection. Moreover, there is no spectral overlap because of narrow vibrational bands of

Raman, which can be ideally suited for multiplex detection system. Numerous studies have demonstrated the potential applications of SERS on immunoassays.[7, 160, 161]

2.4.2 Development of SERS-based Immunoassays

Study on SERS-based immunoassay was first reported by Rohr *et al.* in 1989, who employed surface enhanced resonance Raman scattering (SERRS) to detect the human thyroid stimulating hormone (TSH).[162] Silver films coated with anti-TSH antibodies and resonance dye-labelled anti-TSH antibodies were used to capture the TSH antigens. Dou *et al.* demonstrated an enzyme immunoassay based on SERS.[163] The adsorption of reaction product on silver colloids showed strong SERS signals, which can be detected easily. The SERS intensity also had linear relationship with the antigen concentration. The detection limit was found about 1 order of magnitude lower than that of SERRS method reported by Rohr *et al.*[162] Moreover, Dou *et al.* presented a study by using NIR SERS to detect anti-mouse IgG on AuNPs without bound/free antigen separation.[164] The founding demonstrated that the direct detection of antibodies can be achieved using this method and the limit of detection was 10^{-8} M.

Lately, lots of works related to SERS-based immunoassay have been investigated by Porter *et al*.[7, 39, 165-168] They proposed a sandwich-type SERS-based immunoassay approach, which combined SERS and immunogold colloids together as a successful readout method. Gold film contained the capture antibody was used as a base substrate, and AuNPs contained capture antibodies and molecules were used as SERS probes. The antigens were specifically recognised after forming the sandwich structure by capture and labelling antibodies (Figure 2.8). Neither resonance enhancement nor enzymatic amplification was needed during the immunoassay. The detection limit for IgG was 10^{-9} M using this

approach.[7] Free prostate specific antigen can reach the LOD of ~1 pg/mL in human serum and ~4 pg/mL in bovine serum albumin.[39] They also demonstrated the detection of viral pathogen by SERS using this sandwich immunoassay structure. The limit of detection was 10^6 viruses/mL.[165] These studies laid the foundation for the further development of SERS-based immunoassay for disease detection.

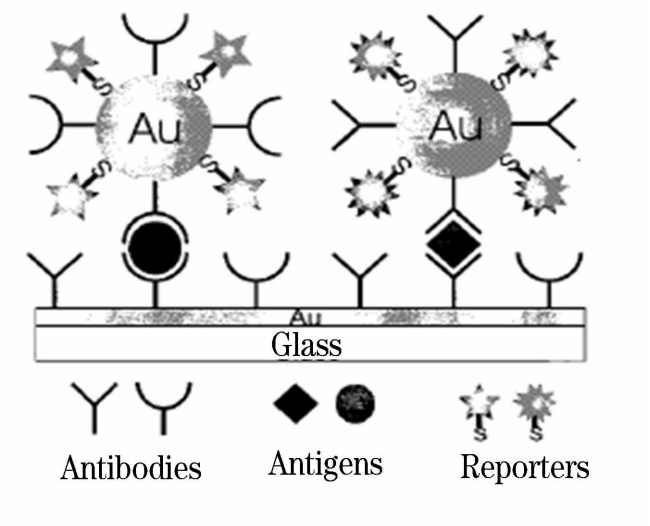

Figure 2.8 A sandwich-type SERS-based immunoassay approach.[7]

2.4.3 SERS Reporters for SERS-based Immunoassays

A typical SERS-based immunoassay mainly contains three parts, including capture substrate, SERS reporter, and capture antigens. The SERS reporters can easily provide valuable information about the presence and distribution of specific target molecules, which is vital important in biomedical applications and detection.[169, 170] SERS tags are composed of metal nanoparticles and Raman-active molecules, where the metal nanoparticles are used to enhance the Raman signals of molecules. The biomolecules such as proteins and antibodies are bond to the SERS tag for the formation of SERS reporter, which can be used to identify specific biomolecules for ultrasensitive detection (as shown

in Figure 2.9). SERS tags can be used to replace fluorescent tags during the practical biomedical applications.

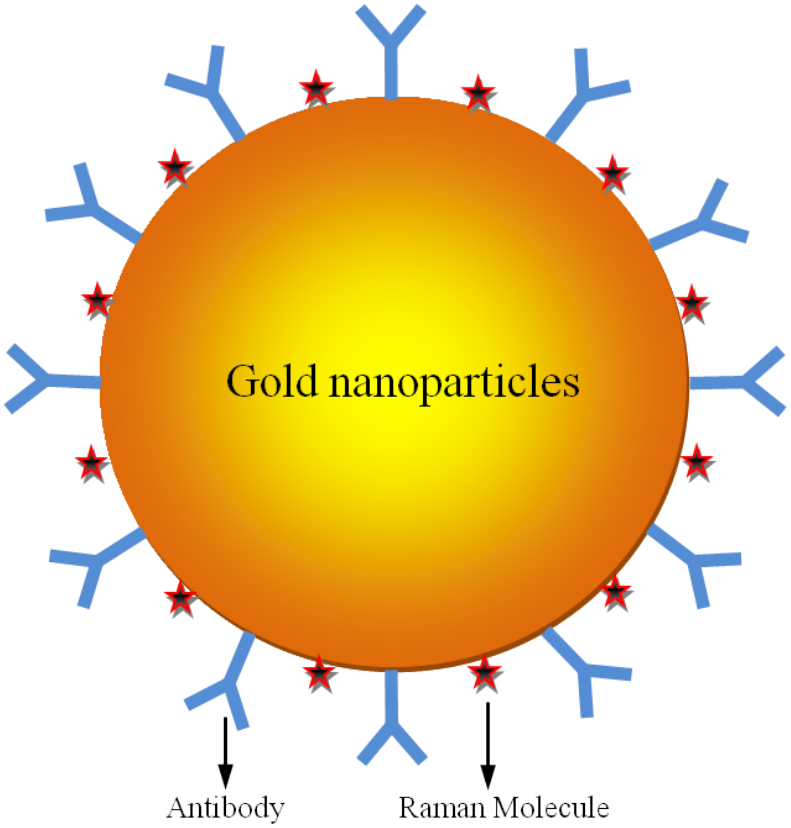

Figure 2.9 Scheme of typical SERS reporter showing the general features of a SERS reporter used for biomolecule detection.

Therefore, the development of SERS tags during the immunoassay is crucial for biodetection. Depending on the application purposes, various SERS tags were widely developed by different shapes, sizes, and compositions of nanoparticles as well as the Raman information of molecules for the improvement of immunological detection techniques. Li *et al*. developed a 30 nm AuNPs based SERS-active substrate for the rapid detection of protein–protein interactions.[171] This method involved in binding the biotin-modified antibodies with protein-stabilised AuNPs and then attaching the avidin-conjugated Raman-active dyes (fluorescein). There was a possibility to detect IgG as low as 1 ng/mL in solution using this standard avidin-biotin chemistry. Gold nanostar-based

SERS tags were reported for the imaging of the tumour suppressor p63 in prostate biopsies.[172] Wang *et al.* developed a new method to prepare SERS tags for the investigation of sandwich-structure immunoassay using SERS.[173] Two different thiolates were used in the system. One thiolate (succinimidyl propionate), which is a weak Raman scatter and used as biofunctional SERS reporter, can covalently bind the antibodies to the surface of particles, while the other thiolate as SERS reporter can generate strong Raman signals. The multiplex detection assay was performed and evaluated using different extrinsic Raman-active molecules, including 4-nitrobenzenethiol, 2-methoxybenzenethiol, 3-methoxybenzenethiol, 4-methoxybenzenethiol, and 2-naphthalenethiol. Qualitative and quantitative detection in a single assay could be achieved using this approach. The examples presented here show that different SERS tags functionalised with specific capture biomolecules have been developed and successfully applied during biomedical applications.

2.4.4 Capture Substrates for SERS-based Immunoassays

2.4.4.1 Solid Surface-based SERS Immunoassays

The detection of a sandwich immunocomplex based on a solid substrate is one of the most popular platforms for SERS-based immunoassay.[174] In the typical solid substrate-based SERS immunoassay, capture molecules, such as antibodies or proteins, are immobilised on the solid substrate, which could be glasses or quartz slides. And then the specific antigens are captured on the substrate, followed by binding with the metal nanoparticles, which are labelled with Raman-active molecules and secondary antibodies (Figure 2.10). The interaction is confirmed by examining the Raman signals of molecule.

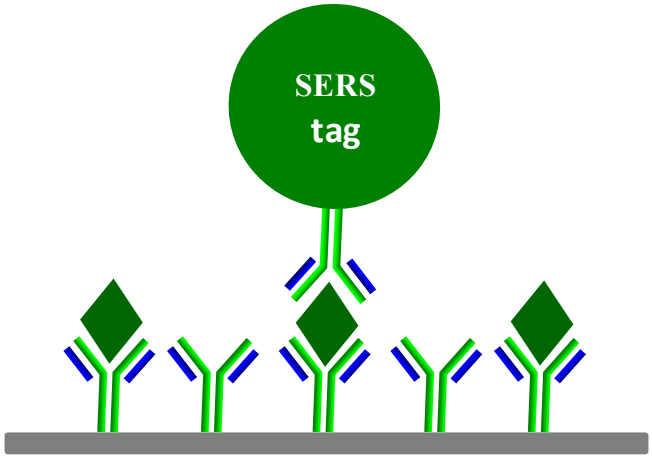

Figure 2.10 Scheme for solid substrate-based SERS immunoassay.

Porter *et al*. have carried out a few studies on sandwich-type solid surface-based SERS immunoassay, which were successfully used for detecting IgG, prostate specific antigen and viral pathogen.[7, 39, 165] Yao *et al*. immobilised the capture antibodies on the solid substrates and utilised the magnetic properties of Fe_2O_3/Au core/shell nanoparticles capped with antibodies to separate the antigens, and subsequently detected them using the SERS-based sandwich immunoassay.[95] Lee *et al*. reported an immunoassay system on a gold-patterned microarray chip based on SERS mapping using hollow gold nanospheres for the detection of the target cancer markers, including angiogenin and alpha-fetoprotein. The limits of detection for these two proteins were 0.1 pg/mL and 1.0 pg/mL, respectively, which were three or four orders of magnitude over that of traditional ELISA method.[175] Domenici *et al.* used the SERS-based biosensing system for the detection of the p53 tumour suppressor on glass substrates, which can reach the low concentration of 5×10^{-13} M.[176] Moreover, the solid-based immunoassay system was also developed for multianalyte immunoassay based on multiple Raman labels.[177] However, extended incubation time and repeated washing process limit the application of solid substrates on immunoassays.[11] It is also difficult to achieve multiplex detection using solid surface-based SERS immunoassay.

2.4.4.2 Living Cell-based SERS Immunoassays

Abnormal cells usually contain various antigens or biomarker on their surface, which provide excellent signal resources for cancer detection. After mixing the SERS reporters with living cell or injecting the SERS reporters into the living bodies, tumour cell can be targeted and detected by selectively binding with antigens (Figure 2.11).

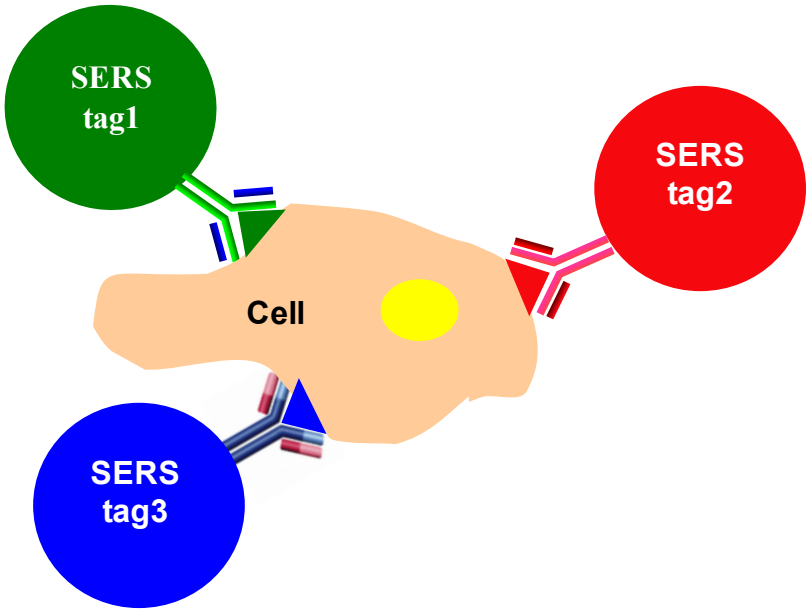

Figure 2.11 Scheme for cell-based SERS immunoassay.

For example, monoclonal anti-epidermal growth factor receptor (anti-EGFR) antibodies/gold nanorod conjugates were incubated with oral cancer cell lines for the investigation of potential cancer detection.[178] It was found that antibody conjugated gold nanorods were aligned on the cancer surface, where EGFR were overexpressed. The presence of cancer cell can be confirmed by strongly SERS signals. Qian *et al.* demonstrated the process for in vivo targeting and detection of tumour based on the utilisation of pegylated SiO_2@gold nanoshells and SERS.[9] Pegylated SERS nanoparticles were more than 200 times brighter than quantum dots on a particle-to-particle basis under

the same experimental conditions, indicating the large optical enhancements can be achieved for tumour detection in live animals using pegylated AuNPs as SERS tags. Keren *et al.* reported the whole-body noninvasive imaging of small living subjects using SERS active nanoparticles (Nanoplex Biotags (Oxonica)) and single-walled carbon nanotubes.[179] The whole-body deep-tissue imaging was achieved in this work. Circulating tumour cells in human peripheral blood have also been targeted using SERS nanoparticles with epidermal growth factor peptide.[42] Recently, a SERS and flow cytometry system was developed for the detection of leukemia and lymphoma cells using antibody-targeted and PEG-coated SERS gold nanoprobes.[180] Fluorescence dyes were used as Raman-active molecules for the nanoprobe preparation. Three proteins on the surface of malignant B cells from lymphoma cell line can be simultaneously detected using different nanoprobes. However, direct detection of abnormal cells by SERS immunoassay might be difficult for early-stage cancer detection since the biomarker concentration at that stage is quite low. The complex environment in the cell may also cover the Raman signals of analytes.[12]

2.4.4.3 Particle-based SERS Immunoassays

Similar to cell-based SERS immunoassay, particle-based SERS immunoassay is also a flow-based assay system. Latex particles, magnetic particles or AuNPs have been used to develop the particle-based SERS immunoassay. The detection platform is presented in Figure 2.12, where solid substrates and cells are replaced by particles during the immunoassay.

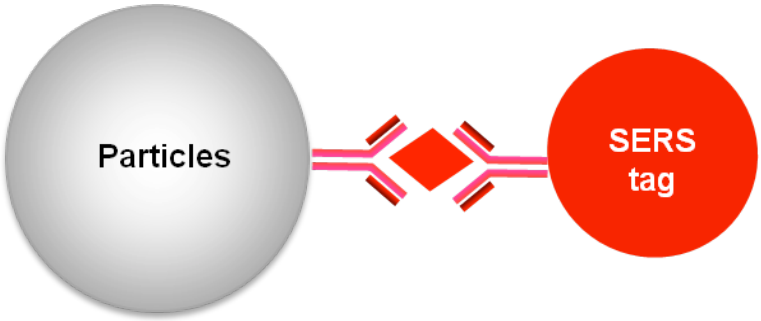

Figure 2.12 Scheme for particle-based SERS immunoassay.

Chon *et al.* developed a higher reproducible SERS-based immunoassay system using hollow gold nanospheres and magnetic beads for cancer marker.[174] Magnetic bar was used to separate the immunocomplex instead of repetition washing process. Compared with solid-based SERS immunoassay, the system overcomes the slow immunoreactions and obtains more reproducible results. This system has also been used for the simultaneous detection of two lung cancer markers.[181] Chen *et al*. developed a direct immunoassay for antigen detection based on magnetic separation and SERS in the absence of solid substrate. The LOD of this method was as low as 1–0.1 fg/mL.[182] Gold nanorods were also used as capture substrate for thrombin detection at subnanomolar concentrations.[13] The results revealed that the strong electromagnetic coupling resonance are presented at the nanorod–nanoparticle junction and could be used as highly sensitive SERS aptasensors for protein detection. In a recent study, magnetic gold nanoparticles were modified with antibodies and gold nanorods were modified with Raman labels and specific anti-gp51 for bovine leukemia virus antigen gp51 detection.[15] The LOD of antigen gp51 in the proposed immunoassay system was 0.95 μg/mL.

The advantage of this system is that the early-stage detection and multiplex detection could be achieved, since different particles can be easily obtained and different antigens are present in solution for detection. These advantages brought our great interests on particle-

based SERS immunoassay, especially polymer microbead-based SERS immunoassay. Because different microbeads can operate as both immuno-supports and individual spectral tags, showing various Raman vibrational information, which can significantly enhance the sensitivity of immunoassay system and improve the ability of SERS-based immunoassay for multiplex detection.

2.5 Polymer Microbead Synthesis and Applications

2.5.1 Fundamentals of Polymerisation

Polymers have been found wide applications in our daily life and industrial processes. Based on the water-solubility, polymers can be classified into hydrophilic polymers (water-soluble) and hydrophobic polymers (water-insoluble). Alternatively, they can be sorted to homopolymers and copolymers according to the chemical composition. Generally, polymer microbeads refer to the spherical microscopic particles in a size range of 1–1000 μm. The synthesis of polymer microbeads attracts lots of attention and considerable research progresses have been obtained in this area. A variety of nano or micro-scaled polymer microbeads with unique molecular structure, various molecular weights, and surface functional properties have been synthesised. The polymer microspheres normally can be prepared using various polymerisation techniques, including suspension, emulsion, precipitation, and dispersion polymerisation. Different polymerisation techniques can be adopted to obtain polymer microbeads with desired particle sizes.

2.5.1.1 Suspension Polymerisation

Suspension polymerisation is suitable for the production of micro-size particles with 50-500 μm in diameter. The regents for suspension polymerisation consist of monomer,

initiator, and suspension regent. Water is a commonly used solvent. 2,2'-azobis(2-methylpropanitrile) (AIBN) or benzoyl peroxide (BPO)) is normally used as initiator.[183] Monomer and initiator are insoluble in the polymerisation medium. Monomer droplets are suspended in the aqueous phase under vigorous mechanical agitation. The suspension regent is used to stabilise and prevent the coalescence of monomer droplets.[184] The mechanical stirring speed and the concentration of monomer and stabiliser can affect the average size of monomer droplets and the resulting particles.[183] Various polymer microbeads with unique Raman and Infrared vibrational fingerprint have been synthesised for styrene and its derivatives using suspension technique.[185] A major drawback of suspension polymerisation is that the synthesised microbeads are highly polydispersed.[186]

2.5.1.2 Emulsion Polymerisation

Emulsion polymerisation usually produces the microbeads in nanometer size. The emulsifying agent is used to disperse the monomer droplets in water and forms micelles, in which polymerisation occurs.[184] The polymerisation is initiated using a water-soluble initiator, such as potassium persulfate and ammonium persulfate. The particle size increases with the increase of monomer concentration and the decrease of emulsifier. It is difficult to produce the polymer microspheres with an uniform particle size larger than 500 nm in diameter using conventional emulsion polymerisation.[187] Emulsifier-free emulsion polymerisation can be used prepare the larger and uniform polymer particles.[183] Seeded emulsion polymerisation was also employed for monodisperse microbead synthesis.[188, 189] The small monodisperse particles are formed as seeds for further growth of larger polymer microbeads after monomer swelling. Furthermore, miniemulsion and microemulsion polymerisation were also employed to prepare the polymer microbeads.[190-193] Miniemulsion polymerisation involves the utilisation of cosurfactant to produce the

particles with the average size less than 500 nm. Cetyl alcohol, hexadecane, dodecyl methacrylate stearyl methacrylates or alkyl methacrylates can act as cosurfactant to stabilise the system during the miniemulsion polymerisation.[191]

2.5.1.3 Precipitation Polymerisation

Precipitation polymerisation is another type of heterogeneous polymerisation. It takes place in a medium where monomer and initiator are absolutely soluble in the solvent and the resulting polymers are insoluble and precipitate.[194] Precipitation polymerisation produces the polymer particles in the absence of a suspension agent or emulsifier. Thus, the polymer microbeads formed by precipitation polymerisation are usually polydispersed and the synthesised particles tend to aggregate together due to the lack of stabiliser. The polymers of vinyl chloride, acrylic acid, divinylbenzene, and glycidyl methacrylate-co-divinylbenzene were prepared by precipitation polymerisation.[195-198]

2.5.1.4 Dispersion Polymerisation

Dispersion polymerisation is a method that can form the micron-size monodisperse polymer microbeads in a size range of 1-15 μm. It is also considered as one type of precipitation polymerisation.[199] Because the monomer in dispersion polymerisation is also soluble in the reaction solution but the corresponding polymer is insoluble in solvent, which is the same as precipitation polymerisation. However, stabiliser is needed in the dispersion polymerisation and the particle size is highly monodispersed. Dispersion polymerisation typically consists of solvent (e.g. hydrocarbons, ethanol or ethanol/water mixture), monomer, initiator (e.g. AIBN), and stabiliser (e.g. poly(vinylpyrrolidone) (PVP)). Reaction parameters, such as monomer type, solvent, and the molecular weight of stabiliser, can affect the size and monodispersity of the resulting particles.[200] The

polymerisation of styrene and methyl methacrylate has been reported using this technique.[201-204] Monodisperse polystyrene particles with the size up to 12 μm were prepared using cellulosic derivatives as steric stabilisers in various solvents.[205] Moreover, the addition of crosslinking agents (e.g. divinylbenzene (DVB) and ethylene glycol dimethacrylate (EGDMA)) or costablizers (e.g. Triton X-305 and Triton N-20) in the reaction will result in the polystyrene particles with a very narrow size distribution.[202, 206]

2.5.2 Applications of Polymer Microbeads on Immunoassay

2.5.2.1 Pure Polymer Microbeads

Polymer microbeads have been widely applied as protein carriers in the development of immunoassay systems. As early as 1956, polystyrene latex particles with 0.81 μm have been used in the diagnosis of rheumatoid arthritis based on the aggregation of particles.[16] The interactions between antigen in the blood serum and gamma-globulin on the surface of polymer microspheres lead to the agglutination of latex particles which could be distinguished directly using eyes. The rapid detection of human rotaviruses has also been reported based on latex agglutination.[207] Various monodisperse functional polymeric microspheres with aldehyde, carboxyl, epoxy, or amino groups on the surface were discussed for immunoassay. Bioligands can be easily covalently bound to the surface of functional microspheres.[208]

Microbeads can also be used in flow cytometry based assays. Holmes *et al*. reported a bead-based immunoassay using glycidyl methacrylate microspheres as solid support based on the microfabricated flow cytometer.[209] Fluorescence-labelled proteins have been immobilised on the surface of polymer beads. The fluorescence signals were measured when the beads flowed through the chip. This device can quantitatively analyse the binding

of antibodies to surface-immobilised antigens and the result is comparable to the commercial flow cytometer. Polystyrene nanobeads with 80 nm in diameter were developed for sandwich immunoassay.[210] The efficacy of IgG binding on the surface of nanobeads was evaluated. The results showed that both fluorescent dye-labelled IgG and vascular endothelial growth factor A were detected using this system.

2.5.2.2 Fluorescence Microbeads

Fluorescence microbead-based immunoassay has been established for biodetection. Polymer microbeads encoded with fluorescence dyes were employed to provide optical identification during the detection.[211-214] The quantitative measurement of multiple human cytokines can be achieved via high-throughput analysis with flow cytometry. Fluorescence dyes (R6G) encoded polymer microbeads were also synthesised and applied on the detection of human alpha fetoprotein antigen in a suspension assay. The detection limit was 80 pg mL^{-1}.[215] QDs have also been used to encode microbeads because of their excellent optical properties. These small semiconducted nanoparticles have many advantages compared with fluorescent dyes. The QDs have a wide excitation and narrow emission, which are brighter and more photostable than fluorescence dyes, making them more attractive for optical encoding. In 2001, Nie's group reported a technology to prepare the multiplexed coding microbeads using QDs.[216] Since then, various QDs-barcoded polymer microbeads have been fabricated and applied on immunoassay.[217-220] QDs are either embedded inside the polymer microbeads or deposited on the surface of polymer microbeads. Furthermore, a method for the preparation of polymer microbeads with stable fluorescence signals and biocompatibility was developed by the encoding of both magnetic nanoparticles and QDs into polymer microbeads for a fast separation and multiplex detection.[221] However, there are a few crucial disadvantages, which hinder the application

of QDs on biosciences, including their unstable ability, toxicity, and difficulty and high costs to synthesise QDs.

2.5.2.3 Infrared/Raman and SERS Microbeads

Polymer microbeads contain many repeat units. Each repeat unit can operate as individual bioanalytical tag, displaying specific IR and Raman fingerprint information. Various spectroscopic encoded polymer microbeads can be easily synthesised and give rise to different IR/Raman spectra. Fenniri *et al.* have synthesised twenty-five polymer microbeads with unique Raman and infrared vibrational fingerprints which can be converted into a 'spectroscopic barcode' system for multiplexed detection.[185] The spectroscopic encoded polymer microbeads were applied for antigen detection.[18] The barcoded microbeads were used not only as the solid support for antibody−antigen recognition but also as the fingerprint vibration spectrum reporter. The antigen concentration as low as 150 ng/mL could be detected using this platform. Tetraplex assays were also performed for pathogen antigen identification using barcoded microbeads, with a detection limit of 1 ng/mL.[222] They also synthesised the robust SERS-active polymer microspheres using 4-mercaptomethylstyrene coated AgNPs as crosslinkers.[223] AgNPs together with 4-mercaptomethylstyrene were dispersed in the polymer matrix during the suspension polymerisation. This method could be using to fabricate a wide range of spectroscopic encoded polymer microbeads by replacing 4-mercaptomethylstyrene with other functionalised mercaptostyrene monomers for high-throughput analysis. SERS-labelled microbeads were also achieved by the encapsulation of dye-labelled silver nanoparticles with outer polymer shell for potential applications in biological assays.[224, 225] Metal nanoparticles were also deposited on the surface of polymer microbeads for SERS-active microbead development and immunoassay. For instance, Jun *et al.* embedded the

AgNP labels into sulfonated PS microbeads for SERS-encoded microbead development.[226] Different organic compounds, such as 4-methylbenzenethiol, 2-naphthalenethiol, and benzenethiol, were used as labels. It was also proven that multiplex detection could be achieved using different SERS-encoded microbeads.

There are a few advantages of IR/Raman and SERS microbead-based immunoassays, such as no photobleaching, narrow emission spectra, and vibrational information of molecules, which make spectroscopic barcoded microbeads more valuable than fluorescence microbead-based immunoassays. As discussed in section 2.4.4.3, there are many advantages using different particles as support substrates for SERS immunoassays. However, particle-based SERS immunoassays are still not well studied till now, especially using spectroscopic encoded microbeads. There are still large demands on the development of microbead-based SERS immunoassays for multiplex detection, which will not only improve the detection sensitivity significantly, but also benefit the multiplex detection. Since human diseases tend to become assorted and complicated nowadays, multiplex detection becomes more important for modern bioanalytical applications. In order to understand, diagnose and cure complex human diseases effectively, and to reduce the side effects and operation costs associated with clinical therapy, a robust technique capable to capturing large amount of information is demanded. By combining SERS-based immunoassay and microbead-based immunoassay together, it is expected a novel multiplex research direction for complex disease diagnostics will be developed.

CHAPTER 3 Methodology

This chapter describes the methods and the instruments used for the synthesis and characterisation of AuNPs and polymer microbeads. More detailed information is presented in each relevant chapter.

3.1 Synthesis of Gold Nanoparticles

All the glassware used for AuNP preparation were cleaned thoroughly using fresh 'aqua regia' (HCl/HNO_3:3:1), rinsed with deionised water (DI water, 18.2 MΩ·cm) thoroughly and dried in oven before use. The preparation of gold colloidal solution was carried out by the citrate reduction method.[109] An amount of 50 mL 10^{-3} M aqueous solution of gold (III) chloride trihydrate ($HAuCl_4 \cdot 3H_2O$) was added to a 250 mL flask and brought to boiling under vigorous stirring. 1% trisodium citrate (Na_3Ct) was quickly added to the boiling solution. After the colour of solution turned to purple or red, the heating was continued for another 15 min to ensure the complete reaction. The colloidal solution was cooled to room temperature and adjusted to 50 mL using DI water.

3.2 Synthesis of Polymer Microbeads

Suspension polymerisation was employed to synthesise the large polystyrene microbeads.[18] In a typical microbead preparation, all the reagents and solvent were charged to a three-neck flask, which was equipped with nitrogen inlet/outlet, condenser and mechanical stirrer (Figure 3.1). The mixture was bubbling by nitrogen for 30 min to remove oxygen and the flask was then put into preheated oil-bath to initiate polymerisation. The reaction condition was set at 340 rpm, 85 °C for 24 h. After the reaction, polymer microbeads were collected using the sieves between 130 and 600 μm, and washed with DI water for several times. The PS microbeads were further purified by Soxhlet extraction. Finally, the polymer microbeads were dried under vacuum.

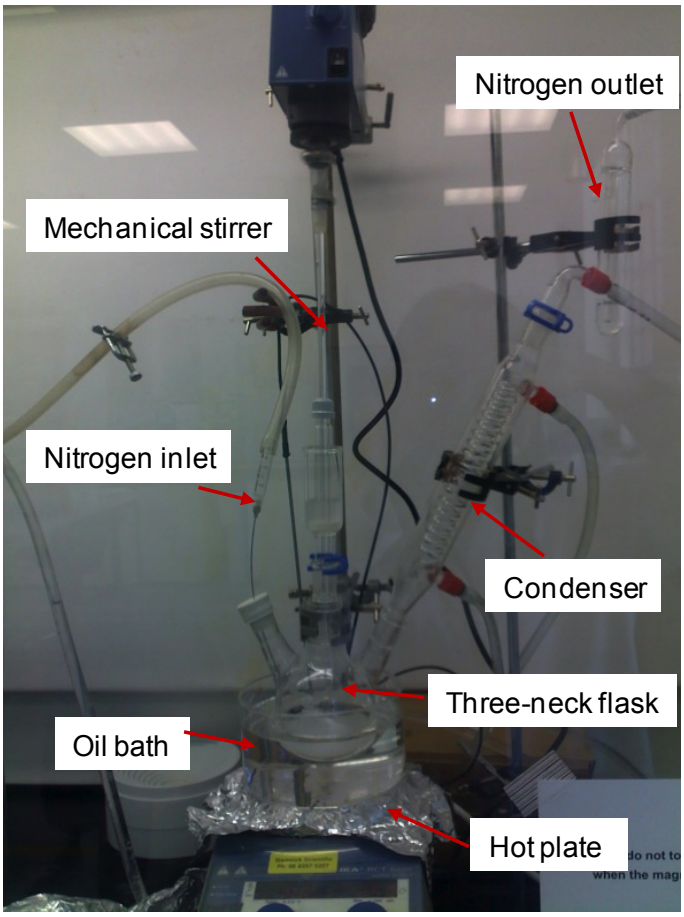

Figure 3.1 Experimental setup for the preparation of polymer microbeads.

Dispersion polymerisation was used to produce monodisperse polystyrene microbeads and copolymer microbeads.[206] The reaction system employed in the dispersion polymerisation was the same as the one for the suspension polymerisation (Figure 3.1). The reaction condition for dispersion polymerisations was set at 100 rpm, 70 °C for 24 h. After the synthesis, polymer microbeads were washed with ethanol and DI water several times to purify the microbeads. The conversion of each synthesis was calculated by gravity analysis.

3.3 Characterisation Techniques

3.3.1 Ultraviolet-Visible Analysis

Metal nanoparticles show unique surface plasmon resonance properties resulting in an absorption peak in visible or near infrared region, which can be easily recorded using Ultraviolet-Visible (UV-Vis) Spectrophotometer. It is the simplest and mostly commonly used technique for quickly observing the formation of metal nanoparticles and estimating the particle size, solution concentration, and aggregation condition of formed nanoparticles.[227] In this project, UV-Vis spectra of AuNP samples were acquired with a spectral range between 300-1100 nm and 1 nm resolution using a Lambda Scientific LIUV-201 UV-Vis spectrophotometer (Helios Gamma, England). Disposable acrylic cuvettes with 1 cm travel path were used for the measurements.

3.3.2 Transmission Electron Microscope

Transmission electron microscope (TEM) is an essential tool for the characterisation of materials to obtain the accurate morphology, particle size and size distribution of nanoparticles. The TEM micrographs were imaged using a CM200 TEM operating at 200 KV accelerating voltage at the Adelaide Microscopy, the University of Adelaide. The AuNP solution was first diluted with water. A drop of diluted solution was deposited onto the carbon-coated copper grid (200-mesh). Then it was allowed to dry at room temperature prior to characterisation.

3.3.3 Scanning Electron Microscope

Scanning electron micrographs were recorded using a Philip XL 30 Field Emission Scanning Electron Microscope (FESEM) at the Adelaide Microscopy, the University of

Adelaide. The microscope is equipped with a secondary electron detector, a backscattered electron detector, and an Energy dispersive X-ray Spectrometer (EDX). The accelerating voltage was adjusted to either 10 kV or 5 kV depending on the samples. The working distance was normally set to 10 mm. For the SEM sample preparation, silica wafers were used and adhere onto conducting adhesive. The appropriate amount of the solution was dropped onto the silica wafer and dried at room temperature. No specific coating was applied during the sample preparation.

3.3.4 Raman Spectrometer

Raman spectra were recorded using the Peak Seeker Pro™ spectrometers with a 785 nm wavelength excitation laser and maximum 300 mW laser intensity. Spectral resolution for the Raman spectrometer is about 6 cm^{-1}. For liquid sample measurement, 1 mL sample was injected to the small glass vial and put it to the sample holder. Raman spectra were measured straightforward. For solid sample analysis, dried samples were placed onto a glass slide and putted onto the metallurgical Raman microscope. The surface of the samples was focused on using the 50× long working distance objective len. A single accumulation in the spectral range 200-2000 cm^{-1} was collected for each sample. The integration time for all the measurements is 3 s.

3.3.5 Confocal Raman Microscope

XploRA confocal Raman microscope from HORIBA Scientific offers the full spectral analysis, measurements, and identification of samples. There are three compact lasers at three wavelengths at: 532 nm, 638 nm, and 785 nm. The confocal Raman microscope is powered by the LabSpec 6 software. The sample solution was dropped onto the glass slide and focused under microscope for Raman measurement.

3.3.6 Fluorescence Spectrometer

Shimadzu RF-530/PC Spectrofluorometer was employed to measure the fluorescence spectra of supernatants during the washing in the immunoassays. For the sample labelled with fluorescein (FITC), the measurement condition was 485 nm for excitation wavelength and 500-600 nm for emission wavelengths. The excitation and emission wavelengths for the sample labelled with Dylight 649 were 650 nm and 665-765 nm, respectively.

3.3.7 Fluorescence Microscope

In the project, fluorescence microscopes were used for the detection of fluorescent emission from the fluorescence labelled IgG during the immunoassay. Both inverted Nikon Eclipse TE300 microscope equipped with a Nikon DXM1200 digital camera and Leica SP5 spectral scanning confocal microscope used in this study are at the Adelaide Microscopy, University of Adelaide. The Leica SP5 confocal microscope has seven excitation wavelengths and the intensity of each excitation laser can be adjusted independently.

3.3.8 Flow Cytometry

FACSCalibur flow cytometry (BD Biosciences) was used to measure the fluorescence information during the immunoassay in Chapter 8. The flow cytometry (FC) has two lasers (argon-488 nm and diode-635 nm) and four colour capability. For flow cytometric measurement, a total number of 10 000 events in select region were recorded for each sample to collect the data for forward scatter channel (FSC), side scatter channel (SSC), and FL4 (DyLight^{TM}649). Each sample was measured three times to obtain the average fluorescence signals. The data were recorded and analysed with CellQuest software.

CHAPTER 4 Polymer Microbead-based Surface Enhanced Raman Scattering Immunoassays

Lijuan Wei,[†] Bo Jin,[*,†,‡] and Sheng Dai[*,‡]

†School of Earth and Environmental Sciences, The University of Adelaide, Adelaide, SA 5005, Australia

‡School of Chemical Engineering, The University of Adelaide, Adelaide, SA 5005, Australia

The Journal of Physical Chemistry C 2012, 116:17174-17081

STATEMENT OF AUTHORSHIP

Polymer Microbead-Based Surface Enhanced Raman Scattering Immunoassays
The Journal of Physical Chemistry C 2012, 116:17174-17081

Wei, L. (Candidate)
Performed experiment design; interpreted data; wrote manuscript; manuscript evaluation.

Signed *Date*

Jin, B.
Supervision of manuscript preparation; manuscript evaluation; acted as corresponding author.

I give consent for Wei, L. to present this paper for examination towards the Doctor of Philosophy.

Signed *Date*

Dai, S.
Supervision of manuscript preparation; manuscript evaluation; acted as corresponding author.

I give consent for Wei, L. to present this paper for examination towards the Doctor of Philosophy.

Signed *Date*

Wei, L., Jin, B. & Dai, S. (2012) Polymer microbead-based surface enhanced raman scattering immunoassays.
Journal of Physical Chemistry C, v. 116(32), pp. 17174-17181

CHAPTER 5 Fabrication of Monodisperse SERS-active Substrates by Deposition of AuNPs on Polystyrene Surface

5.1 Introduction

Resent years, the high sensitive surface enhanced Raman scattering (SERS) makes its broad application in biomolecule recognition. Researchers have given their effort on the multiplex detection using SERS technique, which will allow simultaneously detection of multiple analytes in one sample.[173, 250, 251] Good SERS-active substrates are of great importance for practical applications. Various SERS-active substrates have been developed, including rough electrodes, solid structures and nanoparticles.[20] Rough electrodes are the earliest SERS substrates, but the effect enhancement factors are relatively low. Solid substrate-based micro/nanostructures are mostly developed as SERS-active substrates, where precious metal nanoparticles are deposited on the glass or film surface.[97, 98] The solid substrate-based system is a two-dimension structure system for molecular detection. It is hard to be applied for multiplex detection due to their structure properties. On the other hand, three-dimension SERS-active substrates have also been developed for multiplex detection, where the SERS-active substrates are in suspension. Colloidal metal solutions, like AgNPs and AuNPs are directly used in the three-dimension system. However, precious metal nanoparticles tend to aggregate together in order to achieve high Raman signals, which make the metal nanoparticles unstable and irreproducible. The researches were attempted to deposit metal nanoparticles inside or on the surface of microspheres to form the stable composite microspheres, which can be employed as SERS substrates for molecular detection.[226, 252] Such kind of structures have many advantages, such as easy operating, be applied in flow-based detection, and highly-multiplexed.

There have been numerous studies on the fabrication of composite microspheres in recent years. Different kinds of composite microspheres have been developed, including silica-gold,[253, 254] polystyrene-silica,[255] polystyrene-gold,[256] gold-silica,[257, 258] silver-silica,[259] and

polystyrene-silver.[260] These core-shell composite particles may show special properties which are different from those of the core or the shell. The polystyrene/silica (PS/SiO_2) composite microspheres were formed by thermodynamically driving effect based on colloidal steric stabilisation theory.[255] Besides that, gold nanoparticle (AuNP)-coated PS composite particles were also synthesised based on the thermodynamically driving effect.[261] By changing amounts and types of reducing agent, the composite particles with different morphologies can be easily achieved. A dual mode composite nanoparticle, which is composed of a SERS core as silica-coated gold aggregates and a fluorescent shell as dye-doped silica shell has been developed and applied in multiplex immunoassay.[262] Both fluorescence and SERS signals of composite nanoparticles can be separately produced using different excitation wavelengths. Lately, Li *et al*. presented a study for the preparation of AgNP-coated PS composite microspheres using polyvinylpyrrolidone (PVP) as the reducing agent. They utilised the synthesised composite microspheres as SERS substrates for melamine and DNA detection.[263-265]

Combining the properties of composite microspheres and SERS, the research presented in this study focuses on the preparation of polystyrene/AuNP composite microspheres for the development of monodisperse SERS-active substrates. PS microbeads were synthesised via dispersion polymerisation in alcoholic solvent. Two different methods were applied to prepare polystyrene/AuNP composite microspheres. One method is the direct adsorption of pre-synthesised AuNPs on the polymer microbeads at a room temperature and the other is the in-situ reduction of $HAuCl_4$ using sodium citrate as reducing agent in the presence of polymer microbeads. Both methods can produce the composite microspheres in a simple process without employing seeding or chemical functionalisation of nanoparticles and microbeads. An aromatic thiol, 4-mercaptophenol (4MP) was chosen as model molecule

for investigating the SERS properties of different polystyrene/AuNP composite microspheres.

5.2 Experimental Section

5.2.1 Materials

Gold (III) chloride trihydrate ($HAuCl_4 \cdot 3H_2O$), 4-mercaptophenol (4MP), styrene, Triton X-305 (70% in H_2O), and polyvinylpyrrolidone (PVP 360 000) were purchased from Sigma-Aldrich. Trisodium citrate dehydrate (Na_3Ct) was obtained from ACE chemical company. Acrylic acid (AA) and 2, 2'-azobis (2-methylpropanitrile) (AIBN) were supplied by Acros organics. Absolute ethanol was supplied by Merck. Deionised water (DI water, 18.2 MΩ·cm) was from an EASY pure II ultrapure water purification system.

5.2.2 Synthesis of Polystyrene Microbeads

The monodisperse PS microbeads with or without carboxyl groups were synthesised using dispersion polymerisation according to the procedure with some modification.[206, 248] PS microbeads with no surface carboxyl functional groups (PS) were synthesised by one-stage reaction, while PS microbeads with carboxyl groups on the surface (PS-COOH) were synthesised by two-stage reaction.

For the PS microbead preparation, monomer (6.0 g styrene), initiator (0.24 g AIBN, 4 wt% to styrene), stabilisers (0.27 g PVP 360 000 and 0.30 g 70% Triton X-305) and 50 g 95% ethanol were charged to a 250 mL three-neck flask equipped with nitrogen inlet/outlet, condenser and mechanical stirrer. The mixture was deoxygenated by nitrogen bubbling for 40 min at room temperature. The flask was then merged into a pre-heated 70 °C oil bath and stirred mechanically at 100 rpm. The reaction was allowed for 24 h.

For the PS-COOH microbead preparation, monomer (6.0 g Styrene), initiator (0.24 g AIBN), stabilisers (0.27 g PVP 360 000 and 0.30 g 70% Triton X-305) and 34 g 95% ethanol were charged to a 250 mL three-neck flask in the first stage. The mixture was also deoxygenated by nitrogen bubbling for 40 min at room temperature. The flask was then merged into a pre-heated 70 °C oil bath and stirred mechanically at 100 rpm for one hour, followed by injecting the preheated AA solution (2 wt% AA to styrene was mixed with 16 g 95% ethanol and pre-heated to 70 °C) to the reaction system as the second stage. The reaction was further continued for 24 h.

After the polymerisation, the solid contents of microbead suspension were obtained by weighting a small amount of polymer microbead solution and letting it dry in oven. In order to purify the polymer microbeads, 1 mL pre-synthesised polymer microbead solution was washed three times with 95% ethanol and four times with DI water. Finally, the washed microbeads were redispersed in 1 mL DI water.

5.2.3 Preparation of PS/AuNP Composite Microspheres

5.2.3.1 Method A-Direct Adsorption

The gold colloidal solution was first prepared according to the following method.[109] 50 mL 10^{-3} M $HAuCl_4 \cdot 3H_2O$ were heated to boiling under stirring, followed by rapidly adding 1% sodium citrate solution with the mixing molar ratio of $HAuCl_4/Na_3Ct$ at 1:1.5. After continuously stirring at boiling temperature for 15 min, the colloidal solution was cooled down to room temperature. In the following step, 0.2 g PS (11%) or PS-COOH (12%) microbead suspension was added to the different concentrations of AuNP solution. The mixture was stirred for an hour at room temperature.

5.2.3.2 Method B-In-situ Growth

In the in-situ growth process, 50 mL 10^{-3} M $HAuCl_4 \cdot 3H_2O$ were heated to boil while stirring. 0.2 g PS or PS-COOH microbead solution and 2.206 mL 1 % sodium citrate were simultaneously added to the boiling solution. The resulting mixture was boiled for 15 min and cooled down to the room temperature. The total volume was adjusted to 50 mL using DI water.

All the resulting PS/AuNP composite microspheres prepared by the above two methods under different reaction conditions were centrifuged (3000 rpm, 1 min) and washed with DI water several times till the supernatant became colourless. Finally, the PS/AuNP composite microspheres were redispersed in 0.5 mL DI water.

5.2.4 Preparation of SERS-active PS/AuNP Composite Microspheres

An amount of 50 μL of various composite microspheres was mixed with 1.0 mL of different concentrations of 4MP in ethanol solution (10^{-3} M to 10^{-7} M) and stirred for 1 h at room temperature. The dispersion was then centrifuged and washed with ethanol three times to remove free 4MP. The SERS-active PS/AuNP composite microspheres were redispersed in 1.0 mL water for Raman measurement.

5.2.5 Instrumentation

The scanning electron microscope (SEM) images were taken using a Phillips XL30 SEM operating at an accelerating voltage of 5 kV. Ultraviolet-Visible (UV-Vis) absorption spectra of AuNPs and supernatants of composite microspheres were recorded using a Shimadzu UV-1601 UV-Vis spectrophotometer. The SERS spectra of 4MP enhanced by different composite microspheres were monitored using a Peak Seeker Pro™ Raman

spectrometer equipped with a 200 mW 785 nm laser. The integration time is 3 s. Zeta potential was measured using the Malvern Zeta Particle Analyser.

5.3 Results and Discussion

5.3.1 Morphologies of Polymer Microbeads and PS/AuNP Composite Microspheres

The monodisperse polystyrene microbeads were prepared by dispersion polymerisation technique using PVP as stabiliser. The solid contents for PS microbeads without carboxyl groups were 11% and the average size of PS microbeads was 1.37 μm in diameter. The deposition of AuNPs on the surface of PS microbeads was achieved by direct adsorption, which was done by means of straightly mixing the pre-synthesised polymer microbeads and AuNPs together at room temperature. Different concentrations of AuNPs and pure PS microbeads were mixed to examine the influence of AuNP and PS microbead concentrations on the preparation of composite microspheres, followed by SEM examination.

Figure 5.1 shows the SEM images of pure PS microbeads (Figure 5.1A) and the PS/AuNP composite microspheres obtained at different reaction conditions (Figure 5.1B-E). It is notable to see that AuNPs can be deposited onto the surface of PS microbeads for the formation of composite microspheres under all reaction conditions. By increasing AuNP concentrations from 10 mL (10^{-5} mol), to 20 mL (2×10^{-5} mol), and then to 50 mL (5×10^{-5} mol) at the fixed amount of PS (0.2 g 11% suspension), the number of AuNPs on PS microbead surface increases correspondingly (Figure 5.1B-D). On the other hand, more AuNPs can be deposited onto the surface of PS microbeads by reducing the PS concentration four times while keeping AuNP concentration at 50 mL (Figure 5.1E).

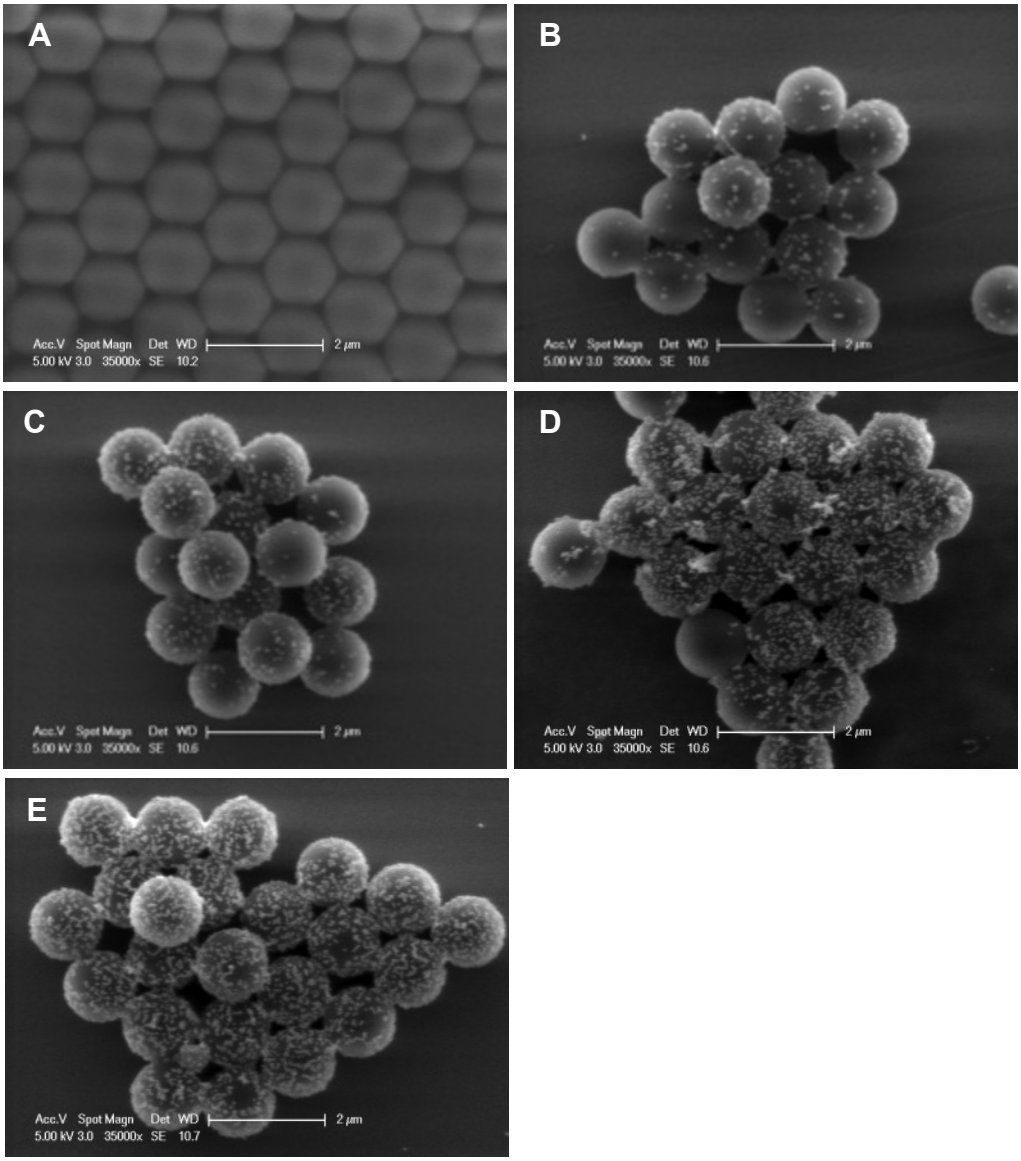

Figure 5.1 SEM images of PS (A) and PS/AuNP composite microspheres (B-E) prepared by the different amounts of AuNPs and PS solutions. (B). 0.2 g PS/10 mL AuNPs, (C). 0.2 g PS/20 mL AuNPs, (D). 0.2 g PS/50 mL AuNPs, and (E). 0.05 g PS/50 mL AuNPs.

Precious metal nanoparticles exhibit a strong absorption band in visible region, which is different from both atom and bulk materials. The physical origin of the light absorption of metal nanoparticles is the coherent oscillation of the conduction band electrons induced by interaction with an electromagnetic field.[266, 267] The resonance is known as the localized surface plasmon resonance (LSPR), which can be used to calculate the size, size

distribution and solution concentration of precious metal nanoparticles. Gold colloidal solution also presents the unique LSPR properties. In this study, AuNPs were adhered onto the surface of PS microbeads after mixing AuNPs with PS microbeads. Therefore, the first-time supernatant after direct adsorption should contain less AuNPs and the UV-Vis absorption intensity decreased correspondingly, which is an important evidence to check the average amount of AuNPs adsorbed on the surface of PS microbeads. The maximum surface plasmon resonance for AuNPs synthesised in this study was at 529 nm. Figure 5.2 shows that nearly no absorption intensity can be observed in the first-time supernatants for 0.2 g PS solution reacting with 10 mL or 20 mL AuNP solution, which indicates that almost all AuNPs have been deposited to the surface of PS microbeads. By increasing the AuNP concentration to 50 mL, a very low intensity of surface plasmon resonance can be seen. Furthermore, decreasing the PS concentration to 0.05 g means the increase of AuNP concentration four times to 200 mL. More free AuNPs were found in the supernatant after centrifugation.

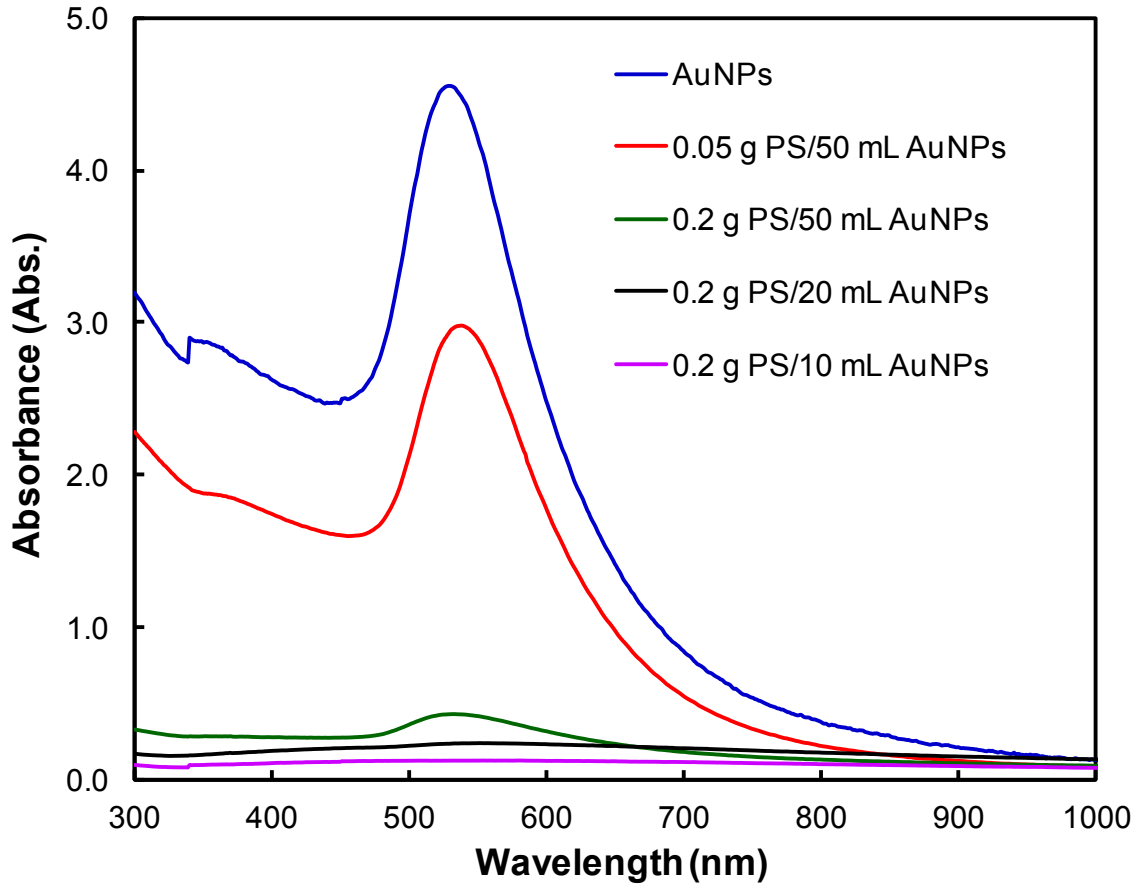

Figure 5.2 UV-Vis spectra of AuNP solution and various first-time supernatants of each adsorption between the different amounts of AuNPs and PS solutions after the centrifugation.

Figure 5.3 presents the relationship between the volume of AuNP solution mixed with the PS microbead suspension and the total numbers of AuNPs adsorbed on the PS microbead surface. All the AuNPs were considered as the same size with the average diameter of 50 nm and the calculated AuNP stock concentration was 1.56×10^{11} particles/mL in water. The total number of AuNPs adsorbed on the microbead surface was calculated by the difference in the UV-Vis absorption intensities of AuNP stock solution and the first-time supernatants after direct adsorption. It is worth noting that the volume of AuNP solution added in Sample D (0.05 g PS/50 mL AuNPs) was calculated by the same concentration of

PS microbeads (0.2 g) as the others, which means that 200 mL AuNP solution was added during the process. The experimental result indicates that the number of AuNPs adsorbed on the microbead surface sharply increases when the volume of AuNP solution was less than 50 mL and increased slowly when further increasing the AuNP volume to 200 mL. Furthermore, the average number of AuNPs on each microbead will follow the same trend as that plotted in the Figure 5.3, since the concentrations of PS microbeads were the same at all the conditions.

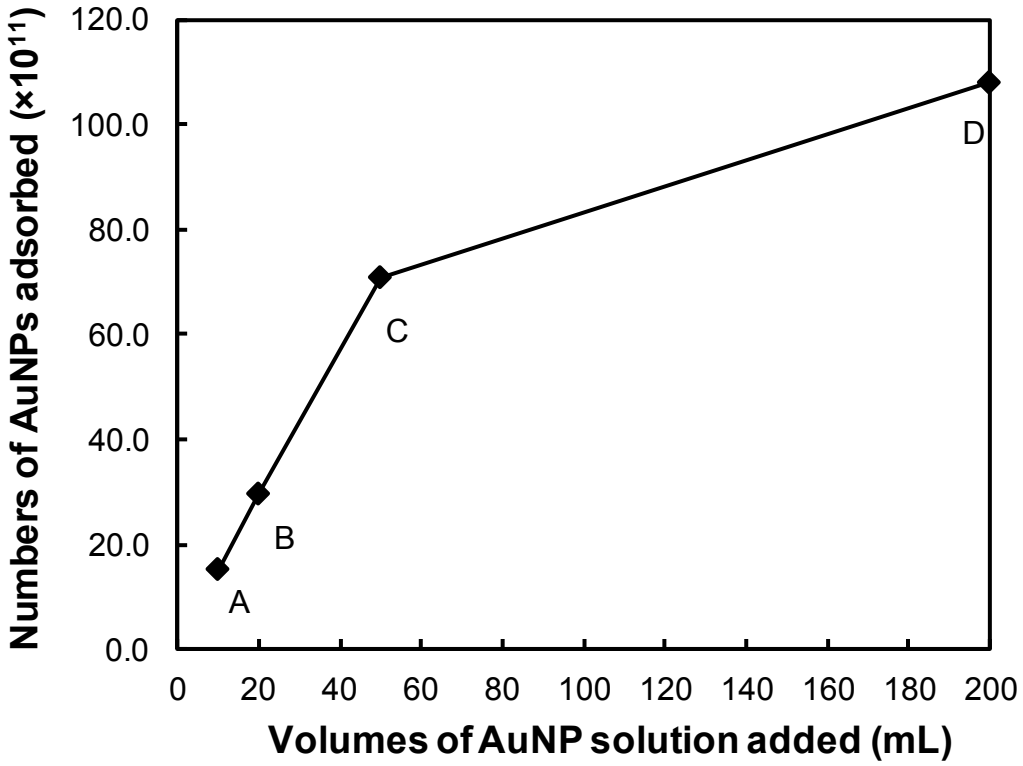

Figure 5.3 The relationship between the volume of AuNP solution mixed with the PS microbead suspension and the total numbers of AuNPs adsorbed on the PS microbead surface. A. 0.2 g PS/10 mL AuNPs, B. 0.2 g PS/20 mL AuNPs, C. 0.2 g PS/50 mL AuNPs, and D. 0.05 g PS/50 mL AuNPs.

During the fabrication of composite microspheres, surface modification were needed in the process.[268] However, the formation of PS/AuNP composite microspheres presented in this study was achieved by the direct adsorption of AuNPs on the microbead surface at room temperature. There was no surface modification applied during the synthesis. A similar report was also presented by Li *et al.* for the fabrication of AuNP-coated PS composite particles by a thermodynamically driving effect.[261] They demonstrated that the PVP-stabilised PS microspheres tended to be metastable after several time washing steps. These metastable PS microbeads intended to be stabilised by AuNPs to form the composite microspheres. We believed that the adsorption principle here is in an essential agreement with that of reported by Li *et al.*, even the reaction is conducted at a room temperature.

Zeta potential analysis can be used to confirm this hypothesis. It is well known that particles with zeta potentials between -15 and 15 mV are normally unstable. The zeta potential measurement indicates that washed PS microbeads had a slight negative charge in water, i.e. -4.5 mV, suggesting that the PS microbeads are metastable. The zeta potential of AuNP solution was -35.5 mV. By mixing the PS microbeads with the AuNPs, the zeta potential of composite microspheres for the 0.2 g PS microbeads with 50 mL AuNP was -26.4 mV, which was much more stable. This suggests that the AuNPs can act as a stabiliser to protect the PS microbeads, resulting in the formation of PS/AuNP composite microspheres at room temperature.

The stability of PS/AuNP composite microspheres was also examined using UV-Vis spectrophotometer. There was no UV-Vis absorption monitored in the supernatant of PS/AuNP composite microsphere solution after their preparation for one year, indicating the strong adsorption ability between AuNPs and PS microbeads. The synthesised

composite microspheres are stable at room temperature without any AuNP leakage from the surface of PS microbeads.

5.3.2 SERS Properties of PS/AuNP Composite Microspheres

4MP was chosen as the model Raman-active molecules and self-assembled with various synthesised composite microspheres. SERS spectra of 4MP on different PS/AuNP composite microsphere substrates and on AuNPs are illustrated in Figure 5.4. The SERS signatures of 4MP on different composite microspheres are identical to that on AuNPs, with featured peaks at 1076 cm^{-1} and 1594 cm^{-1}. The intense Raman signals at approximately 1076 cm^{-1} and 1594 cm^{-1} arise from the ring breathing band (υ_1) and the ring vibrational band (8a) of 4MP, respectively.[269] Since the band at 1076 cm^{-1} was the strongest Raman peak, it was chosen as a reference peak for the spectrum intensity comparison. Figure 5.4 indicates that the Raman intensity at 1076 cm^{-1} increases with an increase in AuNP concentration from 10 mL to 50 mL. Highest Raman intensity was obtained by reducing the PS concentration four times, where more AuNPs were adsorbed on the surface of PS microbeads.

The Raman spectrum of pure PS microbeads is also shown in Figure 5.4, which contains two main vibrational peaks at 999 cm^{-1} and 1029 cm^{-1}. They are assigned to υ_1 symmetrical ring and the υ_{18A} vibrations of PS, respectively.[249] By comparison the SERS spectra of 4MP on the composite microspheres with the Raman spectrum of pure PS microbeads, there is no obvious peak associated with the Raman spectrum information of PS microbeads, which indicates the highly enhancement of composite microspheres after self-assembled with 4MP. The Raman spectrum of first-time supernatant in each reaction was also examined and is presented in Figure 5.4. Only the Raman spectrum of ethanol can be

measured, which confirms that there is no AuNP released from the surface of PS microbeads during the addition of 4MP. The polystyrene/AuNP composite microspheres demonstrated a high stability and can be used for the development of SERS-active microbeads.

The plot in Figure 5.5 shows the relationship between the Raman signals of composite microspheres at 1076 cm^{-1} and the numbers of AuNPs adsorbed on the polymer microbeads. More AuNPs deposited onto the surface of PS microbeads, higher SERS signals of 4MP were achieved correspondingly. However, we can see from Figure 5.2 that there were lots of free AuNPs left in the first-time supernatant at the reaction condition of 0.05 g PS solution with 50 mL AuNPs. The reaction condition at 50 mL AuNP concentration and 0.2 g PS solution was chosen in the following study, since nearly no free AuNPs present in the supernatant at this reaction condition, which means almost all the AuNPs are adsorbed on the PS microbeads surface.

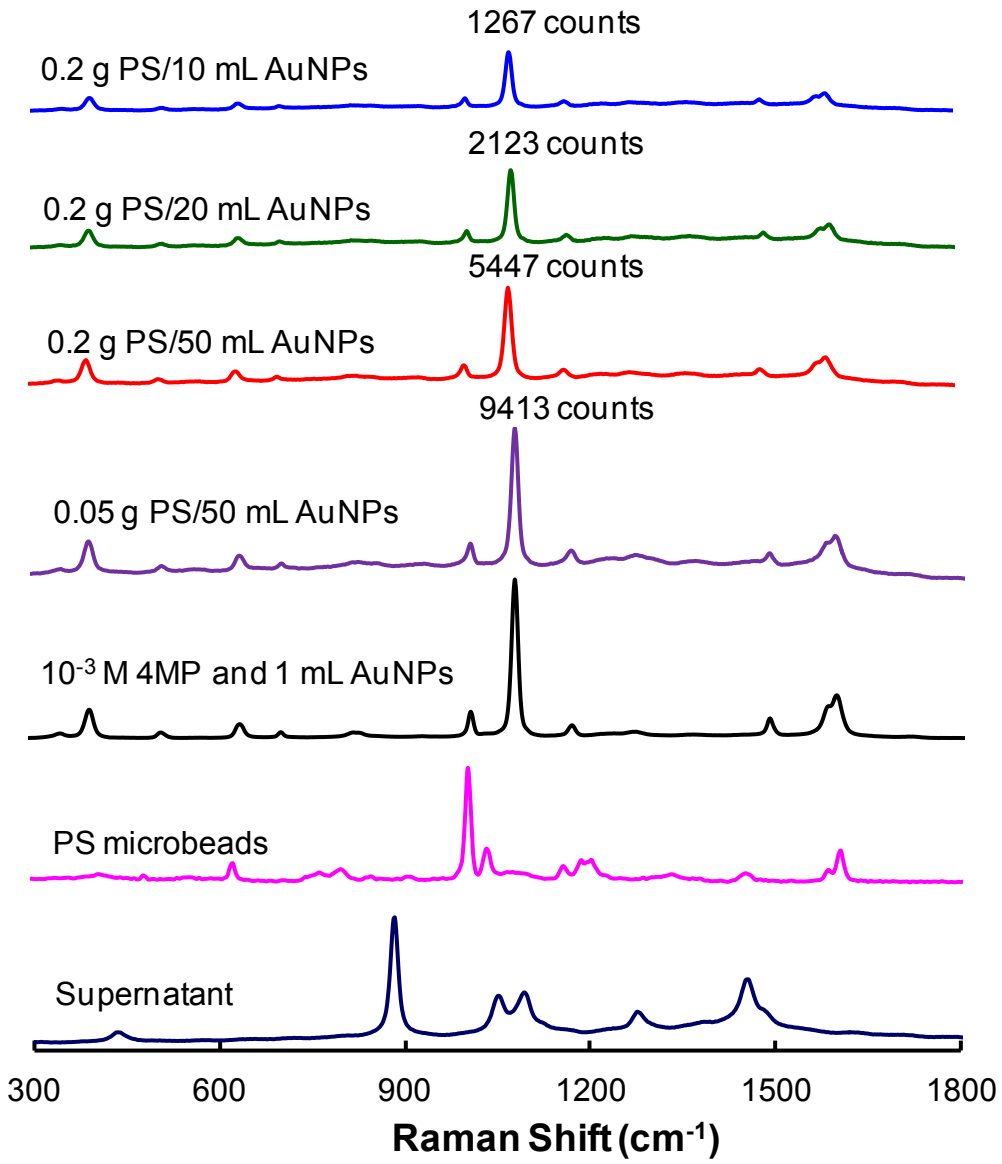

Figure 5.4 SERS spectra of different kinds of composite microspheres prepared by direct adsorption after reacting with the same concentration of 4MP (1 mL 10^{-3} M in ethanol solution) (top 4) and 1 mL AuNPs reacted with 10^{-3} M 4MP in ethanol solution, and the Raman spectra of pure PS microbeads and the first-time supernatant after the reaction between composite microspheres and 4MP.

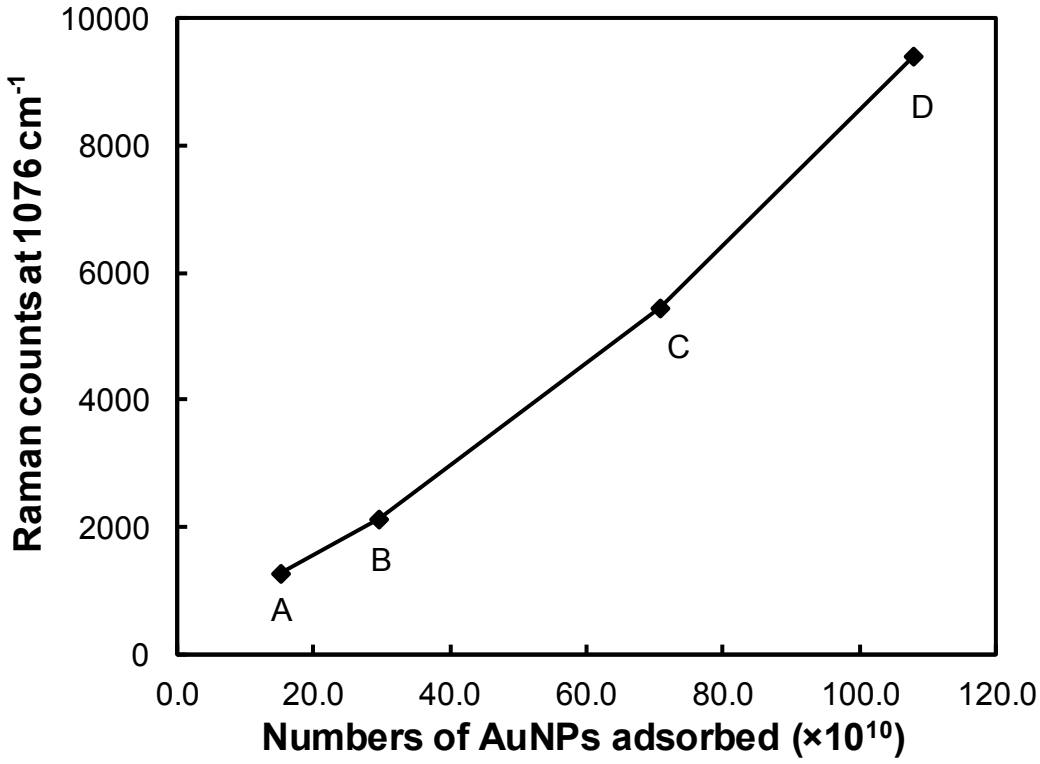

Figure 5.5 The relationship between the Raman intensity at 1076 cm^{-1} and the total number of AuNPs adsorbed on PS microbead surface. A. 0.2 g PS/10 mL AuNPs, B. 0.2 g PS/20 mL AuNPs, C. 0.2 g PS/50 mL AuNPs, and D.0.05 g PS/50 mL AuNPs.

5.3.3 Detection Limit of PS/AuNP Composite Microspheres

PS/AuNP composite microspheres prepared by 0.2 g PS and 50 mL AuNPs using direct adsorption approach were used for studying on the detection limit of 4MP. The SERS spectra of 4MP on PS/AuNP composite microspheres at various concentrations are presented in Figure 5.6a-f. A clear SERS spectrum of 4MP appeared with featured peaks at 1076 cm^{-1} and 1594 cm^{-1} at the 4MP concentration down to 10^{-5} M (Figure 5.6a-c). At 10^{-6} M 4MP concentration (Figure 5.6d), a low intensity at 1076 cm^{-1} can be seen, but an extra peak at 995 cm^{-1} is dominated. Further decreasing the 4MP concentration to 10^{-7} M (Figure 5.6e), the SERS signals of 4MP at 1076 cm^{-1} could not be detected and the Raman

spectrum is the same as the one without 4MP (0 M in Figure 5.6f). This indicates the background signals of PS/AuNP composite microspheres occur at low 4MP concentrations (Figure 5.6d-f), which might be from the contribution of polystyrene after the adsorption of AuNPs to their surface. Furthermore, PS microbeads were also reacted with 10^{-3} M 4MP. Figure 5.6g shows that no Raman signals of 4MP can be measured due to the lack of AuNPs to enhance the Raman signals, compared with the strong signals generated using PS/AuNP composite microspheres as SERS-active substrates. The results demonstrate that the prepared PS/AuNP composite microspheres are good SERS-active substrates and the detection limit is down to 10^{-5} M, by using 4MP as model Raman-active molecule.

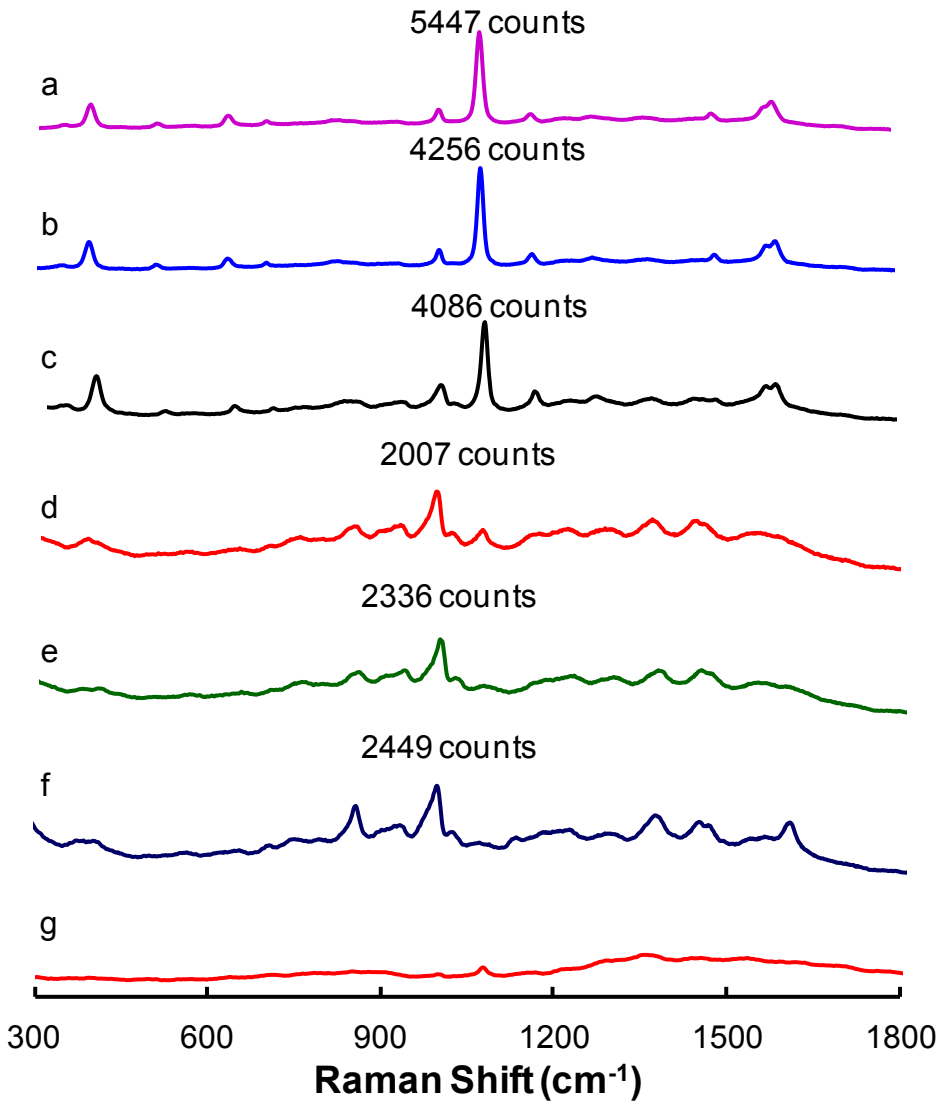

Figure 5.6 The Raman spectra of PS/AuNP composite particles prepared by direct adsorption after reacting with different concentrations of 4MP in ethanol solution, a. 10^{-3} M, b. 10^{-4} M, c. 10^{-5} M, d. 10^{-6} M, e. 10^{-7} M, f. 0 M, and PS microbeads reacting with 10^{-3} M 4MP (g).

5.3.4 Effect of Deposition Methods and Different Microbeads

Method B (in-situ growth) was also employed to prepare composite microspheres to compare the effect of deposition method on the formation of composite microspheres. The results indicated that PS/AuNP composite microspheres also can be fabricated by this

method. All the reaction conditions were set at 0.2 g PS microbeads and 50 mL AuNPs (5×10^{-5} mol). The similar deposition ability for both methods can be verified by SEM images (Figure 5.7) and UV-Vis spectrum data (Figure 5.8). SEM images show the high coverage of AuNPs on all PS microbeads can be seen using Method A (Figure 5.7a and c) and Method B (Figure 5.7b and d). As seen from Figure 5.8, the first-time supernatants by method A have slight higher UV-Vis absorption than those by Method B. But generally speaking, all the first-time supernatants after the reactions only contain fewer amounts of AuNPs compared with the UV-Vis adsorption of AuNP stock solution, indicating almost the full adsorption of 50 mL (5×10^{-5} mol) gold colloidal solution on the polystyrene microbead surface using both methods.

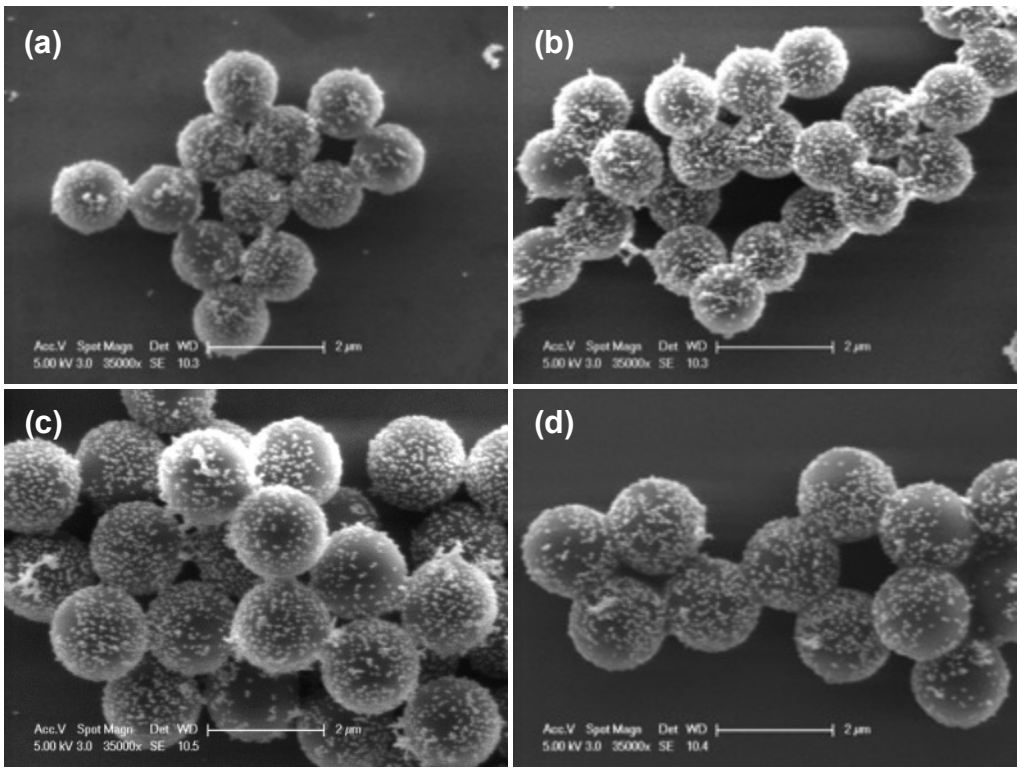

Figure 5.7 SEM images of polystyrene/AuNP composite microspheres prepared by different methods and different microbeads at 0.2 g PS/50 mL AuNPs. (a). PS-Method A, (b). PS-Method B, (c). PS-COOH-Method A, and (d). PS-COOH-Method B.

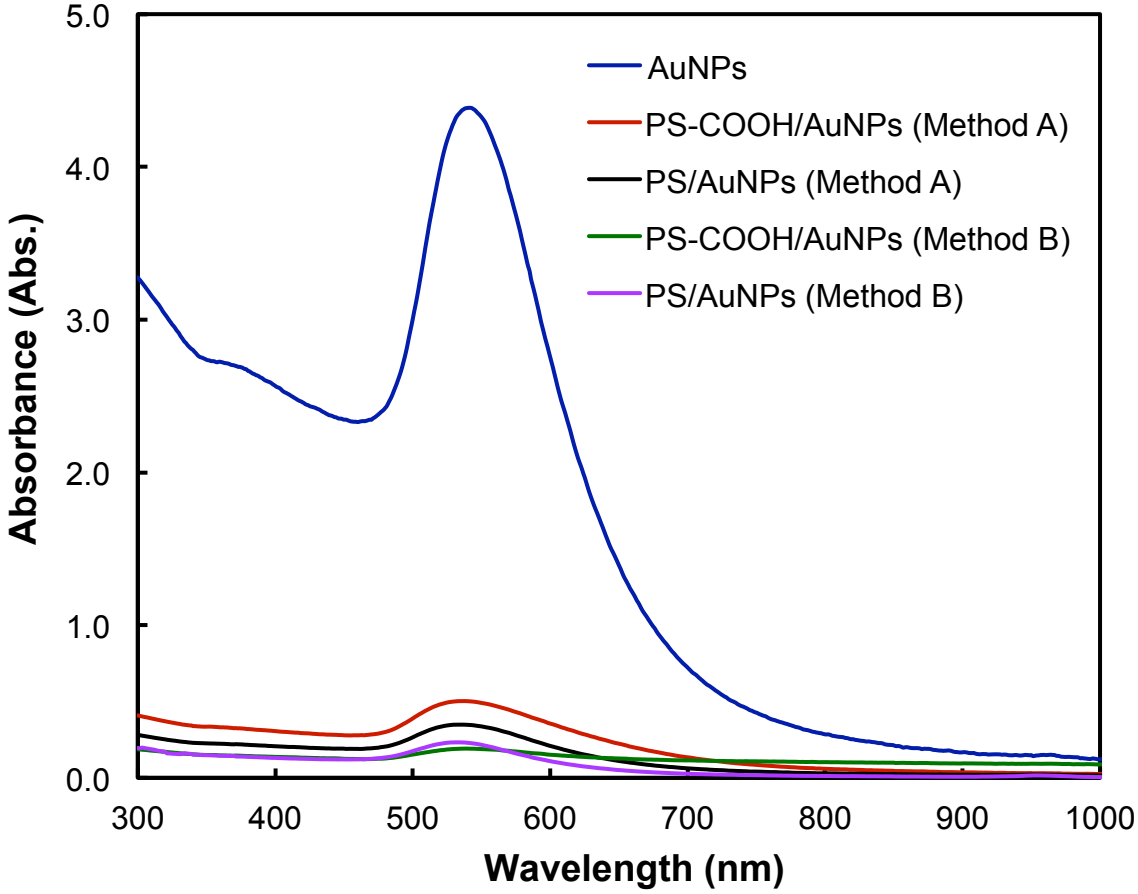

Figure 5.8 UV-Vis spectra of AuNP solution and the first-time supernatants after the formation of different kinds of polystyrene/AuNP composite microspheres by different methods and different microbeads.

The only difference for the formation of composite microspheres using both methods is the adsorption speed. In the in-situ growth of composite microspheres (Method B), AuNPs can be simultaneously deposited on the surface of microbeads after their formation. This reaction only needed about 15 min to complete, which is the same time as that for the preparation of AuNPs. The reaction speed for Method A was slower, compared with Method B. For the reaction at 10 mL and 20 mL AuNP concentration, the dark purple-colour composite microspheres can be observed and the mixture became colourless around 20 minutes. While many coloured composite microspheres using 50 mL AuNP

concentration and 0.2 g PS solution can be seen on the wall of glassware in about 20 minutes. The mixture solution was still purple colour, showing there were still lots of free AuNPs in the mixture solution at that time. By continuously stirring one hour, the mixture became colourless and AuNPs were deposited onto the polymer surface. Temperature might be an important factor in adsorption process for direct adsorption and in-situ growth. The movement of the particles at a boiling temperature is faster than that at a room temperature. There is more collision between particles, resulting in a short adsorption time required. There may be other possible mechanism due to the small nuclei formed during the early-satge of AuNP formation, which can move fast. After these nuclei deposited on the surface of polymer microbeads, more reduction and aggregation take place on the surface of polymer microbeads to form the polystyrene/AuNP composite microspheres using the in-situ growth method.

In order to evaluate the influence of temperature on the formation of composite microspheres, PS/AuNP composite microspheres were also fabricated by mixing the AuNP solution and PS microbead solution at boiling temperature. 50 mL pre-synthesised AuNP solution was brought to boiling, followed by rapidly adding 0.2 g PS solution and stirring for 15 min at boiling temperature. The UV-Vis spectra of AuNP solution before adsorption and the first-time supernatant of composite microsphere solution after the adsorption are presented in the Figure 5.9. The SPR intensity of first-time supernatant is quite low, indicating that there were nearly no AuNPs present in the supernatant and the almost fully adsorption of AuNPs on the PS microbead surface occurred. The result is similar as Method A and B, and confirms the importance of temperature on the formation of composite microspheres. Fabricating the composite microspheres using Method A at

boiling temperature will shorten the deposition time and obtain the same result as that of Method B.

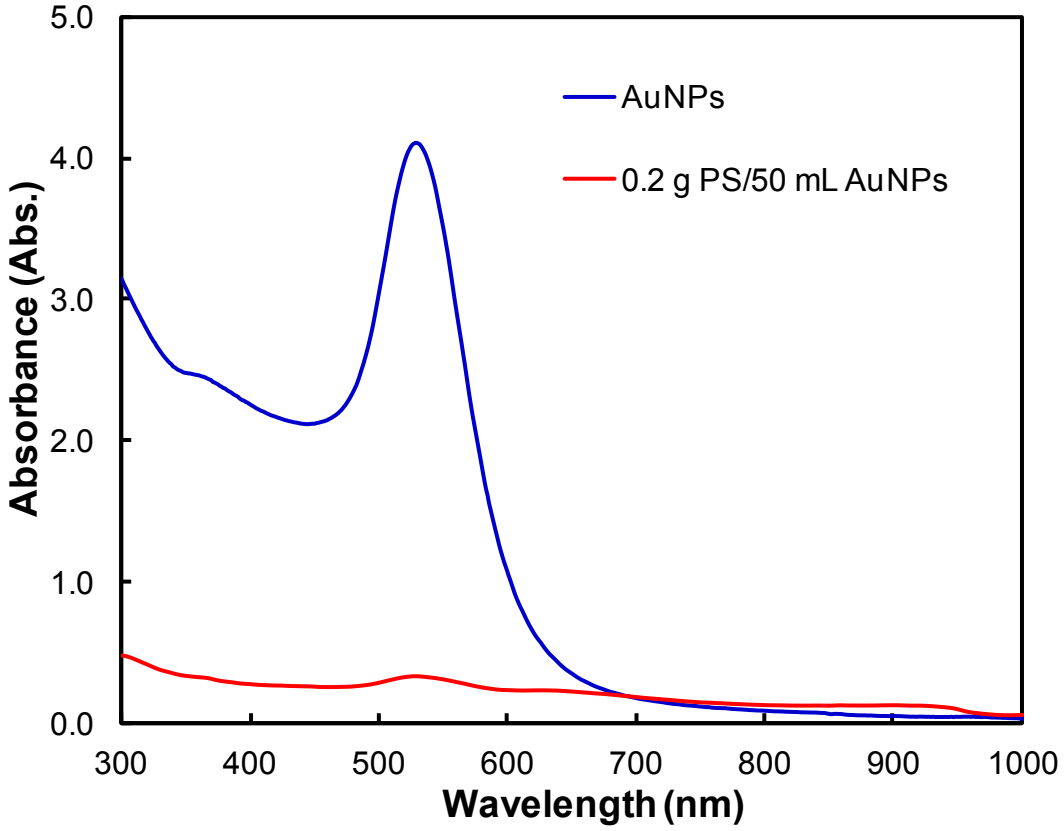

Figure 5.9 UV-Vis spectra of AuNP solution and the first-time supernatant after the adsorption of 50 mL AuNPs on 0.2 g PS microbeads using Method A at boiling temperature for 15 min.

The influence of carboxyl groups on the PS/AuNP composite formation was investigated. The carboxyl group-functionalised PS microbeads (PS-COOH) were produced using AA (2 wt% related to styrene) as functional monomer. The solid contents for the PS-COOH microbeads were 12 % and the size of PS-COOH microbeads was 1.60 μm in diameter. It was calculated there was about 85.3% of the feed –COOH groups of AA on the surface of the polymer microbeads using potentiometric and conductometric titration method. The reaction condition was setting up using 50 mL AuNP and 0.2 g PS solution. It can be seen

from the SEM images (Figure 5.7) and UV-Vis spectrum data (Figure 5.8), there are no obvious differences for the AuNP coverage on the PS-COOH microbeads compared with that on the pure PS microbeads using both methods.

Li *et al*. presented the deposition of AgNPs on the surface of poly (styrene-*co*-acrylic acid) nanospheres by in-situ reduction of $AgNO_3$ using PVP as a reducing agent.[263] Their results indicated that AgNPs on the composite nanospheres gradually increased with increasing the AA contents of PS nanospheres from 5 to 20 wt%. Our results were different from their reported results. This might be due to the lower concentration of AA (2 wt%) added for the microbead preparation in our study during dispersion polymerisation. It might also be because the different deposition mechanism is applied in our study. In their study conducted by Li *et al*., the carboxyl groups of PS microspheres can facilitate the attachment of silver ions onto the nanosphere surfaces by ion-pairing, which allowed the AgNP formation on the nanosphere surfaces reduced by PVP.[263] Therefore, more carboxyl groups on the nanospheres will result in forming more AgNPs on the nanospheres. However, in our study, AuNPs were formed before depositing them to the surface of microspheres. The principle is based on direct adsorption and AuNPs actually stabilise the PS microbeads. Hence, the difference was not observed for the composite microsphere formation between pure PS microbeads and PS-COOH microbeads at 2 wt% AA as functional monomer.

5.3.5 SERS Properties of Composite Microspheres by Different Methods and Different Microbeads

The Raman intensities of 4MP enhanced by four kinds of composite microspheres synthesised by different methods and different microbeads were also investigated. The

results in Figure 5.10 indicate that the Raman intensities of 4MP at 1076 cm^{-1} enhanced by the composite microspheres formed by pure PS microbeads and AuNPs were nearly the same using both methods, while the Raman intensities at 1076 cm^{-1} enhanced by the composite microspheres formed by PS-COOH microbeads and AuNPs were similar. But the Raman intensities between composite microspheres formed using pure PS microbeads and PS-COOH microbeads were slight different. This might be due to the size difference between pure PS microbeads (1.37 μm) and PS-COOH microbeads (1.60 μm). The average number of AuNPs adsorbed on each pure PS microbead and PS-COOH microbead were different, resulting in the different SERS signals. All in all, strong SERS signals of 4MP can be obtained for all the composite microspheres.

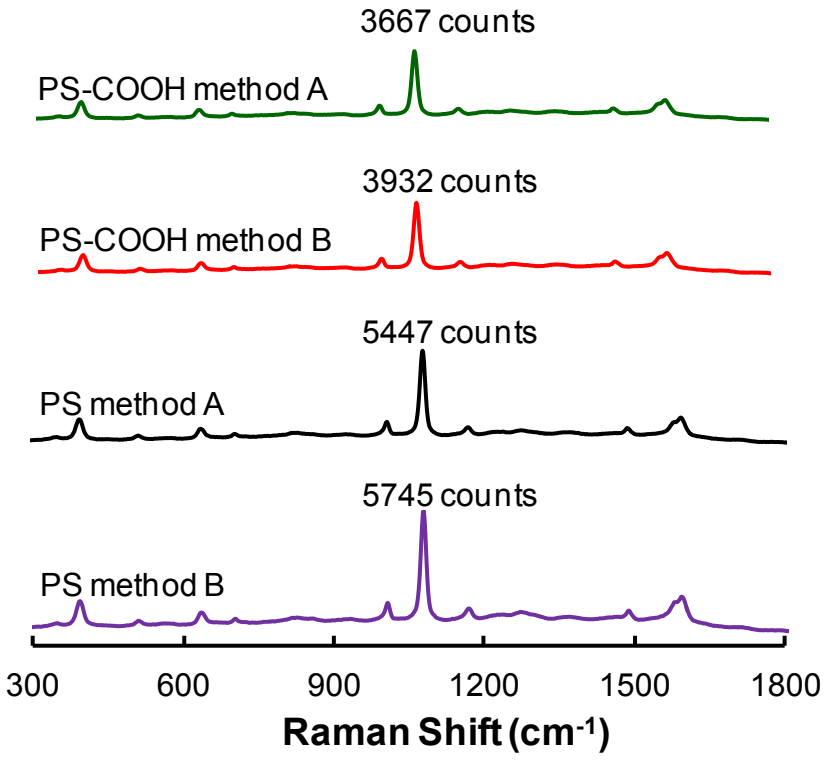

Figure 5.10 SERS spectra of different kinds of composite microspheres by two methods and two different microbeads with the same concentration of 4MP (10^{-3} M).

5.4 Summary

This study demonstrated the feasibility of SERS-active substrate preparation using polystyrene/AuNP composite microspheres. Direct adsorption (Method A) and in-situ growth (Method B) methods were introduced in details to prepare the polystyrene/AuNP composite microspheres, which can be used as SERS-active substrates. The AuNPs can be deposited onto the surface of polymer microbeads in a simple process by Method A without employing seeding or other chemical functionalisation of the nanospheres and microbeads at room temperature. The result showed a high coverage of AuNP layer was formed on the microbead surface for each sample. The composite microspheres were also fabricated using Method B. The deposition principle for both methods was the same and based on the stabilisation of metastable microbeads with small AuNPs. The only difference is the reaction speed. The formation speed for the composite microspheres prepared by in-situ growth was faster than that of direct adsorption at room temperature, but it was the same when conducted the direct adsorption at boiling temperature, indicating the importance of temperature on composite microsphere formation. SERS properties of different PS/AuNP composite microspheres were investigated by choosing 4MP as a model molecule. Both methods had the similar SERS activity. The detection limit of 4MP for composite microspheres formed using direct adsorption at 0.2 g PS/50 mL AuNPs could be down to 10^{-5} M.

CHAPTER 6 Silica Coating of Polystyrene/Gold Nanoparticle Composite Microspheres for SERS-active Microbead Development

6.1 Introduction

In recent years, a numbers of materials with various core-shell structures have been developed for specific applications, such as increasing the stability and biocompatibility of cores,[270] incorporating the different materials into one structure for multifunction applications,[264, 271-273] and improving the surface functionalisation properties.[274] Silica coated core-shell composite materials have been extensively investigated for a wide range of applications due to the following advantages: (1) chemical inert and stability, (2) high biocompatibility, (3) good optical transparency, and (4) easy to be functionalised.[275] The Stöber method is the most popular procedure on the formation of silica layer via the hydrolysis and condensation of tetraethyl orthosilicate (TEOS).[276] Different materials, in particular gold nanoparticles (AuNPs),[257, 277] silver nanoparticles (AgNPs),[278, 279] magnetic nanoparticles,[280] quantum dots (QDs),[281] and polymer microbeads,[282, 283] have been investigated to be coated with silica shell.

Normally, the coupling agents or surfactants are necessary during the formation of silica shell on the core materials. For instance, Liz-Marzάn *et al*. described a method for silica coating of gold colloid using (3-aminopropyl)-trimethoxysilane (APS) as silane coupling agent.[277] APS acted as a primer is used to modify the AuNP surface, making it vitreophilic. The silica shell thickness can be totally controlled under this reaction. Graf *et al*. reported a general method for the silica coating of colloidal particles using poly(vinylpyrrolidone) (PVP) as a coupling agent.[284] PVP, an amphiphilic and nonionic polymer, was employed to stabilise the particles during the silica shell growth process. Various particles, such as gold and silver colloids, boehmite rods, gibbsite platelets, and positively or negatively charged polystyrene spheres, can be directly transferred into an ammonia/ethanol mixture and form the smooth silica shell after the adsorption of PVP. Moreover, Li *et al*. also prepared

polymer core and silver nanoparticles/silica shell composite microspheres and the coupling agent (3-aminopropyl)-triethoxysilane (APTES) was used in the synthesis process.[264]

On the other hand, Lu *et al*. have demonstrated that uniform silica shell can be formed on AuNPs with controllable thickness without the application of coupling agent and surfactant.[257] The surface modification was also not needed using this method. Lately, they employed the same method to form the silica shell on the polymer beads by controlling the pH value of reaction medium, TEOS concentration and deposition time.[282] The result indicated that uniform silica shell could be formed on the surface of positively charged polymer beads. But it is hard to be achieved on the negatively charge PS beads. More studies were also carried out for the formation of silica shell on positively charged polymer core. Different cationic stabilisers and initiators, such as polyethyleneimine,[285] 2,2'-azobis (2-methylpropionamide) dihydrochloride,[286] and azobisisobutyramidine dihydrochloride,[287] can be used to generate the positively charged polymer microbeads prior to silica coating.

In our previous study, polystyrene/AuNP composite microspheres were prepared using both direct adsorption and in-situ growth methods and showed good surface enhanced Raman scattering (SERS) enhancement capability. It is essential to improve the surface biocompatibility of composite microspheres for further applications. Since silica coating has many advantages and great achievements have been made on the formation of silica shells on different materials using the Stöber method, this study focused on the formation of silica layer on the polystyrene/AuNP composite microspheres in a sol-gel process. AuNPs were first deposited on the surface of negatively charged polystyrene microbeads (PS-COOH) using an in-situ growth method for the formation of PS-COOH/AuNP composite microspheres, which was proved to be more efficient for the preparation of composite microspheres than direct adsorption. Systematic studies on the silica coating of

PS-COOH/AuNP composite microspheres were carried out. Although the PS-COOH/AuNP composite microspheres synthesised in the present work are negative charged in the water, silica shell can still be formed on the surface of composite microspheres without coupling agent, by changing the reaction conditions, such as deposition time, ammonia concentration, water concentration and TEOS concentration. Moreover, in order to produce SERS-active microbeads for Raman spectroscopic-based applications, 4-mercaptophenol (4MP) molecules were self-assembled on the PS-COOH/AuNP composite microspheres prior to encapsulation with silica layer.

6.2 Experimental Section

6.2.1 Materials

Styrene, Triton X-305 (70% in H_2O), polyvinylpyrrolidone (PVP 360 000), gold (III) chloride trihydrate ($HAuCl_4 \cdot 3H_2O$), 4-mercaptophenol (4MP), tetraethyl orthosilicate (TEOS), and 3-aminopropyl-trimethoxysilan (APTMS) were supplied by Sigma-Aldrich. Acrylic acid (AA), 2, 2'-azobis (2-methylpropanitrile) (AIBN), N-hydroxysuccinimide (NHS), and N-(3-dimethylaminopropyl)-N'-ethylcarbodiimide hydrochloride (EDC) were purchased from Acros organics. Trisodium citrate dehydrate (Na_3Ct) was obtained from ACE chemical company. Absolute ethanol and 2-propanol were from Merck. 30% ammonia solution was obtained from Chem-supply. FITC-conjugated AffiniPure rabbit anti-human IgG was from Jackson ImmunoResearch (PA). All the chemicals were used as received without further purification.

6.2.2 Synthesis of Polystyrene Microbeads

Dispersion polymerisation was used to prepare monodisperse polystyrene microbeads with carboxyl groups (PS-COOH) according to the reported procedure with some modification.[206] Typically, there were two stages for the microbead preparation. In the first stage, monomer (6.0 g Styrene), initiator (0.24 g AIBN), stabiliser (0.27 g PVP 360 000), costabiliser (0.30 g 70% Triton X-305), and 34 g 95% ethanol were charged to a 250 mL three-neck flask. The mixture was deoxygenated by nitrogen bubbling for 40 min at room temperature, followed by merging the flask into a pre-heated 70 °C oil bath and stirring mechanically at 100 rpm for one hour. In the second stage, the preheated AA solution (2 wt % to styrene was mixed with 16 g 95% ethanol and preheated to 70 °C) was injected to the reaction system. The reaction was continued for another 24 h. After the polymerisation, the solid concentration of polymer solution was obtained and calculated by weighting a small amount of solution and letting it dry in oven at 65 °C for 24 h.

6.2.3 Preparation of PS-COOH/AuNP Composite Microspheres

Prior to the fabrication of composite microspheres, the obtained PS-COOH microbeads were washed three times with ethanol and four times with DI water. The microbeads were then redispersed in the same amount of water. During the composite microsphere synthesis, 50 mL 10^{-3} M $HAuCl_4 \cdot 3H_2O$ solution were heated to boil under vigorous stirring. An amount of 0.2 g PS-COOH microbead aqueous solution (12 wt%) and 2.206 mL 1% sodium citrate were simultaneously added to the boiling solution. Boiling was continued for 15 min. The solution was cooled down to room temperature after the reaction. The resulting PS-COOH/AuNP composite microspheres were then centrifuged (3000 rpm, 1

min) and washed with DI water three times. The composite microspheres were finally redispersed in 0.5 mL DI water.

6.2.4 Silica Coating of PS-COOH/AuNP Composite Microspheres

The silica coating of PS-COOH/AuNP composite microspheres was achieved by a modified Stöber method.[282] In a typically procedure, 50 μL PS-COOH/AuNP composite microsphere suspension was mixed with 3.95 mL DI water and 20 mL 100% 2-propanol. Different amounts of 30% ammonia solution and TEOS were added to the mixture under stirring. The reaction was continued for 6 h at room temperature. The samples were taken out in certain time intervals and centrifuged (3000 rpm, 1 min) to remove the suspension. The residual was washed thoroughly with 2-propanol and DI water, and finally redispersed in DI water.

6.2.5 Silica Coating of SERS-active PS-COOH/AuNP Composite Microspheres

An amount of 50 μL PS-COOH/AuNP composite microspheres reacted with 1 mL 10^{-3} M 4MP in ethanol solution for one hour at room temperature, followed by three-time centrifugation to remove free 4MP. The suspension was redispersed in 1.0 mL DI water for Raman measurement and silica coating. The silica coating process was carried out as stated previously. Amounts of 3.0 mL DI water and 20 mL 100% 2-propanol were mixed with 1.0 mL SERS-active PS-COOH/AuNP composite microsphere solution. Under stirring, 0.1 mL ammonia solution and 20 mM TEOS were added. The reaction was allowed for 15 min at room temperature. Finally, the mixture was washed with 2-propanol several times and redispersed in 1.0 mL DI water.

6.2.6 Antibody Immobilisation of SERS-active Microbeads

Amounts of 0.5 mL SERS-active microbeads were well-dispersed in 12 mL 2-proponal under sonication, followed by adding 0.3 mL APTMS. The mixture was stirred overnight at room temperature. The SERS-active microbeads were purified by centrifugation and redispersed in 0.5 mL DI water. 50 μL APTMS-modified microbeads were mixed with 50 μL freshly prepared EDC/NHS stock solution (20 mg of EDC and 30 mg of NHS in 1 mL phosphate buffer saline (PBS, pH 7.4)) for 15 min, followed by adding 10 μg of FITC-labelled rabbit anti-human IgG. The mixture was gently vortexed for 2 h at room temperature under dark. The microbeads were then washed with phosphate buffer solution three times to remove any unbound antibodies.

6.2.7 Characterisations

The scanning electron micrographs were taken using a Phillips XL30 scanning electron microscopy (SEM) operating at an accelerating voltage of 5 kV. Samples for SEM were prepared by dropping the suspension of PS-COOH/AuNP composite microspheres onto the silica wafer and drying at room temperature. An ImageTool version 3.0 was used to get the average diameter of polystyrene microbeads and silica coated PS-COOH/AuNP composite microspheres by measuring the diameter of 100 particles in the SEM images. The thickness of silica shell was caculcated by the following equation.

$$d = \frac{\overline{D}_2 - \overline{D}_1}{2} \tag{6.1}$$

Where d is the average thickness of silica shell. $\overline{D}_1$ is the average diameter of polystyrene microbeads. $\overline{D}_2$ represents the average diameter of silica coated PS-COOH/AuNP composite microspheres.

The morphologies of PS-COOH/AuNP composite microspheres before and after silica coating were also observed by a Phillips CM200 transmission electron microscopy (TEM). The SERS spectra of 4MP assembled on the composite microspheres before and after silica coating were recorded using a Peak Seeker Pro^{TM} Raman spectrometer equipped with a 200 mW 785 nm laser. The integration time is 3 s. Fluorescence images were taken by Leica TCS SP5 confocal microscopy system.

6.3 Results and Discussion

This study aimed at encapsulating the PS-COOH/AuNP composite microspheres with silica layer and developing the monodisperse SERS-active microbeads. The whole procedure is illustrated in Scheme 6.1. Monodisperse PS-COOH microbeads were first synthesised using dispersion polymerisation. AuNPs were then immobilised onto the surface of monodisperse PS microbeads via an in-situ growth method. The outside of PS-COOH/AuNP composite microspheres was encapsulated with silica shell.

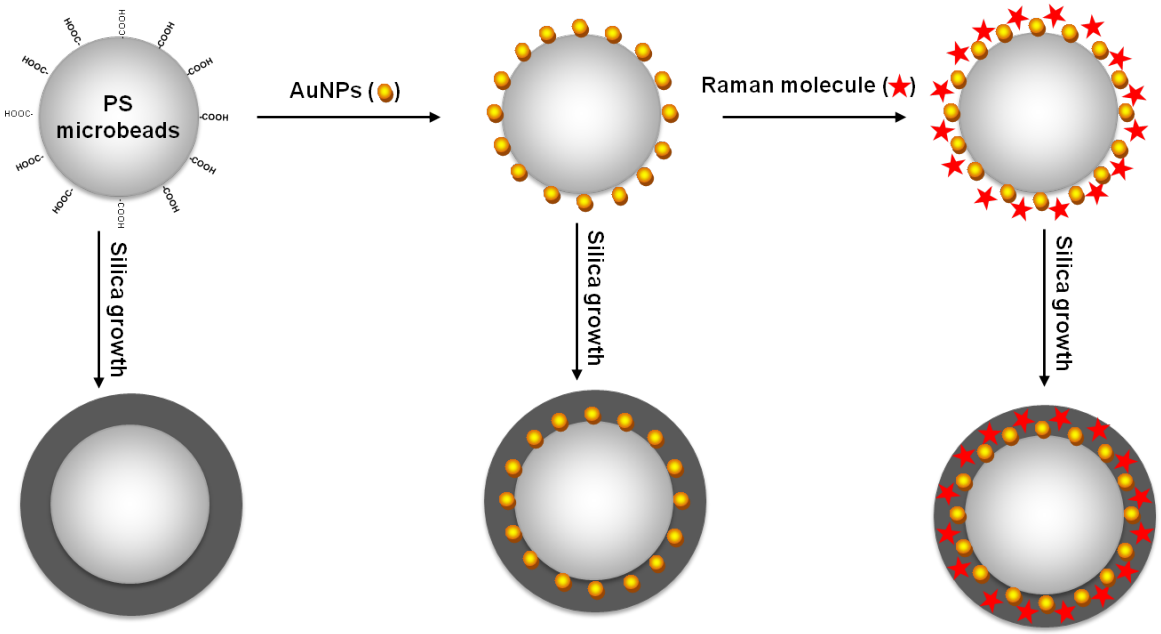

Scheme 6.1 The procedure for the preparation of silica coated PS-COOH microbeads, PS-COOH/AuNP composite microspheres and SERS-active PS-COOH/AuNP composite microspheres.

The silica layer can act as a protect layer and offers the composite microspheres with high chemical and physical stability, biocompatibility, and easy surface functionalisation with other chemicals (such as 3-aminopropyltriethoxysilane (APTES) or succinic anhydride) to produce the amino or carboxyl groups on microbead surface.[288] In the current work, silica

shell was formed onto the surface of PS-COOH/AuNP composite microspheres via the sol-gel method by the hydrolysis and condensation of silica precursor (TEOS) using a reported method.[282] PS-COOH/AuNP composite microspheres both before and after Raman-active molecule assembling were successfully coated with silica layer. The silica coated SERS-active PS-COOH/AuNP composite microspheres can be used as monodisperse SERS-active microbeads and immobilised with proteins for further application on biodetection. It is obvious to note that the formation of silica shell could be influenced by reaction parameters, including deposition time, ammonia concentration, water concentration, and TEOS concentration. Therefore, this study mainly focuses on the formation of silica shell on the surface of PS-COOH/AuNP composite microspheres and the influence of different reaction parameters on the coating process. The formation mechanism is also proposed to explain the silica coating of PS-COOH/AuNP composite microspheres.

6.3.1 Preparation of PS-COOH/AuNP Composite Microspheres

Polystyrene microbeads with carboxyl group (PS-COOH) were first fabricated using dispersion polymerisation, which can produce the polymer microbeads with high monodispersibility. The SEM image in Figure 6.1(a) indicates that the synthesised monodisperse PS-COOH microbeads have an average diameter around 1.6 μm. AuNPs were deposited onto the surface of PS-COOH microbeads using an in-situ growth method by the addition of PS-COOH microbeads into the reaction solution during AuNP formation. It was reported that the polymer microbeads are metastable after several time washing due to the lack of stabiliser, so that the small AuNPs can act as stabilisers and adsorb on the microbead surface, resulting in the formation of composite microspheres.[261] Different sizes of AuNPs can be deposited on the polymer microsphere surface by varying the reducing agents and their concentrations during the composite microsphere preparation. In our

previous study in Chapter 4, it was found that 50 nm AuNPs have a Raman effective enhancement factor higher than 20 nm AuNPs. Thus a molar ratio of $HAuCl_4/Na_3Ct$ at 1:1.5 was chose to form the AuNPs with an average size of 50 nm on the surface of PS-COOH microbeads. It can be seen from the SEM image in Figure 6.1(b) that AuNPs with 50 nm average diameter can directly assemble on the surface of microbeads after their formation. The PS-COOH microbeads were evenly covered with AuNPs.

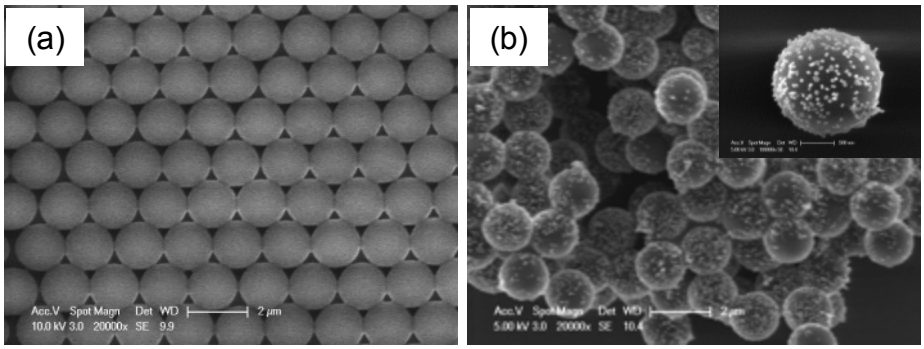

Figure 6.1 The SEM images of PS-COOH microbeads (a) and PS-COOH/AuNP composite microspheres (b). The inset in (b) shows a magnified composite microsphere. The scale bar is 2 μm.

6.3.2 Effect of Deposition Time on Silica Coating

The reaction condition was set up under 0.1 mL ammonia solution, 4 mL water, and 20 mM TEOS. The SEM images of silica coated PS-COOH/AuNP composite microspheres at different deposition times after centrifugation are presented in Figure 6.2 and Figure 6.3. In Figure 6.2, it can be observed that the PS-COOH/AuNP composite microspheres have already fully coated with silica shell within a few minutes by observing the SEM images of silica coated composite microspheres before centrifugation within 15 min (Figure 6.2). Actually, the PS-COOH/AuNP composite microspheres have already been encapsulated with a silica layer at 3 min (Figure 6.2a). The thickness of silica shell is ~70 nm at 15 min (Figure 6.2e and f). After the formation of shell layer, more silica could not be deposited

on the surface of composite microspheres any more with the increase of deposition time. That can be seen by the thickness of shell, which remained constant and did not increase with the deposition time (Figure 6.3a-f). The shell thicknesses at different reaction times from 15 min to 6 h appeared to be similar at approximately 70 nm. The roughness of composite microsphere surfaces presented in TEM image (Figure 6.4b) after silica encapsulation further suggests that the PS-COOH/AuNP composite microspheres are covered by silica shell.

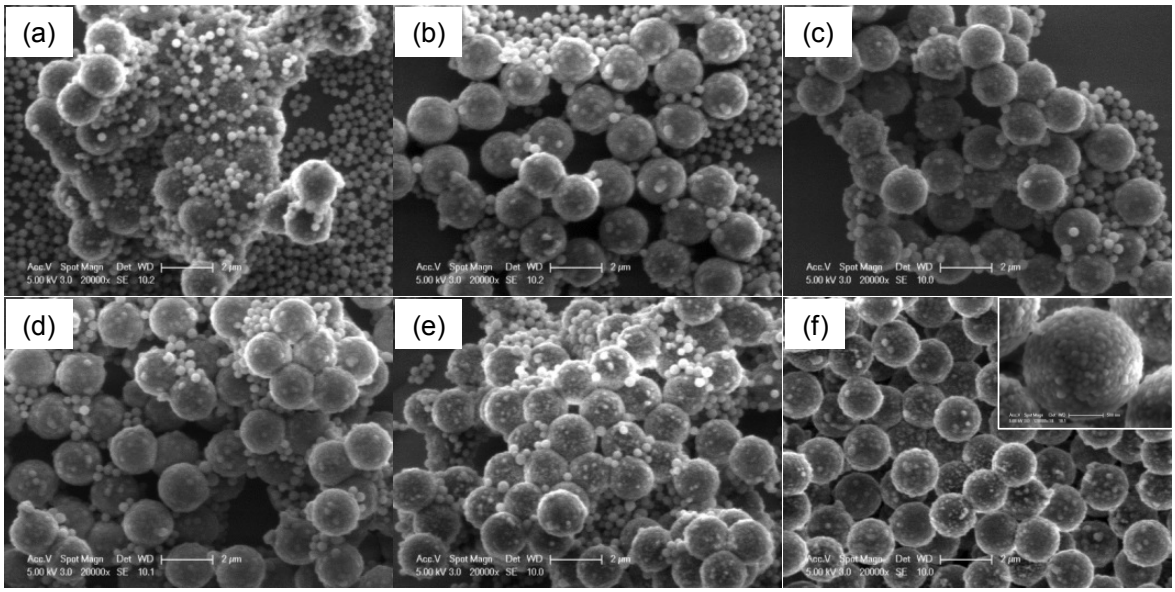

Figure 6.2 The SEM images of silica coated PS-COOH/AuNP composite microspheres using 0.1 mL ammonia, 20 mM TEOS, and 4 mL water before centrifugation at different deposition times: (a) 3 min, (b) 6 min, (c) 9 min, (d) 12 min, (e) 15 min, and (f) 15 min after centrifugation. The inset in (f) shows a high magnification area. The scale bar is 2 μm.

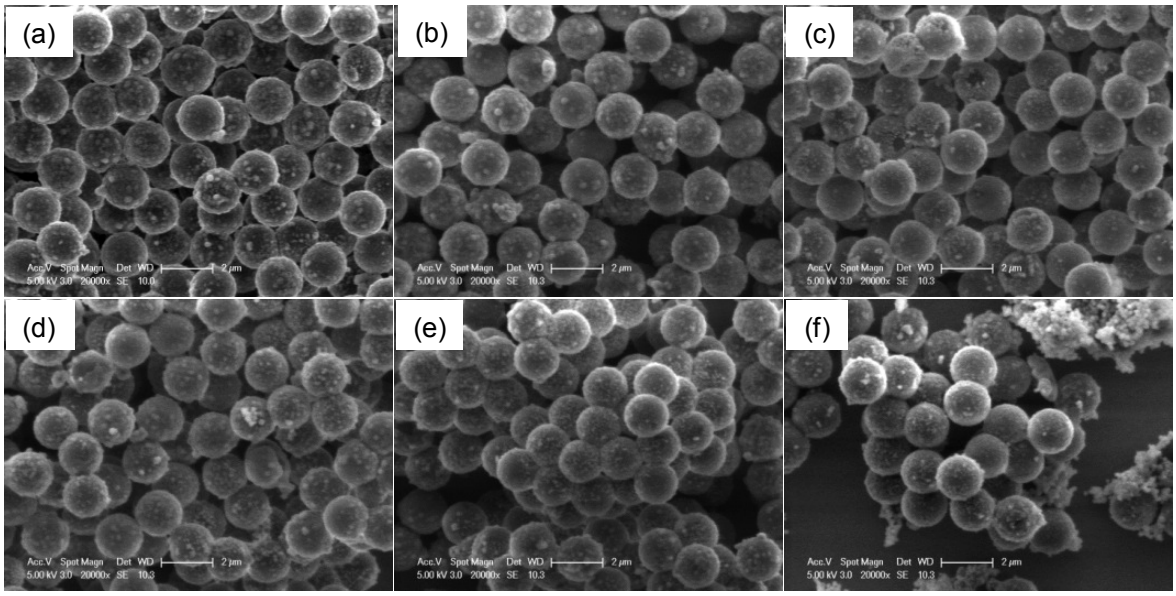

Figure 6.3 The SEM images of silica coated PS-COOH/AuNP composite microspheres using 0.1 mL ammonia, 20 mM TEOS, and 4 mL water at different deposition times: (a) 15 min, (b) 30 min, (c) 1 h, (d) 2 h, (e) 3 h, and (f) 6 h after centrifugation. The scale bar is 2 μm.

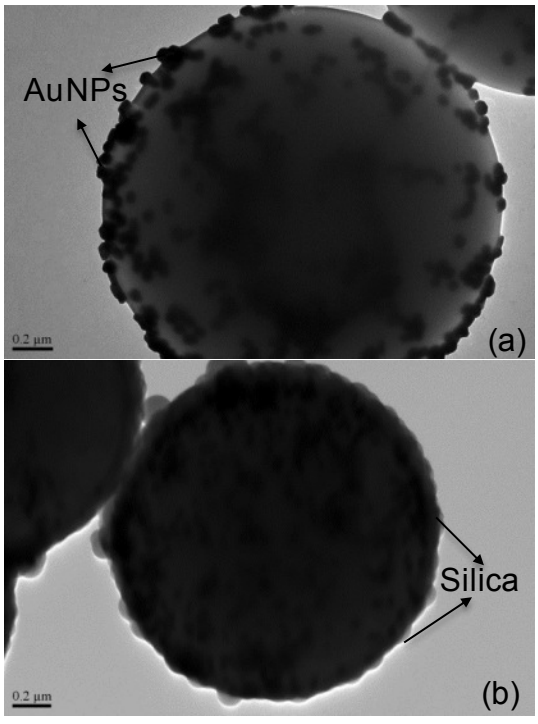

Figure 6.4 TEM images of PS-COOH/AuNP composite microspheres before (a) and after (b) silica coating at 15 min. The scale bar is 0.2 μm.

On the other hand, free silica particles were also formed during the coating process and centrifugation was found to play an important role to remove the free silica particles. SEM images in Figure 6.2a-e show that a number of free silica nanoparticles were formed in addition to the formation of silica shell on the composite microspheres before the centrifugation. The average particle size of these free silica particles was about 300 nm. But the free silica nanoparticles can be easily removed during the centrifugation process (Figure 6.2f). It is worthwhile to note that no free silica nanoparticles can be observed after the centrifugation process within 3 h (Figure 6.3a-e). These free silica particles tend to aggregate together with further increasing the deposition time. Such aggregates could neither be destroyed even under an intense ultrasonic process nor be separated from the silica coated PS-COOH/AuNP composite microspheres during the centrifugation. These aggregates still present in the suspension of silica coated PS-COOH/AuNP composite microspheres after washing. That is why some silica aggregates are seen in Figure 6.3f at 6 h deposition time.

In comparison, silica coating of PS-COOH microbeads was also performed under the same condition as the control experiment. Figure 6.5 presents the silica coating results. Generally, the silica layer with 60 nm average thickness was formed on the PS-COOH microbead surface, which is thinner and smoother than that formed on the surface of PS-COOH/AuNP composite microspheres. This might be due to the contribution of AuNPs on the microbead surface. The surface of PS-COOH microbeads became uneven after the deposition of AuNPs on their surface, which hindered the smooth shell formation in such situation.

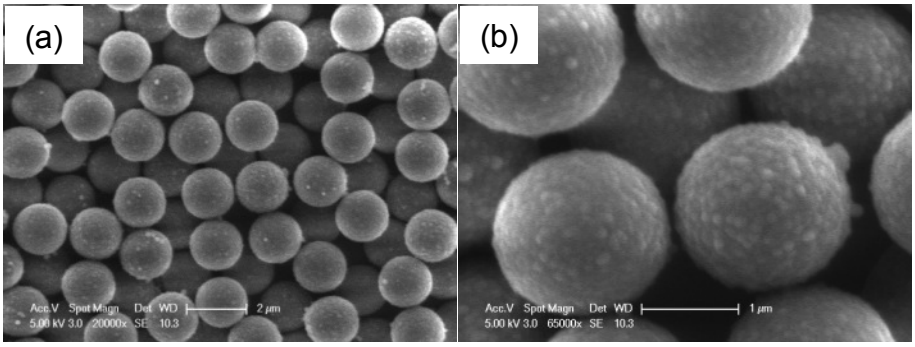

Figure 6.5 The SEM images of silica coated PS-COOH microbeads using 0.1 mL ammonia, 20 mM TEOS, and 4 mL water at 1 h after centrifugation (a) and a higher magnification image (b). The scale bar is 2 μm in (a) and 1 μm in (b).

6.3.3 Effect of Ammonia Concentration

In the Stöber silica preparation, ammonia acts as the catalyst, which catalyses the hydrolysis and condensation of TEOS.[276] In order to investigate the influence of ammonia concentration on the silica coating of PS-COOH/AuNP composite microspheres in the sol-gel process, different amounts of ammonia solution at 0.1 mL, 0.5 mL and 1.0 mL were tested as the catalyst. Figure 6.3, 6.6, 6.7 display the SEM images of the silica coated PS-COOH/AuNP composite microspheres with different ammonia concentrations after centrifugation at different deposition times. The results show that the silica layer could be formed within 15 min under different ammonia concentrations. However, the aggregation of the silica particles at higher ammonia concentrations appeared to occur faster than those at a lower ammonia concentration. The silica aggregates can be seen at 30 min for 1.0 mL ammonia (Figure 6.7b), while they can only be seen until 6 h for 0.1 mL ammonia (Figure 6.3f). They can also been observed at 2 h using 0.5 mL ammonia (Figure 6.6d). Since ammonia is used as a catalyst in the reaction, the higher ammonia concentration would promote the reaction rate and shorten the deposition time.[289] Furthermore, the ionic strength of the reaction mixture increases accordingly with the increase in ammonia

concentration, which lead to destabilise the reaction system. Therefore, the silica particles would aggregate earlier at a higher concentration of ammonia.

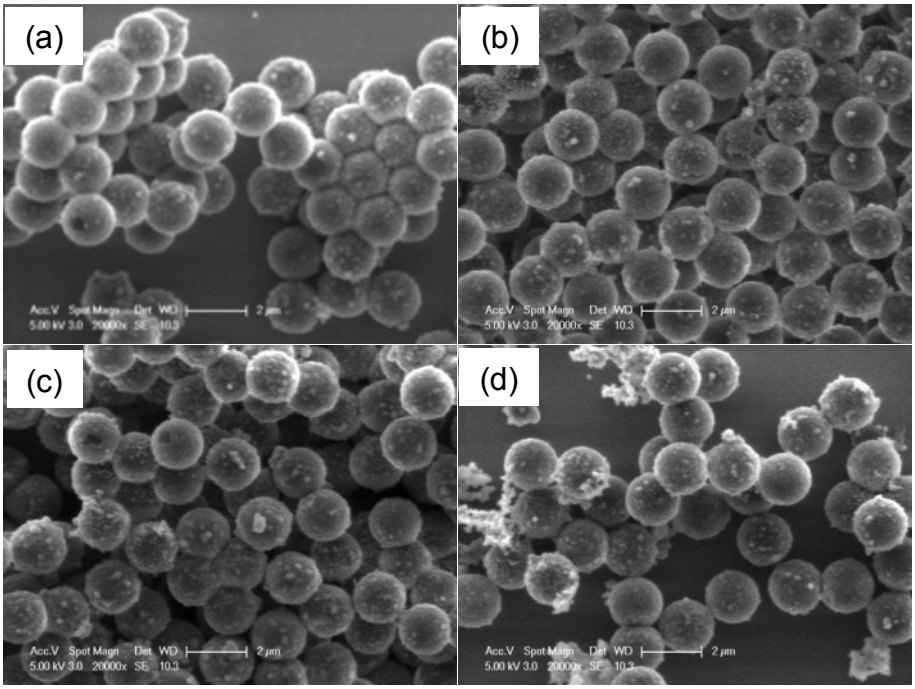

Figure 6.6 The SEM images of silica coated PS-COOH/AuNP composite microspheres using 0.5 mL ammonia, 20 mM TEOS, and 4 mL water at different deposition times: (a) 15 min, (b) 30 min, (c) 1 h, and (d) 2 h after centrifugation. The scale bar is 2 μm.

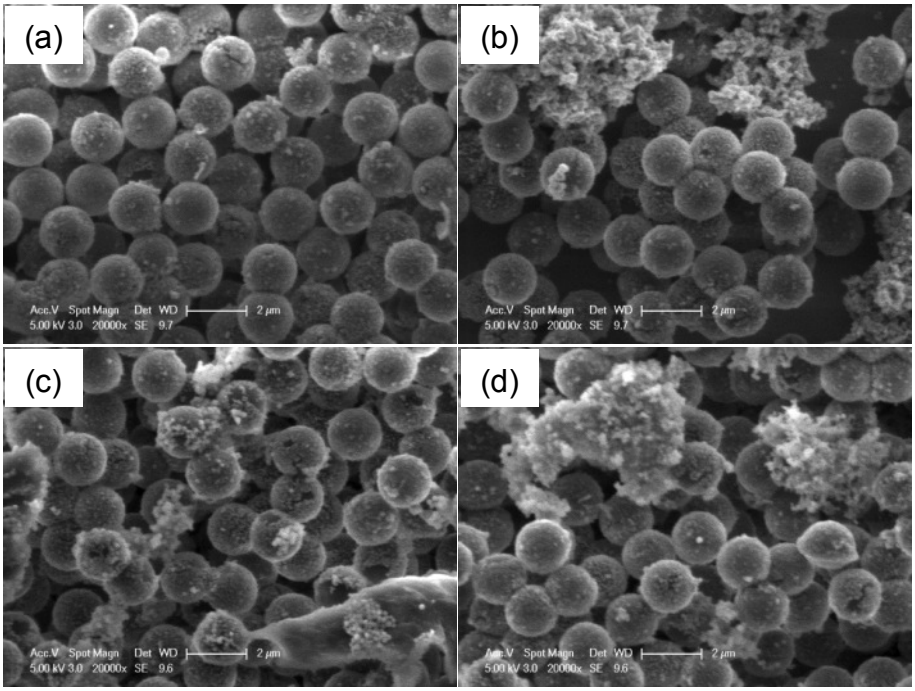

Figure 6.7 The SEM images of silica coated PS-COOH/AuNP composite microspheres using 1.0 mL ammonia, 20 mM TEOS, and 4 mL water at different deposition times: (a) 15 min, (b) 30 min, (c) 1 h, and (d) 2 h after centrifugation. The scale bar is 2 μm.

6.3.4 Effect of Water Concentration

According to the Stöber method, water also plays an important role in the formation of silica particles. The volume ratio of 2-proponal/water was studied on the coating process. The total volume of 2-propanol and DI water was 24 mL. The concentration of water was increased from 0 mL to 6 mL while 2-propanol concentration was decreased correspondingly. Ammonia and TEOS concentrations were kept constant at 0.5 mL and 20 mM for all the reactions. The SEM micrographs of silica coated PS-COOH/AuNP composite microspheres with various water concentrations are shown in Figure 6.8. At a low water concentration (Figure 6.8a), there was no silica shell formed in 3 h reaction and the size of composite microspheres was still at 1.6 μm. The silica layer with poor morphology was formed on the surface of composite microspheres using 2 mL water

concentration. Some of the free silica nanoparticles cannot be removed during the centrifugation (Figure 6.8b). The thickness of silica shell is 100 nm. Increasing the water concentrations to 4 mL and 6 mL resulted in the fabrication of 75 nm silica layer with good morphologies (Figure 6.8c and 6.8d). It was reported that a maximum particle size could be achieved with the increase in water concentration and the results indicated that the particles size first increases and then decreases with the increase of water concentration.[276, 290] In this study, water concentration at 2 mL (~4.5 M) in Figure 6.8b might have already reached or almost reached the optimal water concentration, so the shell thickness is thicker than higher water concentrations at 4 mL (~9.0 M) and 6 mL (~13.6 M).

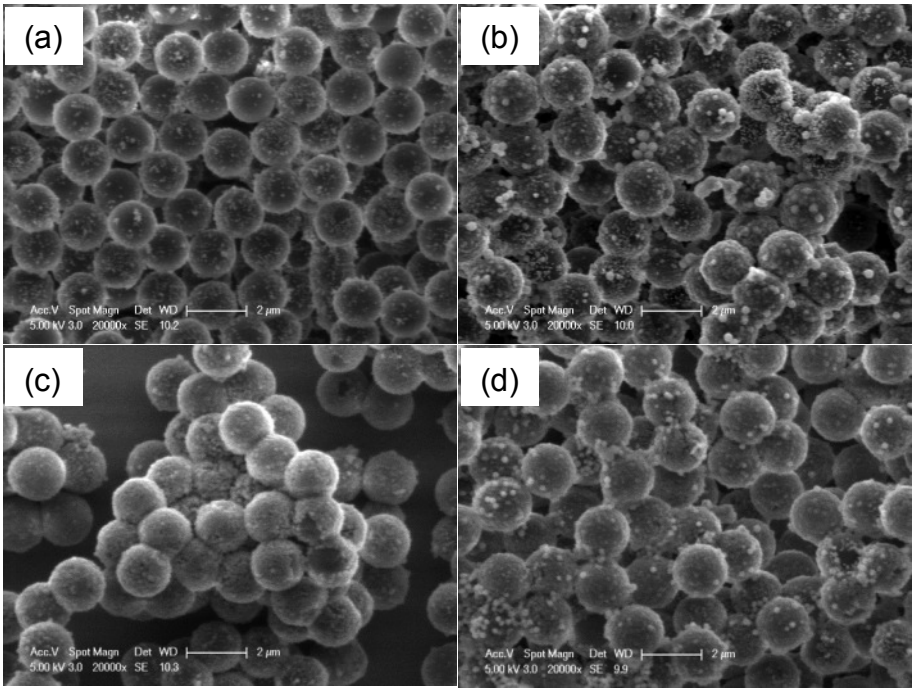

Figure 6.8 The SEM images of silica coated PS-COOH/AuNP composite microspheres using 0.5 mL ammonia and 20 mM TEOS with different water concentrations at different deposition times: (a) 0 mL water at 3 h, (b) 2 mL water at 15 min, (c) 4 mL water at 15 min, and (d) 6 mL water at 15 min after centrifugation. The scale bar is 2 μm.

6.3.5 Effect of TEOS Concentration

It is well known that the change of TEOS concentration results in forming the silica shell with different thickness.[258] The high concentration of TEOS means higher silica source and leads to an increase in the thickness of the silica shell. Figure 6.9 shows the SEM images of silica coated composite microspheres at different concentrations of TEOS ranging from 0.2 mM to 40 mM by fixing ammonia and water concentration at 0.5 mL and 4 mL, respectively. Figure 6.9a indicates that TEOS at a low concentration of 0.2 mM can not trigger the formation of silica shell due to the shortage of silica source. TEOS at 2 mM can introduce the silica shell with 50 nm on the surface of composite microspheres, but there were some uncoated composite microspheres available in the suspension (Figure 6.9b). Increasing the TEOS concentration to 20 mM can produce 70 nm thickness silica shells with good morphology, which was optimal for the formation of silica shell (Figure 6.9c). Further increasing the TEOS concentration to 40 mM resulted in forming a silica layer with thicker shell of 105 nm (Figure 6.9d). However, in addition to the production of silica shell, there were also some free silica particles with irregular shape presented in the suspension after the centrifugation.

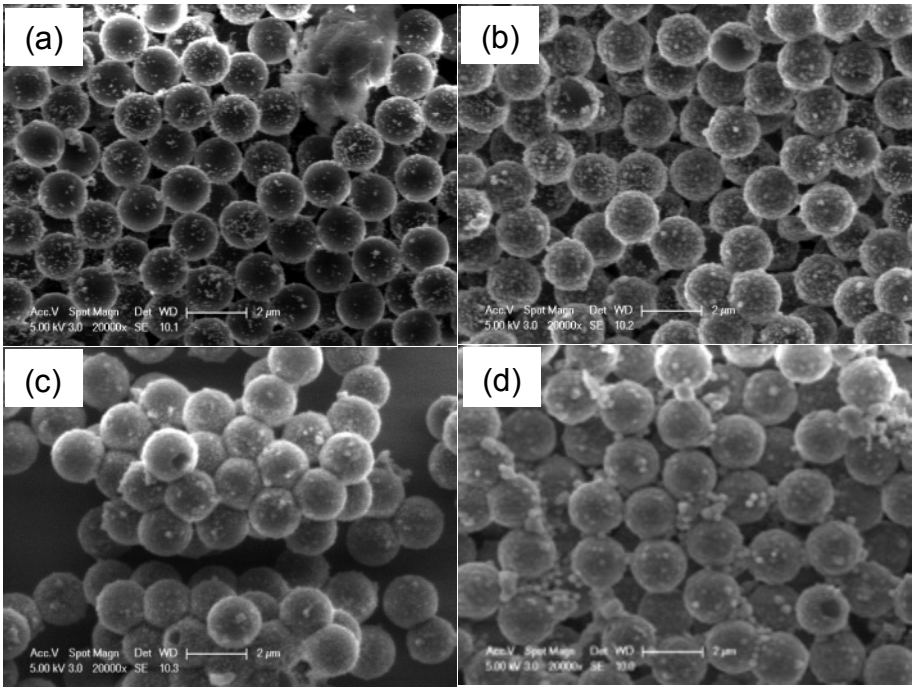

Figure 6.9 The SEM images of silica coated PS-COOH/AuNP composite microspheres using 0.5 mL ammonia and 4 mL water with different TEOS concentrations at different deposition times: (a) 0.2 mM TEOS at 3 h, (b) 2 mM TEOS at 15 min, (c) 20 mM TEOS at 15 min, and (d) 40 mM TEOS at 15 min after centrifugation. The scale bar is 2 μm.

6.3.6 Proposed Mechanisms for the Silica Coating of PS-COOH/AuNP Composite Microspheres

Silica shells were formed on the surface of PS-COOH/AuNP composite microspheres by Stöber method. Previous results revealed that negatively charged microbeads could not be coated with uniform silica shell.[282] In this study, however, two percent of AA was added to fabricate the negatively charge microbeads, which can be formed with smooth silica layer by the sol-gel method. Furthermore, the adsorption of negative-charged AuNPs on the surface of microbeads increased the negative charge of composite microspheres. However, the negatively charged silica particles can still form the silica layer with good coverage on the surface of PS-COOH/AuNP composite microspheres. Since both silica particles and

PS-COOH/AuNP composite microspheres are negatively charged, silicate adsorption is electrostatically unfavourable.

Recently, polymer-silica composite particles were formed by physical adsorption of silica nanoparticles on the surface of poly(2-vinylpyridine) (P2VP) latexes and analysed by small angle X-ray scattering.[291, 292] They reported that both polymer latex and silica nanoparticles were negatively charged at pH 10. Electristaic interaction was unfavourable. The silica can be adsorbed on the latex, becease no repuisive force was generated during the interaction of latex and silica. The results demonstrated that silica adsorption was completed in a few seconds (~2.5 s) after mixing the latex and silica nanoparticles together. Moreover, the adsorption rate depended on the extent of silica coverage on latex surface. It is difficult to adsorb the addition silica nanoparticles at higher silica coverage. In that case, the thickness of silica layer was determined in the first a few seconds and controlled by the latex size. In our study, the similar results were found for the formation of silica shell on the surface of PS-COOH/AuNP composite microspheres. The silica shell was rapidly formed on the surface of composite microspheres within a few minutes and the thickness of shell layer did not increase with the increase in deposition time after 15 minutes.

Aggregative growth model is widely accepted to describe the formation of silica nanoparticles in the Stöber method.[293] In this theory, primary particles (diameter: 5-10 nm) were formed during TEOS hydrolysis and aggregate to produce the silica particles.[294] Figure 6.2a-e indicates that the size of free silica nanoparticles (~300 nm) is much larger than the thickness of silica layer on the composite microspheres (~70 nm). The formation of silica layer might not be associated with the adsorption of free silica nanoparticles, but might be resulted from the adsorption of primary nanoparticles. Therefore, during the silica coating of PS-COOH/AuNP composite microspheres, on the one hand, the primary

particles aggregated on the surface of composite microspheres to stabilise them, leading to the formation of silica shell. On the other hand, the primary particles aggregated with themselves to form the big silica nanoparticles. When the surface of composite microspheres was surrounded by the silica layer, more silica nanoparticles could not be further adsorbed on the surface any more. Only the silica nanoparticles were continuously formed with the deposition time. Furthermore, with further increasing of deposition time, silica nanoparticles preferred to form the big aggregates, which can be seen in the SEM images at longer deposition time in Figure 6.3, 6.6, and 6.7.

6.3.7 Silica Coating of SERS-active PS-COOH/AuNP Composite Microspheres

In order to develop SERS-active microbeads for biodetection, 4MP was added to the PS-COOH/AuNP composite microspheres prior to silica coating. The silica coating procedure was the same as that for PS-COOH/AuNP composite microspheres using 0.1 mL ammonia as a catalyst. Figure 6.10A shows the SEM image of silica coated SERS-active PS-COOH/AuNP composite microspheres. The result indicates that silica layer can still be formed on the surface of SERS-active composite microspheres. The thickness and morphology of silica shell was similar with the one without Raman-active molecules 4MP (Figure 6.3a).

Figure 6.10B presents the Raman spectra of SERS-active PS-COOH/AuNP composite microspheres before and after silica coating. The Raman spectrum signatures of 4MP before and after silica coating were the same. But the Raman intensity after silica coating decreased compare with the Raman spectra of 4MP before silica coating. The strongest characteristic peak at 1076 cm^{-1}, which represents the ring breathing mode of 4MP, was chosen as a reference peak for the comparison of Raman spectrum intensity. The intensity

decreased from 3253 counts before silica coating to 1922 counts after silica coating. Although the Raman intensity of 4MP decreased more than 40%, the SERS-active PS-COOH/AuNP composite microspheres still exhibits good SERS signals, which demonstrates that the silica layer can not block the entire SERS signals. Therefore, the SERS-active PS-COOH/AuNP composite microspheres can be employed as SERS-active microbeads after the silica coating. Various Raman spectroscopic-based microbeads could be developed by changing the Raman-active molecules during the synthesis procedure.

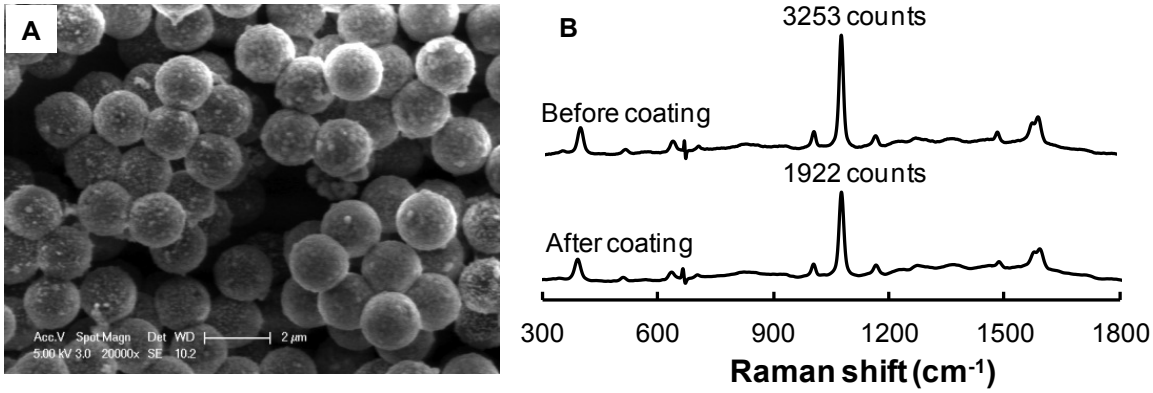

Figure 6.10 The SEM image (A) of silica coated SERS-active PS-COOH/AuNP composite microspheres and the Raman spectra (B) of SERS-active PS-COOH/AuNP composite microspheres before and after silica coating process. The scale bar in A is 2 μm.

The specific molecules, such as DNA-DNA or RNA, antibody-antigen, and biotin-avidin, are very important elements in biological detection. In order to conjugate the biomolecules to the SERS-active microbeads, it is necessary to modify the surface of SERS-active microbeads with the functional groups. APTMS was employed to generate the amino groups on the surface of microbeads. The FITC-labelled IgG was then attached to the surface via the EDC/NHS chemistry (Figure 6.11A). The proteins were successfully loaded to the microbead surface by examining the images using the confocal fluorescence

microscopy. It can be found in Figure 6.11B no fluorescence image can be detected for the bare SERS-active microbeads under blue light illumination. This result reveals that the SERS-active microbeads themselves contain no fluorescence. After conjugating the FITC-labelled rabbit anti-human IgG to the SERS-active microbeads, the image can show up under blue light illumination (Figure 6.11C). This indicated that the proteins can be easily loaded to the surface of SERS-active microbeads. The SERS-active microbeads are able to be employed as biodetection tools after modification and immobilisation with biomolecules, which is of great importance for further biological and biomedical applications.

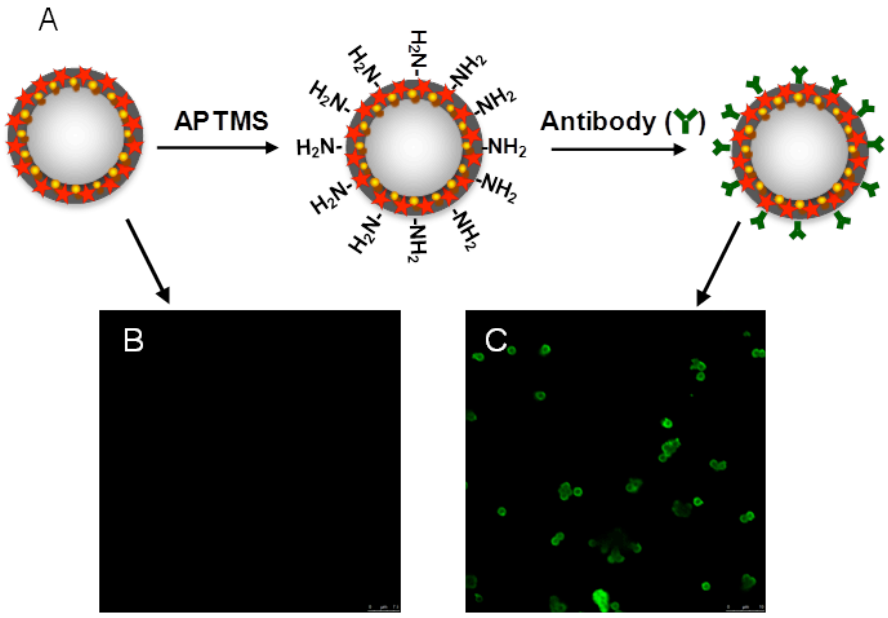

Figure 6.11 The procedure for the protein immobilisation (A) and confocal fluorescence images of SERS-active microbeads before (B) and after (C) conjugated with FITC labelled antibodies.

6.4 Summary

Stable silica layers on the surface of negative charged PS-COOH/AuNP composite microspheres were successfully synthesised via a sol-gel process, by changing the reaction

conditions, such as deposition time, ammonia concentration, water concentration and TEOS concentration. It was revealed that the deposition time plays a significant role in the formation of silica shell on PS-COOH/AuNP composite microsphere surface. Stable silica layer can be encapsulated on the surface of composite microsphere within a few minutes under different ammonia concentrations. Increasing the deposition time does not benefit the silica coating and only results in the formation of free silica nanoparticles and big silica aggregates. The free silica nanoparticles can be easily removed during the centrifugation, while the big silica aggregates cannot be removed any more. A higher ammonia concentration led to a higher reaction rate and a faster aggregation. The concentration of water and TEOS also affected the formation of silica shells on the composite microspheres. By the self-assembling of molecule (4MP) with PS-COOH/AuNP composite microspheres, the silica layer can still be formed on the surface of composite microspheres using the same method. The SERS-active composite microspheres exhibited promising SERS signals after silica coating, and can be modified and immobilised with proteins. Therefore, this functional material would be beneficial for the development of Raman spectroscopic-based microbeads for biosensing application.

CHAPTER 7 Preparation of Raman Spectroscopic-encoded Microbeads by Dispersion Polymerisation

7.1 Introduction

Polymer microbeads have been widely applied as a platform for biodetection. In 1956, polystyrene latex particles was used in the diagnosis of rheumatoid arthritis.[16] The interaction between antigens in blood serum and gamma-globulin on the surface of polymer microspheres led to the agglutination of latex particles and the results could be directly distinguished using eyes. Since then, many studies have been conducted for the disease diagnostics based on latex immunoassays.[207, 295-297] However, human diseases tend to be complicated in modern society. This requires simultaneously measuring different analytes in a single sample. The immunoassays based on the agglutination of latex particles can not meet this requirement. There is a need to develop specific method for multiplex detection.

Fluorescence-encoded microbeads have been prepared by encoding fluorescence dyes or quantum dots (QDs) into microbeads using different methods and applied in the immunoassays for biodetection.[215, 216, 219, 298, 299] For example, various fluorescent polystyrene microbeads with the average diameter of 9.2 μm were synthesised. A high concentration of fluorescent dyes, such as rhodamine 101 and acridine orange, was present on polystyrene microspheres by gradual solvent evaporation method, resulting in the formation of fluorescent beads with high intensity.[299] Polymer microbeads encoded with fluorescence dyes were employed to provide optical identification for the detection of human cytokines during the flow cytometric immunoassays.[211, 213] Microbeads were encoded with fluorescence dyes (R6G) and applied on the detection of human alpha fetoprotein antigen in a suspension assay. The detection limit reached 80 pg mL^{-1}.[215] QDs also can be used for microbead encoding. The QDs have a wide excitation and narrow emission, which are brighter and more photostable than

fluorescence dyes, making them more attractive for optical encoding. Multiplexed coding microbeads have been prepared using QDs by Nie's group.[216] Since then, various QDs-barcoded polymer microbeads have been fabricated and applied on immunoassay.[217-220]

However, there are some limitations using fluorescence labels in polymer microbead coding, including photobleaching and broad emission of organic dyes, surface modification problem and safety issues of QDs.[226] In comparison, Raman spectroscopic-encoded polymer microbeads have shown many advantages over fluorescence-encoded polymer microbeads, such as narrow vibration spectra, photo-stability, and high sensitivity. Furthermore, polymer microbeads contain many repeat units (monomers), which display specific Infrared and Raman fingerprint information. Different polymer microbeads with unique spectroscopic information can be produced by changing the repeat units during the polymerisation process, which allows the potential applications of polymer microbeads for multiplex detection.

Twenty-five polystyrene-poly(ethylene glycol) graft copolymers, obtained using six monomers: styrene, 2,5-dimethylstyrene, 4-methylstyrene, 2,4-dimethylstyrene, 4-tert-butylstyrene, and 3-methylstyrene, have been successfully synthesised using suspension polymerisation.[185] These microbeads can be used to build up the barcoded system by charactering their Raman and infrared fingerprints.[300] They have also been applied for antigen detection for high-throughput multiplex assays.[18] Moreover, 630 copolymer microbeads with unique vibration fingerprints can be obtained by increasing the styrene monomers to fifteen, which enable to generate large libraries of barcoded resins.[17] However, large particle size and broad size distribution are crucial issues, which hinder their application in flow cytometric-based detection. Because common flow cytometry

normally measured the microbeads in size range between 0.2 to 150 μm.[301] Therefore, monodisperse polymer microbeads with unique vibrational information are required to be synthesised for high-throughput analysis.

Surfactant-free emulsion polymerisation and dispersion polymerisation can be used to synthesise monodisperse polymer microbeads with different particle sizes. Generally, surfactant-free emulsion polymerisation produces uniform microbeads with small particle sizes (50-1000 nm) and dispersion polymerisation can generate monodisperse polymer particles with large particle size ranging from 1 to 15 μm.[184] In a typical dispersion polymerisation process, monomers, initiator, stabiliser are dissolved completely in solvent and then react to form polymer particles, which are insoluble in solvent. Reaction parameters, such as monomers, stabiliser, solvent, stirring speed, and temperature are important factors influencing the particle sizes and molecular weights of polymer particles, and the kinetics of dispersion polymerisation process.[200] The polymerisation of styrene and methyl methacrylate has been studied using this technique.[201-204, 302] Poly(styrene-*co*-4-vinylpyridine) copolymer microbeads were also fabricated using dispersion polymerisation.[303] However, there is still lack of studies on the fabrication of copolymer microbeads with both narrow particle size distribution and unique spectroscopic information.

This study aims to produce copolymer microbeads not only with narrow size distribution, but also with specific Raman spectrum signatures using dispersion polymerisation. Styrene (Sty), 4-tertbutylstyrene (4tBS), and 4-methylstyrene (4MS) were chosen as model monomers to prepare different Raman spectroscopic-encoded copolymer microbeads through dispersion polymerisation process.

7.2 Experimental Section

7.2.1 Materials

Styrene (Sty), Triton X-305 (70% in H_2O), polyvinylpyrrolidone (PVP 360 000), 4-tert-butylstyrene (4tBS), and 4-methylstyrene (4MS) were purchased from Sigma-Aldrich. Acrylic acid (AA) and 2, 2'-azobis (2-methylpropanitrile) (AIBN) were supplied by Acros organics. Absolute ethanol was supplied by Merck. All the chemicals were used as received without any further purification.

7.2.2 Preparation of Copolymer Microbeads by Dispersion Polymerisation

The monodisperse copolymer microbeads were synthesised using dispersion polymerisation according to the reported procedure with some modification.[206] In a typical two-stage polymer microbead preparation, Sty and comonomer (6.0 g), initiator (0.24 g AIBN, 4 wt% to monomers), stabilisers (0.27 g PVP 360 000 and 0.30 g 70% Triton X-305), and 34 g 95% ethanol were charged to a 250 mL three-neck flask equipped with nitrogen inlet/outlet, condenser and mechanical stirrer. The mixture was degassed with bubbling nitrogen gas at room temperature for 40 min and then merged into a 70 °C oil bath. The stirring speed was fixed at 100 rpm. After the reaction was conducted for one hour, functional monomer AA (0.12 g), dissolved in 16 g 95% ethanol, was injected to the reaction system and the polymerisation was continued for another 24 h under the protection of nitrogen atmosphere.

7.2.3 Characterisation

The morphologies of synthesised polymer microbeads were monitored using a Phillips XL30 scanning electron microscope (SEM) operating at an accelerating voltage of 10

kV. More than 100 microbeads were counted to calculate the average size using an ImageTool version 3.0. The number-average diameter (D_{n}) and the coefficient of variation (CV) of the particles were calculated according to the following formula:[304]

$$D_{\mathrm{n}} = (\sum n_i d_i / n_i) \tag{7.1}$$

$$CV = \frac{\left(\sum\left(d_i - (\sum n_i d_i / \sum n_i)\right)^2 / \sum n_i\right)^{1/2}}{(\sum n_i d_i / \sum n_i)} \times 100 \tag{7.2}$$

where n_i is the number of microbeads with the diameter d_i.

The conversion was calculated gravimetrically. A small amount of sample was weighted and dried under oven at 65 °C until no changing of weight. The samples for Raman measurements were washed three times with 95% ethanol and dried at 65 °C for 24 h. Raman spectra of polymer microbeads were monitored using a Peak Seeker Pro™ Raman spectrometer equipped with a 200 mW 785 nm laser. The integration time is 3 s for all the measurements.

7.3 Results and Discussion

Figure 7.1 presents the chemical structures of monomers used for the synthesis of polymer microbeads in this study. All monomers contain vinyl group, which allows monomers to be synthesised through addition polymerisation. The characteristics of Raman spectra of three monomers used in the synthesis of copolymer microbeads are depicted in Figure 7.2. Each of them has unique Raman spectrum and can be easily distinguished from each other. Successful fabrication of copolymer microbeads with these monomers will allow a large pool of potential microbeads with specific Raman spectroscopic information. In this study, different Raman spectroscopic-encoded copolymer microbeads were fabricated by dispersion polymerisation, because

dispersion polymerisation is able to produce highly monodisperse polymer microbeads with 1-15 μm.

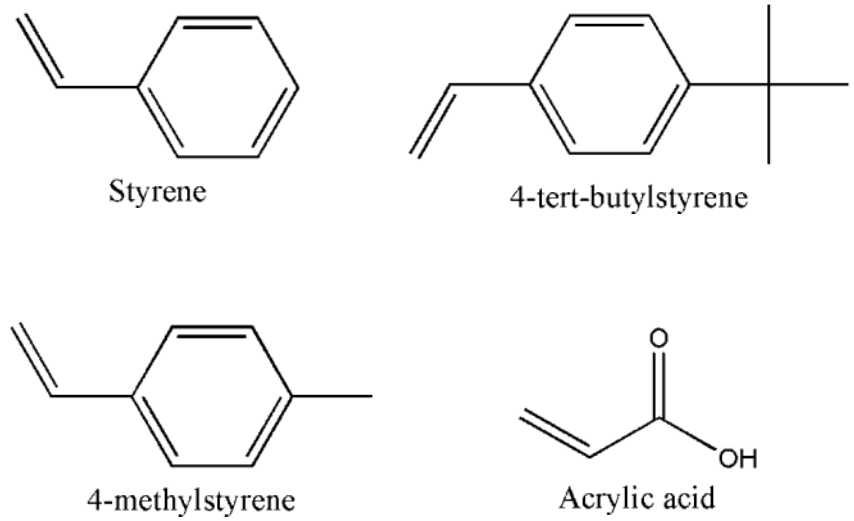

Figure 7.1 Chemical structures of different monomers used for the synthesis of Raman spectroscopic-encoded microbeads.

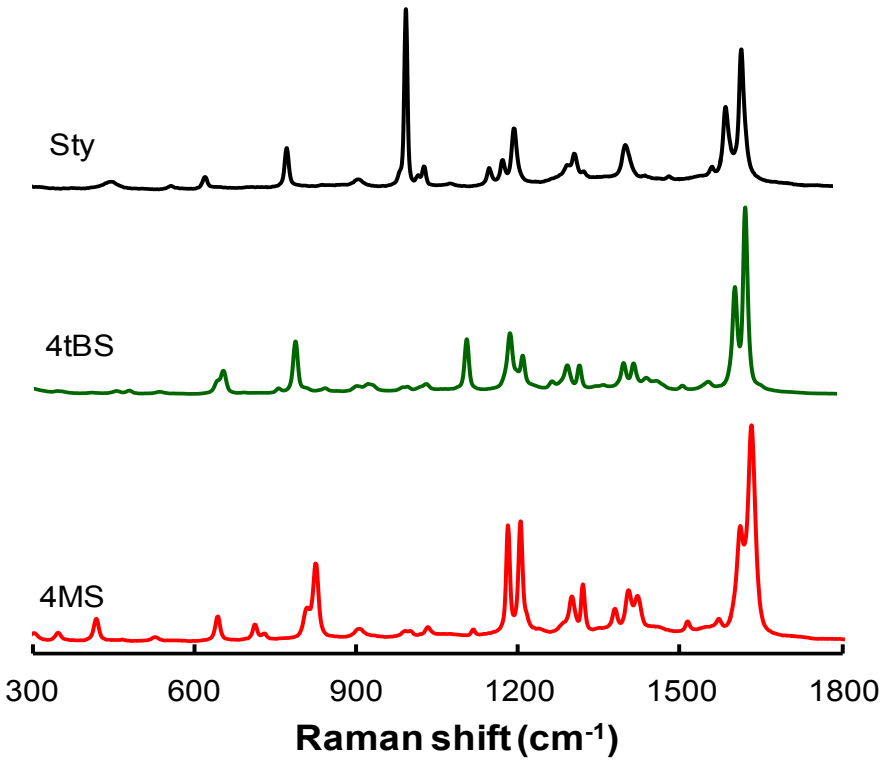

Figure 7.2 Raman spectra of different monomers used.

7.3.1 Poly(Sty-4tBS-AA) Microbeads

The poly(Sty-4tBS-AA) microbeads with various concentrations of 4tBS were synthesised by two-stage dispersion copolymerisation. The AA comonomer (2 wt% to Sty) was used to introduce surface functional groups on copolymer microbeads. The SEM images of poly(Sty-4tBS-AA) copolymer microbeads are presented in Figure 7.3, which shows that the synthesised copolymer microbeads are highly monodispersed. Varying the 4tBS concentrations from 0 wt% to 100 wt%**,** copolymer microbeads with narrow size distribution were obtained.

The weight ratio of Sty/4tBS, conversion and the size of the copolymer microbeads synthesised are listed in Table 7.1. The conversions for all reactions are more than 94% corresponding to the 4tBS concentration of 0-100 wt%. The average sizes (D_{n}) of the poly(Sty-4tBS-AA) copolymer microbeads do not change too much with the average diameters between 1.07-1.60 μm. For all the microbeads, the coefficients of variation (CV) of the microbeads are less than 5%, indicating the monodispersity of the synthesised copolymer microbeads.

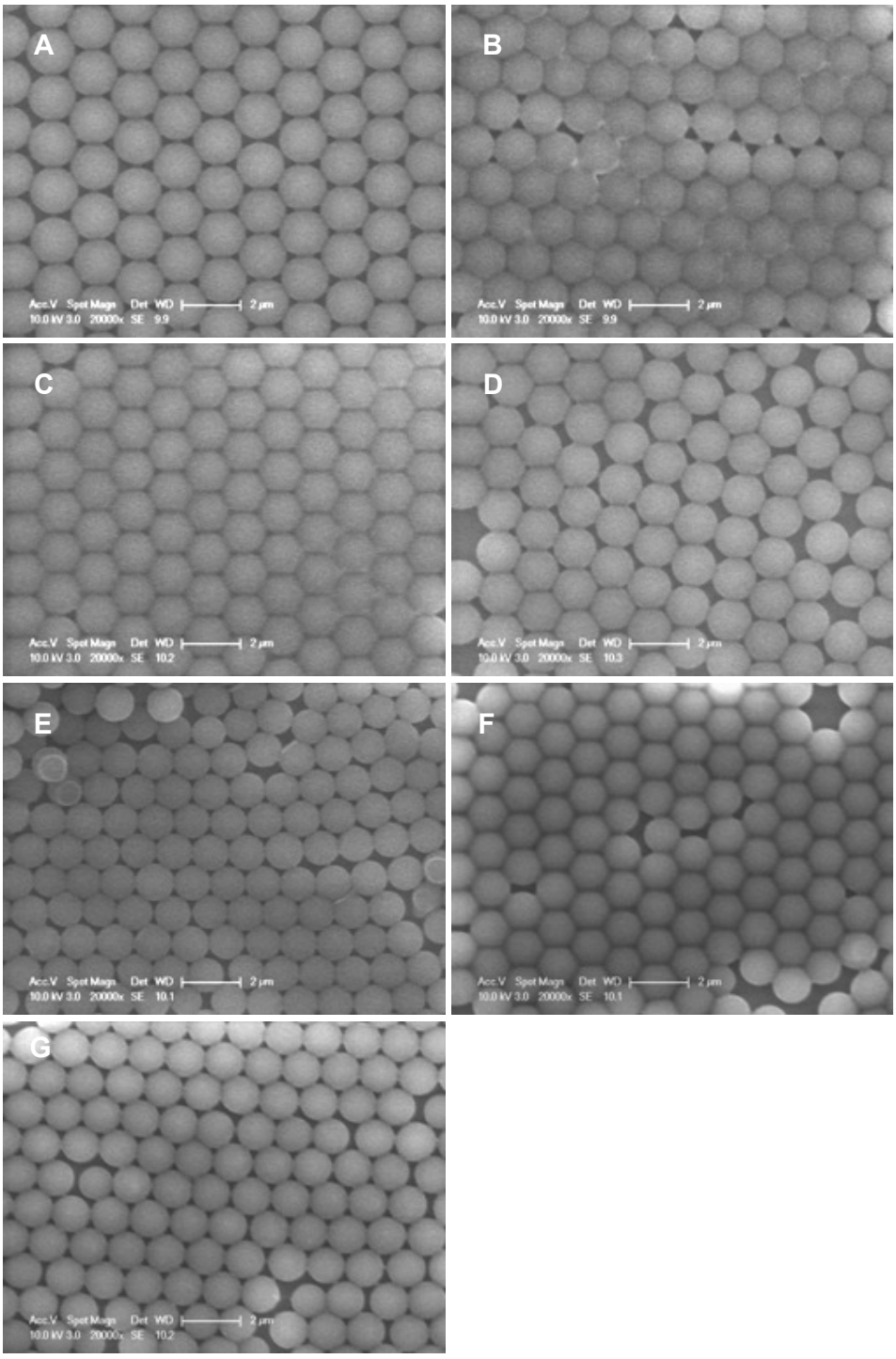

Figure 7.3 SEM images of various poly(Sty-4tBS-AA) microbeads in the presence of different concentrations of 4tBS: A: 0, B: 5, C: 10, D: 25, E: 50, F: 75, G: 100 wt% with respect to the amount of Sty monomer. AA was 2 wt% to Sty.

Table 7.1 Conversion, D_n and CV of poly(Sty-4tBS-AA) microbeads prepared with various concentrations of 4tBS through two-stage dispersion polymerisation.

Sample	Sty/4tBS (wt%)	Conversion (%)	D_n (μm)	CV (%)
A	100/0	96	1.60	1.9
B	95/5	97	1.43	3.0
C	90/10	98	1.40	2.9
D	75/25	97	1.37	3.6
E	50/50	97	1.07	4.7
F	25/75	94	1.14	3.5
G	0/100	96	1.18	4.2

Raman spectrometer was used to investigate the Raman spectroscopic information of the synthesised copolymer microbeads, as displayed in Figure 7.4. The Raman vibrational information of Sty monomer and poly(Sty-AA) microbeads are listed in Table 7.2 and the peak assignments of Raman spectra of 4tBS monomer, poly(4tBS-AA), and poly(Sty-4tBS-AA) microbeads are presented in Table 7.3. At low concentrations of 4tBS ranged as 0-10 wt%, only the Raman peaks of Sty can be observed in Figure 7.4A-C. The characteristic bands of Sty at 999 cm^{-1} and 1029 cm^{-1} are assigned to α and α+β vibrations of Sty. There is no difference observed between the Raman spectra of poly(Sty-AA) (Figure 7.4A) and poly(Sty-4tBS-AA) microbeads at 5 and 10 wt% 4tBS concentrations (Figure 7.4B and C). By increasing the concentration of 4tBS to 25 wt% (Figure 7.4D), extra signals corresponding to 4tBS at 641 cm^{-1} and 1107 cm^{-1} are found, but with very low intensities. They are assigned to the α and ν_a(CC) of 4tBS. The intensities of these two points increase with the increase of 4tBS concentration and more Raman signals belonging to 4tBS can be detected, such as 793,

922 and 1610 cm^{-1} (Figure 7.4E and F). At 100 wt% 4tBS (Figure 7.4G), only the peaks of 4tBS can be observed. The poly(4tBS-AA) microbeads in the absence of Sty show totally different Raman fingerprints compared with poly(Sty-AA) microbeads. In all case, AA can not be monitored due to their low concentration (2 wt% with respect to the amount of Sty monomer). Therefore, three kinds of copolymer microbeads with unique Raman signatures, poly(Sty-AA), poly(Sty-4tBS-AA), and poly(4tBS-AA), can be obtained by varying the concentrations of Sty and 4tBS during the polymerisation.

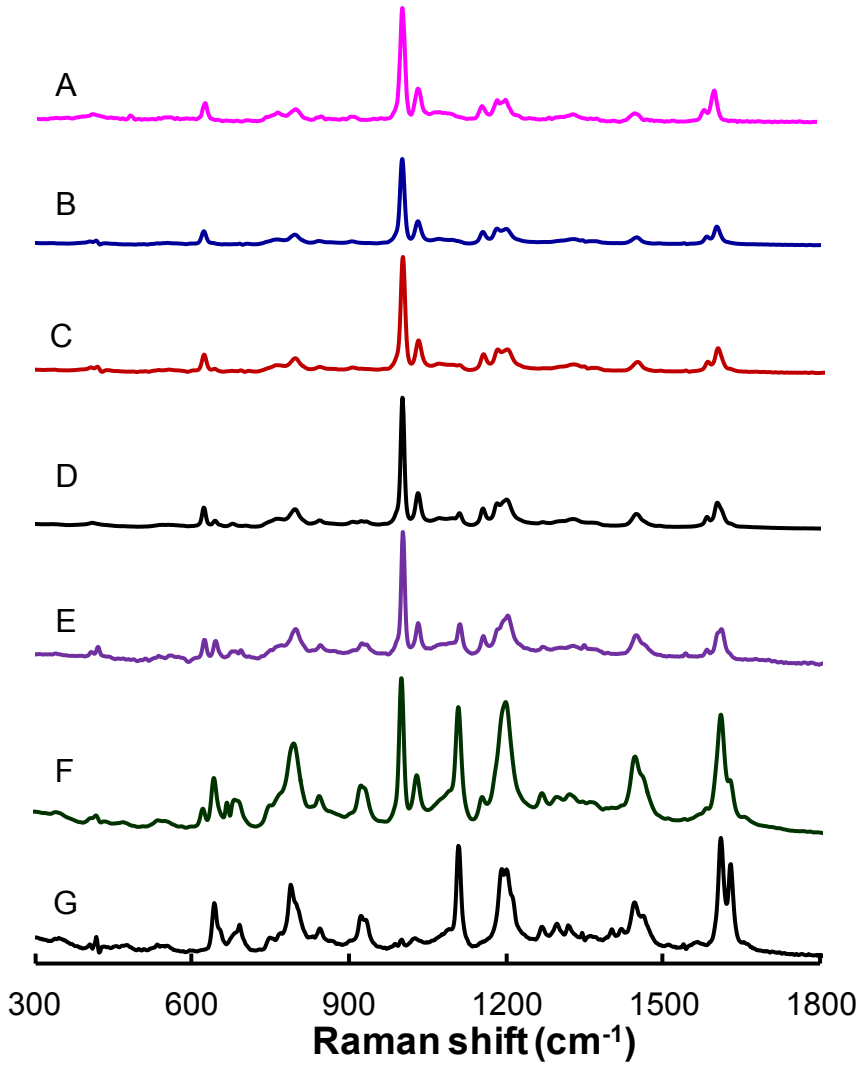

Figure 7.4 Raman spectra of poly(Sty-4tBS-AA) microbeads with various concentrations of 4tBS: A: 0, B: 5, C: 10, D: 25, E: 50, F: 75, G: 100 wt% with respect to the amount of Sty monomer.

Table 7.2 Raman vibrational information of Sty monomer and poly(Sty-AA) microbeads.

Sty monomer		Poly(Sty-AA)		Peak assignment[185]
Raman (cm^{-1})	Intensity	Raman (cm^{-1})	Intensity	
1631	s			γ(829+826)
1600	s	1603	s	α+β
1576	w	1584	m	α+β
		1449	m	α+β, $\delta_s(C' H_2)$
1411	m			-
		1328	w	β
1314	w			-
1200	s	1199	m	ν(CC')+α
1181	w	1182	m	α+β
1154	w	1154	m	α+β
1031	w	1030	s	α+β
997	s	1000	s	α
907	w	904	w	γ
		794	m	α
772	m			-
		760	w	γ
618	s	620	s	α

s, strong; m, medium; w, weak; α, in–plane ring deformation; β, in–plane ring bending; γ, out–of–plane ring bending; δ, deformation; ν, stretch; C, carbon in ring; C', carbon in chain; subscripts "s" , symmetric modes.

Table 7.3 Raman vibrational information of 4tBS monomer, poly(4tBS-AA), and poly(Sty-4tBS -AA) microbeads.

4tBS monomer		Poly(4tBS-AA)		Poly(Sty-4tBS-AA) (25/75 wt%)		Peak assignment[185]
Raman (cm^{-1})	Intensity	Raman (cm^{-1})	Intensity	Raman (cm^{-1})	Intensity	
1630	s	1630	s	1629	w	γ(829+826)
1611	s	1611	s	1610	s	α+β
		1462	w			$\delta_a(CH_3)$
		1446	s	1447	s	$\delta_s(CH_2)$
1420	m	1420	w			-
1402	m	1402	w			-
1318	m	1318	w	1322	w	-
1297	m	1297	w			-
1267	w	1267	w	1268	w	ν_a(CC in *t*-Bu)+rk(CH_3)
1212	s	1200	s	1199	s	ν(CC)+α
1188	s	1190	s			ν_s(CC in *t*-Bu)+rk(CH_3), ν(CC)+α
				1154	w	α+β
1107	s	1107	s	1108	s	ν_a(CC)
				1029	s	α+β
				999	s	α
		920	m	922	s	ν_s(CC)+ rk(CH_3)
		842	w	842	w	γ
786	s	786	s			α
				793	s	α
		688	m	680	m	α

				665	m	-
651	m					-
		640	s	640	s	α
				619	w	α

s, strong; m, medium; w, weak; α, in–plane ring deformation; β, in–plane ring bending; γ, out–of–plane ring bending; δ, deformation; ν, stretch; rk, rocking; C, carbon in ring; C', carbon in chain; subscripts "s", symmetric modes; subscripts "a", asymmetric modes.

7.3.2 Poly(Sty-4MS-AA) Microbeads

Figure 7.5 shows the morphologies of copolymer microbeads with different amounts of 4MS. Monodisperse poly(Sty-4MS-AA) microbeads could be fabricated using two-stage dispersion polymerisation at different concentrations of 4MS (25-100 wt% with respect to the amount of Sty monomer). The conversion, average size (D_n) and coefficient of variation (CV) of the synthesised microbeads are summarised in Table 7.4. The conversions for all the polymerisation are higher than 91% and the average diameters of poly(Sty-4MS-AA) microbeads are between 1.20-1.69 μm. Less than 5% CVs also indicate the highly monodispersity of synthesised poly(Sty-4MS-AA) microbeads at various concentrations of 4MS.

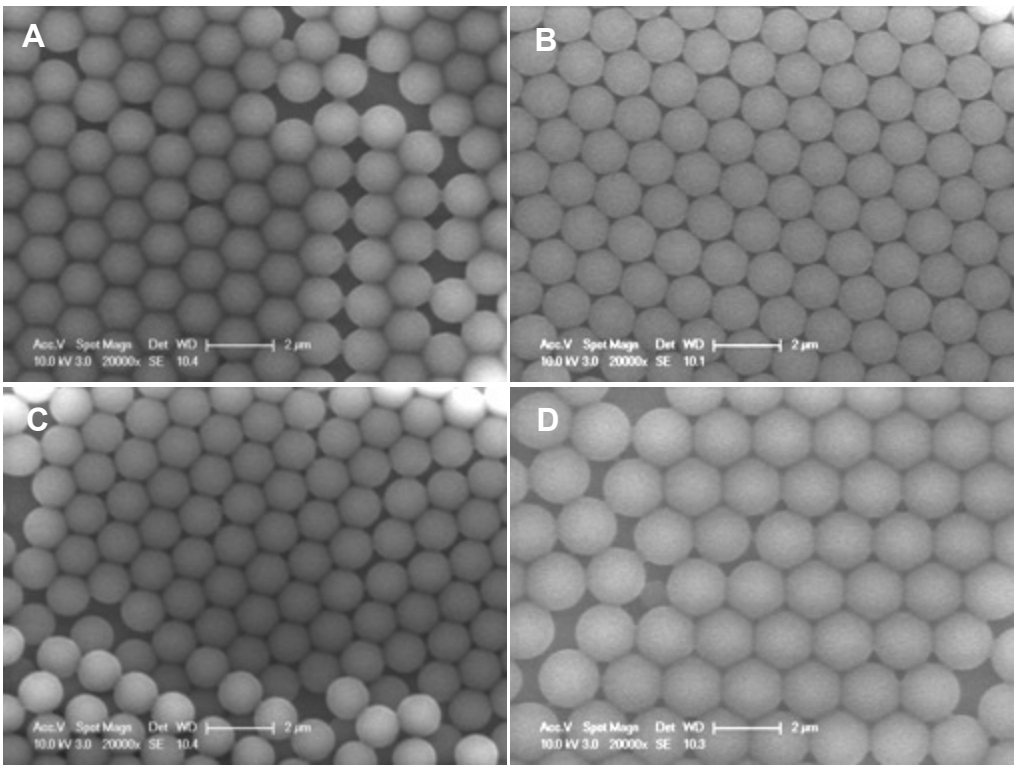

Figure 7.5 SEM images of poly(Sty-4MS-AA) microbeads with various concentrations of 4MS: A: 25, B: 50, C: 75, D: 100 wt% with respect to the amount of Sty monomer.

Table 7.4 Conversion, D_n and CV of poly(Sty-4MS-AA) synthesised with various concentrations of 4MS.

Sample	Sty/4MS (wt%)	Conversion (%)	D_n (μm)	CV (%)
A	75/25	92	1.26	3.2
B	50/50	96	1.30	3.8
C	25/75	91	1.20	2.5
D	0/100	95	1.69	4.7

The Raman spectra of poly(Sty-4MS-AA) microbeads are presented in Figure 7.6. The Raman assignments for monomer (4MS), polymer (Poly(4MS-AA) microbeads), and copolymer (Poly(Sty-4MS-AA) microbeads at 25/75 wt% of Sty/4MS) are presented in Table 7.5. The most intensified Raman bands of 4MS monomer are at 806, 822, 1179, 1203, 1378, and 1610 cm^{-1}, which can be measured on polymer at 807, 827, 1183, 1202, 1377, and 1614 cm^{-1}. They are assigned to α, α, α+β, ν(CC')+α, $\delta_s(CH_3)$ and α+β of 4MS, respectively. This can be used to distinguish the poly(Sty-4MS-AA) microbeads with poly(Sty-AA), poly(Sty-4tBS-AA), and poly(4tBS-AA) microbeads. At 25 wt% concentration of 4MS (Figure 7.6A), the Raman spectrum is dominated by Sty with two strong peaks at 999 cm^{-1} and 1029 cm^{-1} and the peaks of 4MS are relatively weak. With the increase of 4MS concentrations to 50 and 75 wt%, the peaks of 4MS become stronger (Figure 7.6B and C). In Figure 7.6D, at 100 wt% concentration of 4MS, the featured peaks at 999 cm^{-1} and 1029 cm^{-1} for Sty disappear and the Raman spectrum only shows the vibrational information of 4MS, which is totally different from poly(Sty-4MS-AA) microbeads. Hence, poly(Sty-4MS-AA) and poly(4MS-AA) microbeads with

different Raman signatures can be produced using 4MS and Sty following two-stage dispersion polymerisation.

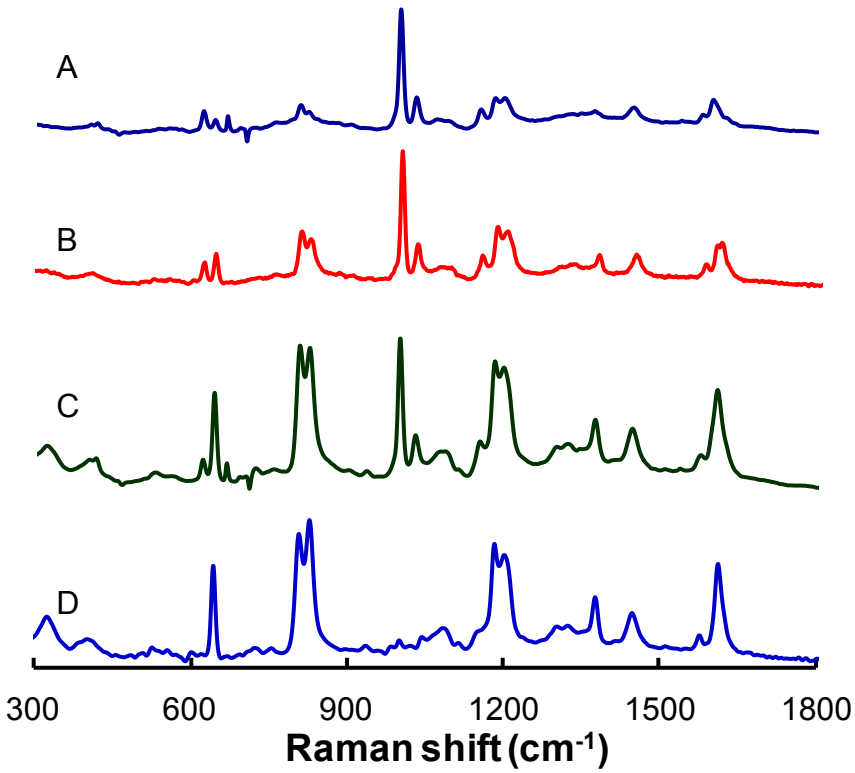

Figure 7.6 Raman spectra of Poly(Sty-4MS-AA) microbeads with various concentrations of 4MS: A: 25, B: 50, C: 75, D: 100 wt% with respect to the amount of styrene monomer.

Table 7.5 Raman vibrational information of 4MS monomer, poly(4MS-AA), and poly(Sty-4MS-AA) microbeads.

4MS monomer		Poly(4MS-AA)		Poly(Sty-4MS-AA) (25/75 wt%)		Peak assignment[185]
Raman (cm^{-1})	Intensity	Raman (cm^{-1})	Intensity	Raman (cm^{-1})	Intensity	
1631	s					γ(829+826)
1610	s	1614	s	1612	s	α+β
1571	w	1578	w	1580	w	α+β
1513	w					α+β
		1448	s	1448	s	$\delta_a(CH_3)$, $\delta_s(C'H_2)$
1418	m					α+β
1402	m					-
1378	m	1377	s	1376	s	$\delta_s(CH_3)$
1318	s	1324	w	1323	w	-
1297	m	1303	w	1302	w	-
1203	s	1202	s	1200	s	ν(CC')+α
1179	s	1183	s	1184	s	α+β
				1154	m	α+β
1116	w					α+β
		1084	m			-
1031	w			1029	s	α+β
				999	s	α
905	w					-
822	s	827	s	825	s	α
806	w	807	s	806	s	α
727	w					α
709	w					ϕ
				665	w	-

642	m	642	s	641	s	α
				619	w	α
526	w			528	w	ϕ
416	m			412	w	-
		398	w	400	w	-
346	w					-
		321	m	318	m	ϕ

s, strong; m, medium; w, weak; α, in–plane ring deformation; β, in–plane ring bending; γ, out–of–plane ring bending; ϕ, out–of–plane ring deformation; δ, deformation; ν, stretch; C, carbon in ring; C', carbon in chain; δ_s, symmetric deformation; δ_a, asymmetric deformation.

7.3.3 Poly(4tBS-4MS-AA) Microbeads

Poly(4tBS-4MS-AA) microbeads were also fabricated using dispersion polymerisation by the mixing ratio of 4tBS and 4MS at 50/50 wt%. The conversion for the preparation of poly(4tBS-4MS-AA) microbeads is almost 100%. Figure 7.7A shows the SEM image of resulting microbeads. The average size (D_n) of microbeads is 1.35 μm by analysing the SEM image. The coefficient of variation (CV) is 3%, indicating the highly monodispersity of poly(4tBS-4MS-AA) microbeads. The Raman spectrum and detailed vibrational information of poly(4tBS-4MS-AA) microbeads are presented in Figure 7.7B and Table 7.6, respectively. The featured peaks of both 4tBS and 4MS can be found in the poly(4tBS-4MS-AA) microbeads. The strong Raman signals at 1108 and 1199 cm^{-1} are assigned to ν_a(CC) and ν(CC')+α of 4tBS, while the peaks at 806 and 823 cm^{-1} are associated with α vibration of 4MS. There are also more peaks assigned to 4tBS or 4MS listed in Table 7.6. The result shows that the synthesised poly(4tBS-4MS-AA)

microbeads have unique Raman signatures, which is different from the poly(4tBS-AA) and poly(4MS-AA) microbeads.

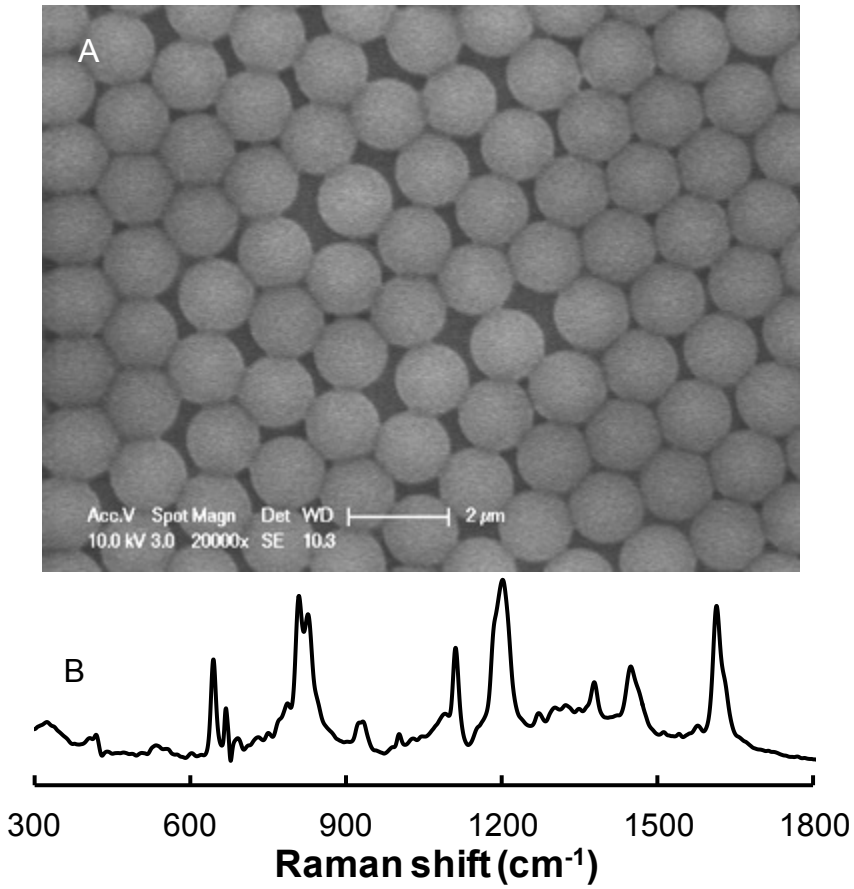

Figure 7.7 SEM image and Raman spectrum of poly(4tBS-4MS-AA) microbeads fabricated at 50/50 wt% of 4tBS and 4MS.

Table 7.6 Raman vibrational information of poly(4tBS-4MS-AA) microbeads.

Poly(4tBS-4MS-AA) (50/50 wt%)		Peak assignment	Belong to
Raman (cm^{-1})	Intensity		
1613	s	α+β	4tBS; 4MS
1578	w	α+β	4MS
1447	s	$\delta_a(CH_3)$, $\delta_s(C'H_2)$	4tBS; 4MS
1378	m	$\delta_s(CH_3)$	4MS
1199	s	$\nu(CC')$+α	4tBS
1108	s	$\nu_a(CC)$	4tBS
929	m	$\nu_s(CC)$+rk(CH_3)	4tBS
823	s	α	4MS
806	s	α	4MS
688	w	α	4tBS
665	m	-	4MS
641	s	α	4tBS; 4MS
530	w	ϕ	4MS
414	w	-	4MS

s, strong; m, medium; w, weak; α, in–plane ring deformation; β, in–plane ring bending; ϕ, out–of–plane ring deformation; δ, deformation; ν, stretch; rk, rocking; C, carbon in ring; C', carbon in chain; δ_s, symmetric deformation; δ_a, asymmetric deformation.

7.4 Summary

In this Chapter, various spectroscopic-encoded microbeads with narrow size distribution and unique Raman signatures were synthesised by dispersion polymerisation approach. The conversions for all the monodisperse Raman spectroscopic-encoded microbeads are

higher than 91% and the coefficients of variation are less than 5%. Poly(Sty-4tBS-AA) microbeads can be synthesised with different concentrations of comonomer 4tBS. At low 4tBS concentrations, only the Raman peaks of Sty can be monitored. When the concentration of 4tBS reaches 25 wt%, the Raman peaks of 4tBS and Sty can be observed in the copolymer microbeads and the intensity of Raman peaks of 4tBS increases with the increasing 4tBS concentration. Poly(Sty-4MS-AA) microbeads at four different concentrations of 4MS were also fabricated with narrow size distribution and unique Raman signatures. Furthermore, monodisperse poly(4tBS-4MS-AA) microbeads with unique Raman signatures can be prepared using the mixing ratio of 4tBS and 4MS at 50/50 wt%.

CHAPTER 8 Polystyrene Microbead-based Immunoassays using Flow Cytometry and Surface Enhanced Raman Scattering

8.1 Introduction

Rapid, high-throughput and multiplex detection is ungently required for the effective detection and treatment of life-threaten human diseases. Flow cytometry is an effective tool for counting and sorting cells/microspheres in a short period of time.[305] High-throughput detection methods based on flow cytometry are widely used in health related research. Thousands of cells or particles in suspension can be analysed per second, which provides the high-speed quantitative measurements of analytes. Microspheres are fascinating materials and have been considered as the solid support for various molecular reactions. After the conjugation of molecules on the surface of microspheres, the analytes are captured and recognised accordingly by a fluorochrome-conjugated detection molecule using flow cytometry.[212] Dyes and quantum dots have been used to prepare fluorescent microbeads for flow cytometric analysis.[306, 307] The combination of different fluorescent microbeads allows us to simultaneously measure several analytes in one test tube, which offers significant influence on the multiplex detection of analytes.[211, 213, 308] Because conventional flow cytometry-based approach typically performs by the detection of fluorescence signals, it is limited by photobleaching, broad emission spectra, spectral overlapping, and different excitation wavelengths of fluorophores.

A great deal of effort has been given to explore new methods for bioassays. One approach is to develop Raman-based flow cytometry. Unlike conventional fluorescence flow cytometry, Raman-based flow cytometry is based on the measurement of Raman information in a flow cytometric system.[309-313] Raman vibrational information is dependent on the structures of molecules and no photobleaching. Moreover, the narrow Raman bands allow us to distinguish a variety of molecules with high similarity, which is extremely important for multiplex detection. To date, Raman and surface enhanced Raman scattering

(SERS) have been extensively studied for chemical detection and bioapplications.[5, 7, 9, 30, 35] Raman signals of molecules will be significantly enhanced after the formation of self-assembled monolayer (SAM) on the surface of metal nanoparticles/nanostructures.

High-throughput spectral flow cytometers capable of acquiring Raman spectra of individual particles in flow system have recently been reported. For example, Sebba *et al.* presented a flow spectroscopy-based approach for high throughput analysis of individual surface-enhanced resonant Raman scattering (SERRS) tags by measuring Rayleigh and Raman scattering of single tags. Hundreds of nanoparticles can be analysed per second using this approach.[314] Goddard *et al*. demonstrated an approach for the spectral analysis of individual SERS-active nanoparticle in flow systems. They used a full spectral Raman flow cytometer to investigate the SERS tag populations.[315] This approach enables to simultaneously acquire multiple optical parameters over thousands of individual SERS tags. Recently, AuNPs labelled with reporter molecules (malachite green isothiocyanate) were used to investigate the SERS spectrum of single nanoparticles in a flow-based system.[316] New technique for multiplex detection could be developed based on those studies by analysing the spectral information of individual cell or particle.

In our previous study, large and polydisperse polystyrene microbeads have been prepared using suspension polymerisation for microbead-based Raman/SERS immunoassay, which have the following advantages: label-free, no photobleaching, high sensitivity, and highly multiplexed. The specific recognition between antibody-conjugated PS microbeads and antigen-conjugated AuNPs has been examined by both fluorescence and Raman analysis. There is a possibility that Raman-activated flow cytometry could be developed based on the microbead-based Raman/SERS immunoassay system by taking advantages of flow

cytometry and Raman spectroscopic information obtained from polymer microbeads and SERS reporters.

The polymer microbeads prepared by suspension polymerisation were polydispersed with large particle size up to 600 μm, which can not be analysed using common flow cytometry. The size range measured for common flow cytometry is roughly 0.2 to 150 μm.[301] In order to apply flow cytometry for microbead sorting and develop Raman flow cytometry, small polymer microbeads should be used during the microbead-based Raman/SERS immunoassay. As we know from previous studies, dispersion polymerisation is a technique that can produce monodisperse microbeads with their sizes of 1-15 μm. Therefore, in this study, polystyrene (PS) microbeads were prepared using dispersion polymerisation and used to explore the microbead-based Raman/SERS immunoassay by the combination of flow cytometry and SERS techniques for immunoglobulin (IgG) detection.

8.2 Experimental Section

8.2.1 Materials

AffiniPure goat anti-rabbit IgG and DyLight^{TM}649-conjugated AffiniPure rabbit anti-human IgG (Ex/Em 652/670 nm) were purchased from Jackson ImmunoResearch (West Grove, PA). Gold (III) chloride trihydrate ($HAuCl_4 \cdot 3H_2O$), 4-mercaptobenzoic acid (4MBA), styrene (≥99%), Triton X-305 (70% in H_2O), polyvinyl pyrrolidone (PVP 360 000), and bovine serum albumin (BSA) were purchased from Sigma-Aldrich. *N*-(3-dimethylaminopropyl)-N'-ethylcarbodiimide hydrochloride (EDC), *N*-hydroxysuccinimide (NHS), 2, 2'-azobis (2-methylpropanitrile) (AIBN), and acrylic acid (AA) were obtained from Acros organics. Trisodium citrate dehydrate (Na_3Ct) was supplied by Prolabo.

8.2.2 Preparation of Carboxylated Polystyrene Microbeads

A two-stage dispersion polymerisation was used to prepare monodisperse PS microbeads with carboxyl groups on surface.[206] In the first step, 0.24 g AIBN (initiator), 0.27 g PVP 360 000 (stabiliser), 0.30 g Triton X-305 (co-stabiliser), 6.0 g styrene (monomer) and 34 g 95% ethanol were poured into a 250 mL three-neck flask equipped with nitrogen inlet/outlet, condenser and mechanical stirrer. The solution was stirred and deoxygenated by nitrogen bubbling for 40 min at RT, followed by merging into a preheated oil bath at 70 °C. The mechanical stirrer speed was fixed at 100 rpm. In addition, 0.12 g AA was dissolved in 16 g 95% ethanol. One hour later, the AA solution was heated to 70 °C and immediately injected to the reaction solution. After that, the reaction was maintained at 70 °C for another 24 h. The PS microbead solution was washed by 95% ethanol three times and redispersed in 95% ethanol for further characterisation.

8.2.3 Preparation of AuNPs

The gold nanoparticles (AuNPs) were prepared according to literature.[109] An amount of 50 mL 10^{-3} M $HAuCl_4 \cdot 3H_2O$ aqueous solution was heated to boil under vigorous stirring, following by the rapid addition of 1% sodium citrate aqueous solution by controlling the molar ratio of $HAuCl_4 \cdot 3H_2O/Na_3Ct$ at 1:1.5. The light yellow solution quickly turned to colourless, black, and then changed to purple. The resulting mixture was boiled for another 15 min and cooled down to room temperature. The total volume was adjusted to 50 mL using DI water.

8.2.4 Conjugation of Antibodies with Polymer Microbeads

One hundred microlitres of 1.9 wt% purified PS microbeads and 100 μL EDC/NHS/PBS solution (20 mg of EDC and 30 mg of NHS in 1 mL of phosphate buffer saline (PBS, pH 7.4)) were mixed for 15 min at room temperature (RT), followed by the addition of 10 μg of antibodies (goat anti-rabbit IgG). The mixture solution was incubated at RT for 2 h with gentle rotation and then quenched using 1 M hydroxylamine. The antibody-conjugated polymer microbeads were washed with phosphate buffer (0.01 M sodium phosphate, 0.25 M NaCl, pH 7.6) three times and blocked using 1 mL blocking solution (50 mM Tris, 0.14 M NaCl, 1% BSA, pH 8.0) for 30 min at RT. The microbeads were then washed four times using wash solution (50 mM Tris, 0.14 M NaCl, 0.05% Tween 20, pH 8.0). Finally, the antibody-conjugated microbeads were redispersed in 100 μL DI water. The same as the procedure for the conjugation of goat anti-rabbit IgG with PS microbeads, 10 μg BSA was also conjugated to polymer microbeads as the control.

8.2.5 Absorption of Antibodies to AuNP surface

For the SAM preparation, 1 mL gold colloidal solution and 2.5 μL 10^{-3} M 4MBA in THF were mixed together and allowed to react for 2 min at RT. The mixture solution was centrifuged at 8 000 rpm for 2 min to remove any unreact 4MBA and redispersed in 100 μL DI water. Five microgram antibodies (DyLight^{TM}649 conjugated rabbit anti-human IgG) in phosphate buffer were charged to the SAM sample and standing for 2 h by gentle rotation at RT. A hundred microlitres of 10% BSA solution was added to the mixture and rotated for another 30 min. The solution was then centrifuged and washed three times using DI water, and redispersed in 100 μL DI water.

8.2.6 Immunoassays

Fifty microlitre antibody-conjugated PS microbeads were added to antibody-conjugated gold colloidal solution and allowed to react for 1 h at RT under gentle rotation. The solution was then washed several times using DI water at 3000 rpm, 2 min and dispersed in 50 μL DI water, followed by flow cytometric analysis and Raman analysis.

8.2.7 Characterisation

Absorption spectrum of AuNPs was recorded using Lambda Scientific LIUV-201 UV-Vis Spectrophotometer. The micrographs of AuNPs were taken using a Phillips CM200 TEM operating at 200 KV accelerating voltage. The images of polymer microbeads were taken using a Phillips XL30 SEM at an accelerating voltage of 10 kV. The potentiometric and conductometric titrations of carboxylated PS microbeads were carried out using a SmartCHEM-pH meter (TPS) and a HI8733 conductivity meter (HANNA Instruments) at RT. An amount of 1.0 M NaOH standard solution was used to adjust 120 mL PS microbead aqueous solution to pH about 10 and then back-titrated using 0.01 M HCl to pH around 4. Both conductivity and pH were recorded during the titration. Fluorescence properties of PS microbeads after the bioconjugation and immunoassay were analysed in a FACSCalibur flow cytometer (BD Biosciences). Confocal fluorescence microscope was used to further record the immunoassay results. The Raman spectra were measured using a XploRA Confocal Raman Microscope (HORIBA Scientific), equipped with three laser wavelengths at 532 nm, 638 nm and 785 nm. The samples were dropped onto the glass slide and focused under a long working distance 100× objective lens. The Raman signals were collected using the excitation wavelength at 638 nm. The acquisition time is 3 s.

8.3 Results and Discussion

8.3.1 PS Microbead Synthesis by Dispersion Polymerisation

Dispersion polymerisation technique was chosen to prepare monodisperse PS microbeads with surface carboxyl groups. The morphology of synthesised polymer microbeads produced was examined by SEM with typical images presented in Figure 8.1. The SEM results indicated that the PS microbeads prepared using dispersion polymerisation are monodispersed, and the average size of the polymer microbeads is 1.60 μm associated with a coefficient of variation (CV) of 2%. The calculated conversion was found to be 96% from weight analysis.

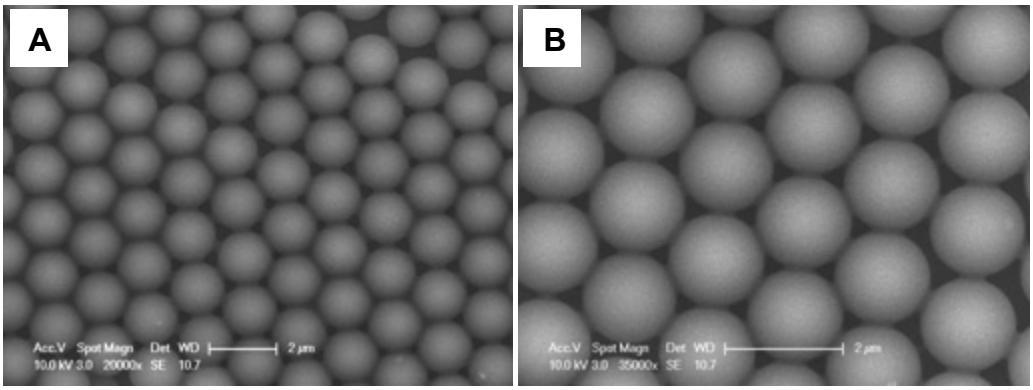

Figure 8.1 SEM images of polystyrene microbeads synthesised using dispersion polymerisation at different magnification. A. Low magnification and B. High magnification.

During the polymer microbead synthesis, AA was added to the reaction system as a functional monomer to generate carboxyl groups on the surface of polymer microbeads. The AA solution should be preheated before charging to the reactors to avoid reaction temperature fluctuation. After the polymerisation, polymer microbead suspension was

washed using ethanol for several times and redispersed in ethanol to remove any unreacted compound and small molecules.

Potentiometric and conductometric titrations were usually performed to characterise the carboxyl groups (–COOH) on the surface of microbeads. Both forward titration and back titration were done to investigate the carboxyl groups on the surface of latex particles and the result showed the quantity of surface carboxyl groups measured by back titration was slighter larger than the forward titration.[317] In this study, backward titration was performed by adjusting the pH of PS microbead suspension to 10 using NaOH. Under this condition, excess OH^- ions and COO^- ions are present in the solution. With the addition of HCl in the solution during backward titration, strong base groups are first neutralised with HCl, so the conductivity decreases quickly. After that, the neutralisation of COO^- ions starts and the conductivity of PS microbead solution changes slowly. After the complete reprotonation of COO^- to COOH, excess HCl gather in the solution resulting in an increase in conductivity. From the conductivity curves, the concentration of carboxyl groups on the microbead surface can be calculated.

Before titration: $COOH + OH^- \rightleftharpoons COO^- + H_2O$

Decreasing: $OH^- + H^+ \rightleftharpoons H_2O$

Changing slowly: $COO^- + H^+ \rightleftharpoons COOH$

Increasing: free ions of strong acid (HCl) present in solution

Figure 8.2 presents the pH and conductivity backward titration curves of the synthesised PS microbeads using 0.01 M HCl aqueous solution. Nitrogen gas was used to eliminate the influence of CO_2 in the titration process. The pH of PS microbead suspension kept decreasing from 10 to 4 with the addition of HCl. The conductivity curve can be divided

into three phases. In phase 1, the strong base groups (OH^-) were neutralised with HCl. Phase 2 indicated the neutralisation of carboxyl groups (COO^-), where the conductivity slightly changed. An increase of conductivity in phase 3 was caused by excess HCl added. By calculating the HCl amounts in Phase 2, the quantity of carboxyl groups can be determined. It is calculated from Figure 8.2 about 85.26% of the feed –COOH group of AA was found on the surface of the synthesised polymer microbeads. This result confirms that the surface of PS microbead contains enough carboxyl groups for the further attachment of antibodies to built immunoassays.

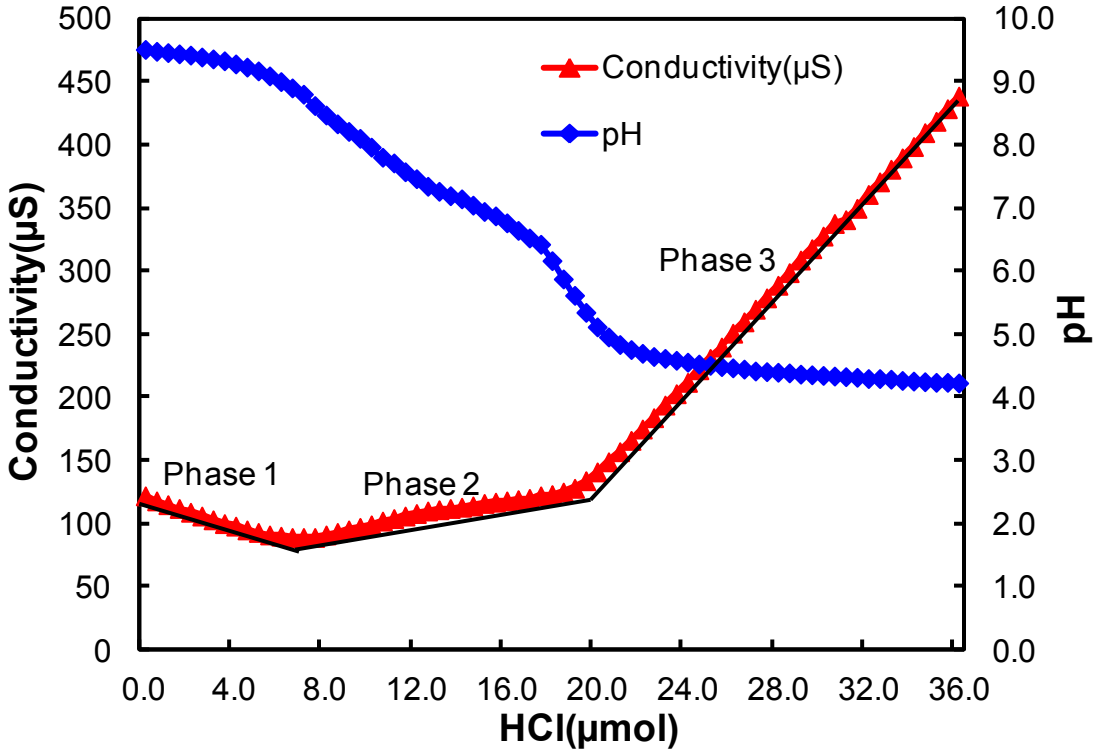

Figure 8.2 Potentiometric and conductometric backward titration curve of polymer microbeads with surface carboxyl groups using HCl standard solution at room temperature.

8.3.2 SERS Reporter Formation

AuNPs with an average particle size of 50 nm, which were proved having higher Raman effective enhancement factors than smaller AuNPs synthesised at the mixing ratio of 1:2 in Chapter 4, were synthesised by citrate reduction method. Figure 8.3 is the UV-Vis spectrum and TEM image of gold colloidal solution. The maximum plasmon band for 50 nm AuNPs is at 543 nm (Figure 8.3A) and the morphology of synthesised AuNPs is mostly irregular (Figure 8.3B). The detailed information for the formation of SAMs on AuNPs by 4MBA and the conjugation with antibodies during the immunoassay system has been described in Chapter 4.3.1. Raman-active molecules (4MBA) can easily form the SAMs on the surface of AuNPs to generate strong SERS signals. Antibodies (DyLight^{TM}649 rabbit anti-human IgG) were further adsorbed onto AuNPs, which is considered as SERS reporter during the immunoassay systems.

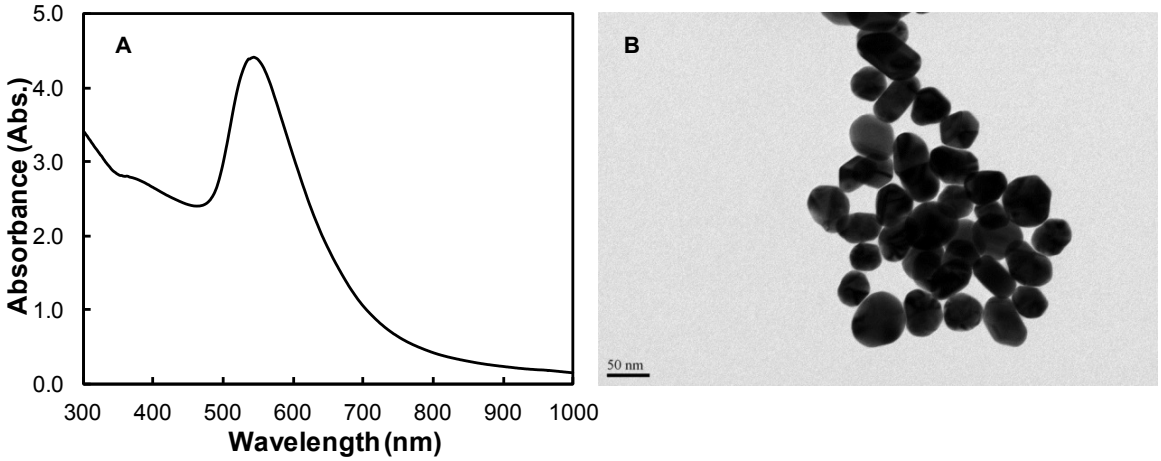

Figure 8.3 UV-Vis absorption spectrum (A) and TEM image (B) of AuNPs.

8.3.3 Immunoassays without AuNPs/4MBA

The preliminary study was first conducted using the immunoassay procedure without AuNPs/4MBA to check the specific recognition between goat anti-rabbit IgG and

DyLight^{TM}649 rabbit anti-human IgG on the PS microbeads. The investigation was achieved by mixing DyLight^{TM}649 rabbit anti-human IgG with goat anti-rabbit IgG conjugated PS microbeads or BSA conjugated PS microbeads for an hour at RT, followed by flow cytometry and confocal fluorescence microscope examination. It can be considered as the control experiments for the further investigation of microbead-based immunoassays using self-assembled and bioconjugated AuNPs as SERS reporters through flow cytometry and Raman analysis.

Figure 8.4 and Table 8.1 indicate PS microbeads (as control) and goat anti-rabbit IgG conjugated PS microbeads have no fluorescence signals (Figure 8.4A and B). When the DyLight^{TM}649 rabbit anti-human IgG was mixed with PS microbeads, they can attach to the surface of goat anti-rabbit IgG conjugated microbeads (Figure 8.4C), but can not attach to the surface of BSA conjugated microbeads (Figure 8.4D). Nearly all the goat anti-rabbit IgG conjugated PS microbeads (99.76%) show the fluorescence signals of DyLight^{TM}649 after the reaction. However, only 2.86% of BSA conjugated microbeads presented DyLight^{TM}649 signals, which might be due to minor non-specific binding. The results have also been verified using fluorescence microscope (Figure 8.5). After the addition of DyLight^{TM}649 rabbit anti-human IgG, all the goat anti-rabbit IgG conjugated PS microbeads can be seen under blue light illumination (Figure 8.5B), while no fluorescence signals can be observed for the BSA conjugated microbeads (Figure 8.5D). The results indicated that goat anti-rabbit IgG (antibody) can specifically recognise DyLight^{TM}649 rabbit anti-human IgG (antigen) during the flow cytometric immunoassays.

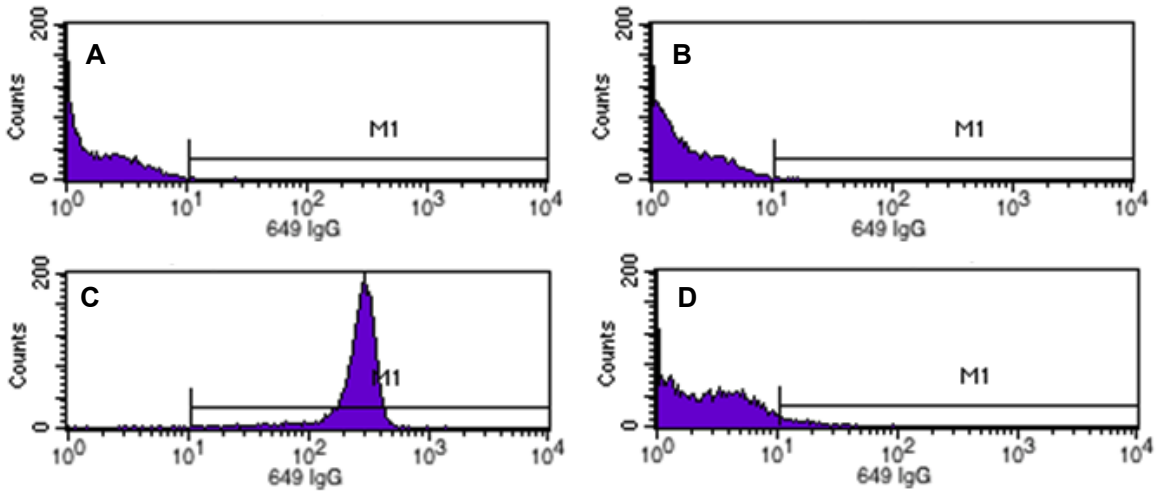

Figure 8.4 Fluorescence histograms of flow cytometric immunoassay results in the absence of AuNPs/4MBA. A: PS microbeads; B: PS microbeads-goat anti-rabbit IgG; C: PS microbeads-goat anti-rabbit IgG/DyLight^{TM}649 rabbit anti-human IgG; and D: PS microbeads-BSA/DyLight^{TM}649 rabbit anti-human IgG.

Table 8.1 Statistics for flow cytometric immunoassay results in the absence of AuNPs/4MBA.

Sample	**% Gated (FL4)**
PS microbeads (as control)	0%
PS microbeads-goat anti-rabbit IgG	0.07%
PS-goat anti-rabbit IgG/DyLight^{TM}649 rabbit anti-human IgG	99.76%
PS-BSA/DyLight^{TM}649 rabbit anti-human IgG	2.86%

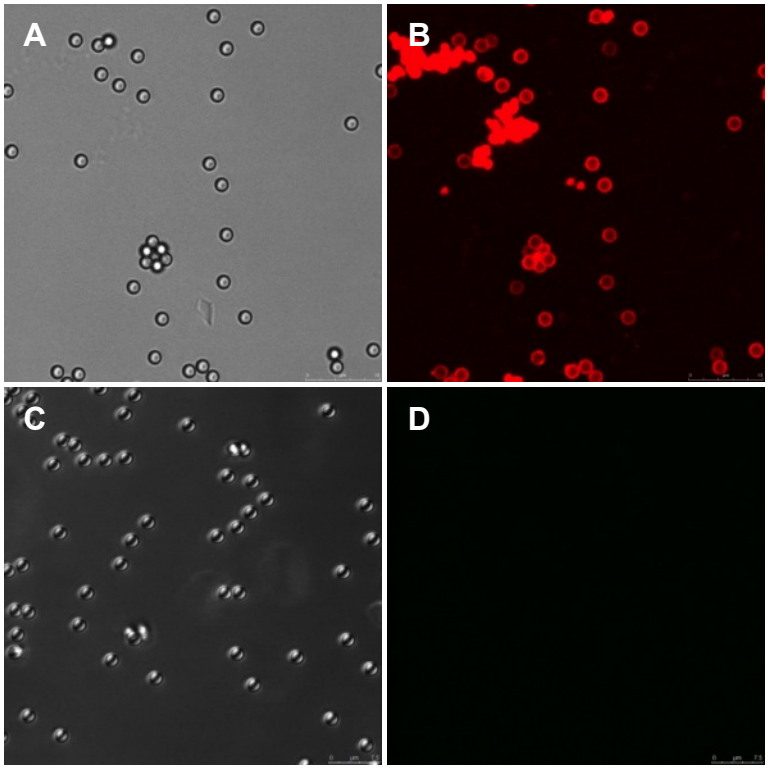

Figure 8.5 Fluorescence images during the immunoassays in the absence of AuNPs/4MBA. Optical (A) and fluorescence (B) images of PS microbeads-goat anti-rabbit IgG/DyLight^{TM}649 rabbit anti-human IgG; Optical (C) and fluorescence (D) images of PS microbeads-BSA/DyLight^{TM}649 rabbit anti-human IgG.

8.3.4 Immunoassays with AuNPs/4MBA

The immunoassays were done by introducing the 4MBA self-assembled AuNPs (AuNPs/4MBA) into the system. Goat anti-rabbit IgG and DyLight^{TM}649 rabbit anti-human IgG were conjugated with PS microbeads and AuNPs/4MBA, respectively. BSA was also bioconjugated with PS microbeads as the control experiment. Flow cytometry and Raman equipment were employed to examine the immunoassay system.

8.3.4.1 Flow Cytometric Analysis

Quantitative flow cytometric analysis was conducted to monitor the specific recognition of goat anti-rabbit IgG and DyLight^{TM}649 rabbit anti-human IgG after mixing the protein

conjugated microbeads and AuNPs/4MBA. The data in Table 8.2 shows the statistic information of flow cytometric results on the polymer microbeads before and after conjugation with antibody (goat anti-rabbit IgG) and antigen (DyLight^{TM}649 rabbit anti-human IgG)-labelled AuNPs/4MBA. PS microbeads are negative control samples, where the microbeads were unconjugated (0%). By conjugated the goat anti-rabbit IgG with PS microbeads, there was still no fluorescence signal (0.03%). 99.31% of goat anti-rabbit IgG conjugated PS microbeads showed fluorescence signals of DyLight^{TM}649 after mixed and reacted with DyLight^{TM}649-labelled goat anti-human IgG conjugated AuNPs/4MBA, which is different from the BSA conjugated PS microbeads (only 3.07%). Figure 8.6 is the forward scattering (FSC) versus side scattering (SSC) data and the histogram plot information of both goat anti-rabbit IgG conjugated PS microbeads and BSA conjugated PS microbeads after their reaction with DyLight^{TM}649-labelled goat anti-human IgG conjugated AuNPs/4MBA. The flow cytometric analysis results indicated that fluorescence-labelled IgG-AuNPs/4MBA can only attach to the surface of IgG conjugated PS microbeads, but can not be detected on the surface of BSA conjugated PS microbeads, which represent the specific binding between antibody and antigen. There was no difference compared with the result from the flow cytometric immunoassay without AuNPs/4MBA, which means the addition of AuNPs/4MBA during immunoassay systems does not affect the specific recognition between antibody and antigen. Furthermore, the addition of Raman-active molecules (4MBA) on AuNPs will benefit the further analysis using Raman equipments.

Table 8.2 Statistics for flow cytometric immunoassay results in the presence of AuNPs/4MBA.

Sample	% Gated (FL4)
PS microbeads (as control)	0%
PS microbeads-goat anti-rabbit IgG	0.03%
PS-goat anti-rabbit IgG/649 rabbit anti-human IgG-AuNPs/4MBA	99.31%
PS-BSA/649 rabbit anti-human IgG-AuNPs/4MBA	3.07%

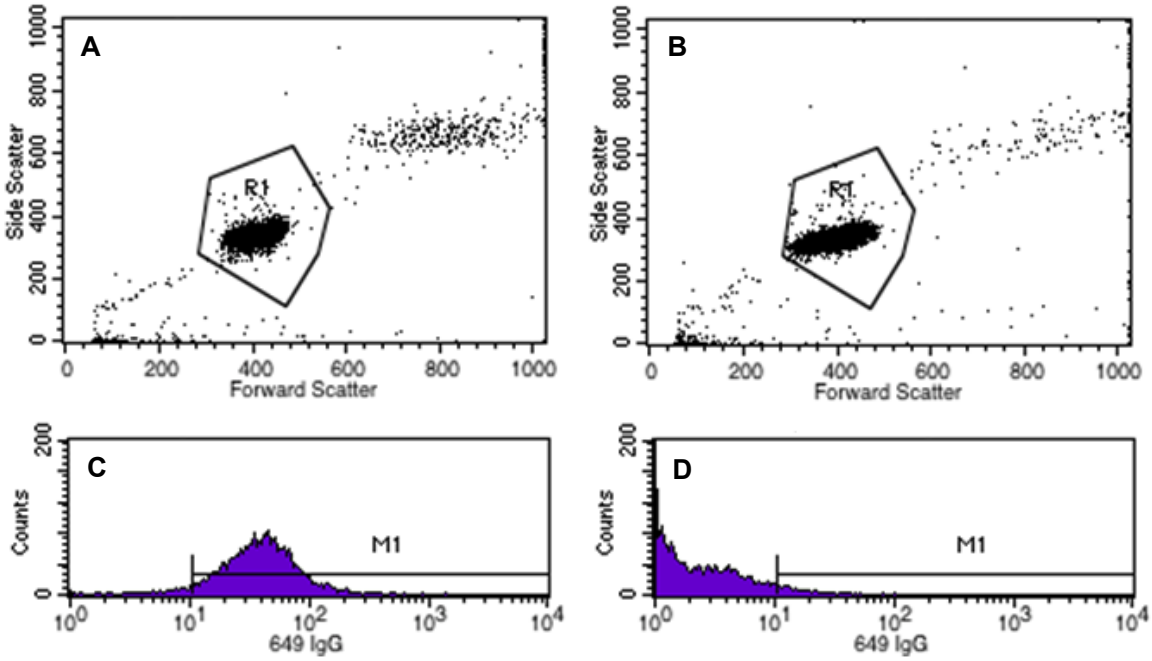

Figure 8.6 Flow cytometric immunoassay results in the presence of AuNPs/4MBA. Forward scattering (FSC) versus side scattering (SSC) of PS-goat anti-rabbit IgG/ 649 rabbit anti-human IgG-AuNPs/4MBA (A) and PS-BSA/649 rabbit anti-human IgG-AuNPs/4MBA (B); Fluorescence histograms of PS-goat anti-rabbit IgG/649 rabbit anti-human IgG-AuNPs/4MBA (C) and PS-BSA/649 rabbit anti-human IgG-AuNPs/4MBA (D).

8.3.4.2 Raman Analysis

The immunoassays were further examined using Raman microscope and the results are shown in Figure 8.7. Herein, monodisperse polymer microbeads were functionalised with goat anti-rabbit IgG, which have been proved to specifically recognise the DyLight^{TM}649-labelled rabbit anti-human IgG by flow cytometry and fluorescence microscope. AuNPs were self-assembled with 4MBA and conjugated with DyLight^{TM}649-labelled rabbit anti-human IgG, which can attach to the surface of goat anti-rabbit IgG conjugated polymer microbeads due to specific recognition. Therefore, when mixing the polymer microbeads and AuNPs together, both the Raman signals of polymer microbeads and the SERS signals of 4MBA can be observed (Figure 8.7b). In Chapter 4, we discussed that the typical Raman spectrum of PS microbeads (Figure 8.7a) has two vibrational bands at 999 cm^{-1} and 1029 cm^{-1}, which are assigned to υ_1 symmetrical ring and υ_{18A} vibrations of polystyrene, and the vibrational bands of 4MBA are located at 1074 cm^{-1} and 1583 cm^{-1} for the SAM, which can be assigned to the υ_{8a} and υ_{12} aromatic ring vibrations. When antibody-conjugated PS microbeads and its matched antigen-conjugated AuNPs were mixed together, both the Raman signals of polymer microbeads and the SERS signals of 4MBA can be observed due to specific recognition between antibody and antigen. Figure 8.7b shows both Raman signatures of PS microbeads and 4MBA are present on goat anti-rabbit IgG conjugated PS microbeads, indicating the recognition between goat anti-rabbit IgG and rabbit anti-human IgG. Furthermore, BSA conjugated PS microbeads were also mixed with DyLight^{TM}649-labelled rabbit anti-human IgG conjugated AuNPs/4MBA. The Raman spectrum is measured as shown in Figure 8.7c, where the SERS peaks of 4MBA at 1074 cm^{-1} and 1583 cm^{-1} can not be observed. The results in this study are similar as those in Chapter 4 where the big and polydisperse polymer microbeads were used during the immunoassay system. The advantage of this immunoassay system is that the results can be analysed using both

flow cytometry and Raman techniques, which benefits the further development of high-throughput screening and detection system, such as Raman-based flow cytometry.

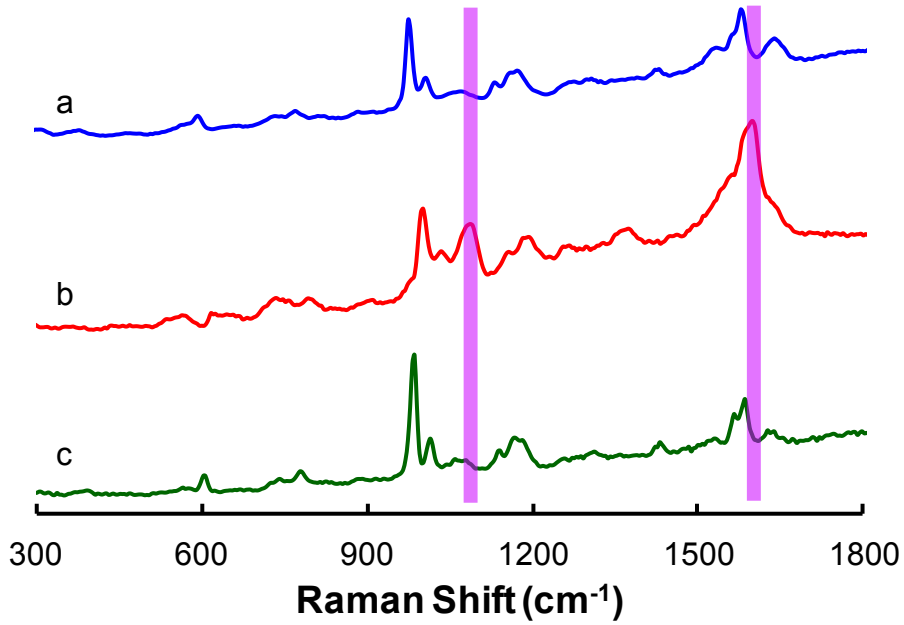

Figure 8.7 Raman spectra of PS microbeads (a), PS microbeads-goat anti-rabbit IgG/649 rabbit anti-human IgG-AuNPs/4MBA (b), and PS microbeads-BSA/649 rabbit anti-human IgG-AuNPs/4MBA (c).

8.4 Summary

The detection of IgG by polymer microbead-based immunoassays using flow cytometric/SERS analysis has been introduced in this study. The specific binding of antibody and antigen has been measured using different techniques, including flow cytometry, Raman microscope, and confocal fluorescence microscope. The flow cytometric results demonstrate that nearly all the goat anti-rabbit IgG conjugated polymer microbeads were attached with DyLight^{TM}649-labelled rabbit anti-human IgG in both conditions: in the absence or presence of AuNPs/4MBA. But the results can not be

observed on the BSA conjugated polymer microbeads. The results indicate the high specificity between corresponding antibody–antigen pairs.

CHAPTER 9 Conclusions and Recommendation

9.1 Conclusions

This thesis focuses on the synthesis of AuNPs, Raman tags, SERS- and Raman-active polymer microbeads, which was aimed at the development of microbead-based Raman/SERS immunoassay systems for multiplex detection. The experimental investigations employed advanced analytical techniques including TEM, SEM, UV-Vis spectrophotometer, Raman spectrometer, Raman microscope, fluorescence microscope, and flow cytometry during the characterisation. The following conclusions have been drown:

9.1.1 AuNP Synthesis and Their SAMs

AuNPs were chosen as SERS-active substrates for the Raman tag preparation after self-assembled with Raman-active molecules (4MBA) during the microbead-based Raman/SERS immunoassay. Different sizes of AuNPs were prepared by varying the feed molar ratios of $HAuCl_4 \cdot 3H_2O/Na_3Ct$ from 1:1.0, 1:1.5 to 1:4.0. The results indicated that it is difficult to obtain stable gold colloidal particles at a $HAuCl_4 \cdot 3H_2O/Na_3Ct$ ratio of 1:1. However, purple-colour AuNP suspension can be obtained by changing the mixing ratio to 1:1.5 and stable red-colour AuNPs with small particle size can be synthesised at the mixing molar ratio beyond 1:2.

Both AuNPs prepared at the mixing ratio of 1:2 and 1:1.5 were reacted with 4MBA to prepare their SAMs. It was found that AuNPs with 50 nm average size prepared at the molar ratio of $HAuCl_4 \cdot 3H_2O/Na_3Ct$ at 1:1.5 have the highest Raman effective enhancement factor among the AuNPs we investigated and is more suitable for producing significant SERS signals of the SAMs. Using the band of 1074 cm^{-1}, the effective

enhancement factor was calculated to be 5.4×10^5. This provides important information for the future utilisation of AuNPs as SERS reporter.

9.1.2 Raman-active Polymer Microbead Preparation

Large and polydisperse PS microbeads with the particle size up to 600 μm were synthesised using suspension polymerisation, and monodisperse PS microbeads with the average particle size 1.6 μm were prepared by dispersion polymerisation. The surface of PS microbeads was functionalised with carboxyl groups by the addition of functional comonomer (AA) during the PS microbead synthesis. The potentiometric and conductometric titrations indicated that carboxyl groups were present on the surface of the polymer microbeads using both polymerisation techniques, which is very important for further bioconjugation with proteins using EDC/NHS chemistry. Both kinds of polymer microbeads can also show clear Raman spectroscopic information of PS.

The copolymer microbeads with narrow size distribution and unique Raman signatures were also fabricated using dispersion polymerisation. Six kinds of copolymer microbeads, poly(Sty-AA), poly(Sty-4tBS-AA), poly(4tBS-AA), poly(Sty-4MS-AA), poly(4MS-AA), and poly(4tBS-4MS-AA), were produced with monodisperse particle sizes (1.07-1.69 μm) and unique Raman signatures. The conversions for all the monodisperse microbead fabrication are higher than 91% and CVs are less than 5%. The produced polymer microbeads could be applied for biodetection due to their narrow size distribution and specific spectroscopic properties.

9.1.3 SERS-active Polymer Microbead Development

The SERS-active microbeads were also fabricated for biodetection. The AuNPs were first deposited on the surface of monodisperse PS microbeads to form polystyrene/AuNP composite microspheres by thermodynamic drive effect, where AuNPs act as stabilisers to stabilise the metastable PS microbeads. So the AuNPs can be deposited on the microbead surface. Direct adsorption and in-situ growth methods were used to prepare the composite microspheres. In the next step, the PS-COOH/AuNP composite microspheres were reacted with Raman-active molecules (4MP) and the outside layer of SERS-active composite microsphere was encapsulated with the silica shell, which can increase the biocompatibility of composite microspheres and make them easy to be functionalised with biomolecules for the practical applications.

The mechanism for the silica coating of PS-COOH/AuNP composite microspheres was also investigated in detail by changing the reaction conditions during the coating process, such as deposition time, ammonia concentration, water concentration and TEOS concentration. The results indicated that the silica layer can be formed on the surface of PS-COOH/AuNP composite microspheres within a few minutes and the shell thickness will not increase any more with the increase of deposition time. The increase of deposition time only results in the presence of free silica nanoparticles and the big particle aggregates.

9.1.4 Microbead-based Raman/SERS Immunoassay System Development

The major purpose of this whole project was to develop different immunoassay systems for the multiplex, specific and sensitive detection of biological molecules. IgG was used as the model proteins. Polymer microbeads served as the solid support and barcoded Raman fingerprint enable to enhance the detection sensitivity and multiplexed ability of the

immunoassay systems. Compared with traditional bead-based fluorescence immunoassays, the developed polymer microbead-based Raman/SERS immunoassays have the following advantages: label-free, no photobleaching, and high sensitivity. It has potential applications for multiplex analyte detection from one homogeneous immunoassay.

A novel technique for IgG detection based on large PS microbeads and AuNPs has been developed. The PS microbeads prepared by suspension polymerisation were first used to develop the polymer microbead-based Raman/SERS immunoassay system. AuNPs with 50 nm average size were self-assembled with 4MBA and being used as the SERS reporters in the Raman/SERS immunoassays. Both fluorescence microscope and Raman spectrometer characterisation demonstrate the core-shell-corona structured SERS reporters can be successfully readout on the polymer microbeads through the specific recognition between donkey anti-goat IgG and goat anti-human IgG.

Since we target to develop the Raman flow cytometry for the microbead-based Raman/SERS immunoassays, monodisperse PS microbeads with 1.6 μm diameter prepared by dispersion polymerisation were also used to develop the microbead-based immunoassays. The specific binding of antibody and antigen has been measured using different techniques, including flow cytometry, Raman microscope, and confocal fluorescence microscope. The flow cytometric and Raman results demonstrate that goat anti-rabbit IgG conjugated polymer microbeads can specifically recognise the DyLight^{TM}649-labelled rabbit anti-human IgG in the absence or presence of AuNPs/4MBA, which was due to the high specificity between corresponding antibody–antigen pairs.

9.2 Recommendation for Future Work

9.2.1 Fabrication of Different SERS-active Microbeads

As discussed in Chapter 5 and Chapter 6, SERS-active microbeads with Raman signature have been fabricated by the deposition of AuNPs on the surface of PS microbeads and the silica coating of SERS-active PS-COOH/AuNP composite microspheres. The advantage of this method is that the dispersion polymerisation only needs to be performed once, and the fabrication of SERS-active microbeads is based on these synthesised monodisperse polymer microbeads. So the resulting SERS-active microbeads are all monodispersed, which is different from the copolymer polymerisation. Although a few copolymer microbeads with narrow size distribution and unique Raman fingerprints have been prepared in this study as reported in Chapter 7, the fabrication of copolymer microbeads is still a challenge. The result in in Chapter 6 showed that only one aromatic thiol (4MP) was used as Raman-active molecules to fabricate the SERS-active microbeads. Therefore, in the future work, different Raman-active molecules, such as 4MBA and 4-aminothiophenol (4ATP), can be self-assembled on the PS-COOH/AuNP composite microspheres prior to silica coating. As a result, various SERS-active microbeads can be developed.

9.2.2 Development of Multiplex Immunoassay System

Different kinds of SERS-active and Raman-active polymer microbeads with unique Raman fingerprints have already been synthesised. Therefore, we can apply these microbeads for the multiplex detection system development. The similar procedure as microbead-based Raman/SERS immunoassay could be used based on different SERS-active microbeads and Raman microbeads for multiplexed detection. By conjugating different Raman spectroscopic-encoded microbeads with different antibodies, the microbeads can

specifically recognise the matched antigens after the formation of sandwich structures with SERS reporters. Because of the unique Raman spectra of microbeads and SERS reporters, the identification of each antigen can be achieved by measuring the Raman signals of polymer microbead and SERS reporter combination.

9.2.3 Build-up of Raman Flow Cytometry System

The Raman and SERS-active polymer microbeads have been demonstrated their importance for multiplex detection. The spectral information of single particle has been analysed in the flow system.[309, 312, 315] Hundreds and thousands of nanoparticles can be analysed per second using this approach. But there is no commercial flow cytometry available to read these Raman signals. The future work can focus on setting up a Raman flow cytometer system to read the Raman signals of polymer microbeads and SERS reporters in the microbead-based Raman/SERS immunoassays. Various monodisperse SERS-active and Raman-active microbeads will be used as the solid supports and barcodes, and self-assembled AuNPs are used as SERS tags. The signals of Raman flow cytometer will be enhanced, which gives rise to the significant improvement in detection limit. Since various Raman spectroscopic-encoded microbeads have been produced using various polymerisation techniques, the system could have a promising application in multiplex detection after the conjugation of microbeads and SERS tags with different antibodies and antigens. Therefore, such systems could make it possible to quickly measure multiple analytes simultaneously and decrease related analytical cost.

REFERENCES

1. C. Kendall, M. Isabelle, F. Bazant-Hegemark, J. Hutchings, L. Orr, J. Babrah, R. Baker and N. Stone, *Analyst*, 2009, **134**, 1029-1045.
2. Z. W. Huang, A. McWilliams, H. Lui, D. I. McLean, S. Lam and H. S. Zeng, *International Journal of Cancer*, 2003, **107**, 1047-1052.
3. E. B. Hanlon, R. Manoharan, T. W. Koo, K. E. Shafer, J. T. Motz, M. Fitzmaurice, J. R. Kramer, I. Itzkan, R. R. Dasari and M. S. Feld, *Physics in Medicine and Biology*, 2000, **45**, R1-R59.
4. P. R. T. Jess, M. Mazilu, K. Dholakia, A. C. Riches and C. S. Herrington, *International Journal of Cancer*, 2009, **124**, 376-380.
5. S. M. Nie and S. R. Emery, *Science*, 1997, **275**, 1102-1106.
6. M. Fleischm, P. J. Hendra and McQuilla.Aj, *Chemical Physics Letters*, 1974, **26**, 163-166.
7. J. Ni, R. J. Lipert, G. B. Dawson and M. D. Porter, *Analytical Chemistry*, 1999, **71**, 4903-4908.
8. X. Y. Zhang, M. A. Young, O. Lyandres and R. P. Van Duyne, *Journal of the American Chemical Society*, 2005, **127**, 4484-4489.
9. X. M. Qian, X. H. Peng, D. O. Ansari, Q. Yin-Goen, G. Z. Chen, D. M. Shin, L. Yang, A. N. Young, M. D. Wang and S. M. Nie, *Nature Biotechnology*, 2008, **26**, 83-90.
10. K. K. Maiti, U. S. Dinish, A. Samanta, M. Vendrell, K.-S. Soh, S.-J. Park, M. Olivo and Y.-T. Chang, *Nano Today*, 2012, **7**, 85-93.
11. M. Vendrell, K. K. Maiti, K. Dhaliwal and Y.-T. Chang, *Trends in Biotechnology*, 2013, **31**, 249-257.
12. K. C. Bantz, A. F. Meyer, N. J. Wittenberg, H. Im, O. Kurtulus, S. H. Lee, N. C. Lindquist, S.-H. Oh and C. L. Haynes, *Phys Chem Chem Phys*, 2011, **13**, 11551-11567.
13. Y. Wang, K. Lee and J. Irudayaraj, *Chemical Communications*, 2010, **46**, 613-615.
14. C. Y. Song, Z. Y. Wang, J. Yang, R. H. Zhang, H. Wu and Y. P. Cui, *Journal of Nonlinear Optical Physics & Materials*, 2011, **20**, 63-73.
15. J. Baniukevic, I. Hakki Boyaci, A. Goktug Bozkurt, U. Tamer, A. Ramanavicius and A. Ramanaviciene, *Biosensors and Bioelectronics*, 2013, **43**, 281-288.

16. J. M. Singer and C. M. Plotz, *The American Journal of Medicine*, 1956, **21**, 888-892.
17. H. Fenniri, S. Chun, O. Terreau and J.-P. Bravo-Vasquez, *Journal of Combinatorial Chemistry*, 2007, **10**, 31-36.
18. J. Raez, D. R. Blais, Y. Zhang, R. A. Alvarez-Puebla, J. P. Bravo-Vasquez, J. P. Pezacki and H. Fenniri, *Langmuir*, 2007, **23**, 6482-6485.
19. C. V. Raman and K. S. Krishnan, *Nature*, 1928, **121**, 501-502.
20. W. Xie, P. Qiu and C. Mao, *J Mater Chem*, 2011, **21**, 5190-5202.
21. R. Loudon, *Advances in Physics*, 1964, **13**, 423-482.
22. F. Tuinstra and J. L. Koenig, *Journal of Chemical Physics*, 1970, **53**, 1126-1130.
23. S. A. Solin and A. K. Ramdas, *Physical Review B*, 1970, **1**, 1687-1698.
24. T. R. Hart, R. L. Aggarwal and B. Lax, *Physical Review B-Solid State*, 1970, **1**, 638-642.
25. A. M. Rao, P. C. Eklund, S. Bandow, A. Thess and R. E. Smalley, *Nature*, 1997, **388**, 257-259.
26. A. C. Ferrari, J. C. Meyer, V. Scardaci, C. Casiraghi, M. Lazzeri, F. Mauri, S. Piscanec, D. Jiang, K. S. Novoselov, S. Roth and A. K. Geim, *Physical Review Letters*, 2006, **97**, 1-4.
27. A. C. Ferrari, *Solid State Communications*, 2007, **143**, 47-57.
28. F. J. Boerio and J. L. Koenig, *Journal of Chemical Physics*, 1970, **52**, 3425-3431.
29. E. W. Small, B. Fanconi and Peticola.Wl, *Journal of Chemical Physics*, 1970, **52**, 4369-4379.
30. S. C. Erfurth, E. J. Kiser and Peticola.Wl, *Proceedings of the National Academy of Sciences of the United States of America*, 1972, **69**, 938-941.
31. D. L. Jeanmaire and R. P. Vanduyne, *Journal of Electroanalytical Chemistry*, 1977, **84**, 1-20.
32. M. G. Albrecht and J. A. Creighton, *Journal of the American Chemical Society*, 1977, **99**, 5215-5217.
33. M. Moskovits, *Reviews of Modern Physics*, 1985, **57**, 783-826.
34. K. Kneipp, H. Kneipp, I. Itzkan, R. R. Dasari and M. S. Feld, *J Phys-Condens Mat*, 2002, **14**, R597-R624.
35. K. Kneipp, Y. Wang, H. Kneipp, L. T. Perelman, I. Itzkan, R. Dasari and M. S. Feld, *Physical Review Letters*, 1997, **78**, 1667-1670.

36. R. G. Freeman, K. C. Grabar, K. J. Allison, R. M. Bright, J. A. Davis, A. P. Guthrie, M. B. Hommer, M. A. Jackson, P. C. Smith, D. G. Walter and M. J. Natan, *Science*, 1995, **267**, 1629-1632.
37. K. Kneipp, A. S. Haka, H. Kneipp, K. Badizadegan, N. Yoshizawa, C. Boone, K. E. Shafer-Peltier, J. T. Motz, R. R. Dasari and M. S. Feld, *Applied Spectroscopy*, 2002, **56**, 150-154.
38. Y. W. C. Cao, R. C. Jin and C. A. Mirkin, *Science*, 2002, **297**, 1536-1540.
39. D. S. Grubisha, R. J. Lipert, H.-Y. Park, J. Driskell and M. D. Porter, *Analytical Chemistry*, 2003, **75**, 5936-5943.
40. C. Y. Song, Z. Y. Wang, R. H. Zhang, J. Yang, X. B. Tan and Y. P. Cui, *Biosensors & Bioelectronics*, 2009, **25**, 826-831.
41. A. Pallaoro, G. B. Braun, N. O. Reich and M. Moskovits, *Small*, 2010, **6**, 618-622.
42. X. Wang, X. Qian, J. J. Beitler, Z. G. Chen, F. R. Khuri, M. M. Lewis, H. J. C. Shin, S. Nie and D. M. Shin, *Cancer Research*, 2011, **71**, 1526-1532.
43. A. Yashchenok, A. Masic, D. Gorin, B. S. Shim, N. A. Kotov, P. Fratzl, H. Moehwald and A. Skirtach, *Small*, 2013, **9**, 351-356.
44. K. E. Shafer-Peltier, C. L. Haynes, M. R. Glucksberg and R. P. Van Duyne, *Journal of the American Chemical Society*, 2002, **125**, 588-593.
45. N. P. W. Pieczonka and R. F. Aroca, *Chemical Society Reviews*, 2008, **37**, 946-954.
46. N. T. B. Thuy, R. Yokogawa, Y. Yoshimura, K. Fujimoto, M. Koyano and S. Maenosono, *Analyst*, 2010, **135**, 595-602.
47. A. Samanta, K. K. Maiti, K.-S. Soh, X. Liao, M. Vendrell, U. S. Dinish, S.-W. Yun, R. Bhuvaneswari, H. Kim, S. Rautela, J. Chung, M. Olivo and Y.-T. Chang, *Angewandte Chemie International Edition*, 2011, **50**, 6089-6092.
48. M. A. Mahmoud, *Langmuir*, 2013, **29**, 6253-6261.
49. A. Campion and P. Kambhampati, *Chemical Society Reviews*, 1998, **27**, 241-250.
50. K. Kneipp, H. Kneipp, R. Manoharan, E. B. Hanlon, I. Itzkan, R. R. Dasari and M. S. Feld, *Applied Spectroscopy*, 1998, **52**, 1493-1497.
51. H. X. Xu, J. Aizpurua, M. Kall and P. Apell, *Physical Review E*, 2000, **62**, 4318-4324.
52. M. Moskovits, in *Top Appl Phys*, 2006, pp. 1-17.
53. X. M. Qian and S. M. Nie, *Chemical Society Reviews*, 2008, **37**, 912-920.
54. T. E. Furtak and D. Roy, *Surface Science*, 1985, **158**, 126-146.

55. A. Otto, I. Mrozek, H. Grabhorn and W. Akemann, *J Phys-Condens Mat*, 1992, **4**, 1143-1212.
56. A. Otto, T. Bornemann, U. Erturk, I. Mrozek and C. Pettenkofer, *Surface Science*, 1989, **210**, 363-386.
57. K. Kneipp, H. Kneipp, R. Manoharan, I. Itzkan, R. R. Dasari and M. S. Feld, *Bioimaging*, 1998, **6**, 104-110.
58. E. J. Blackie, *Ph.D thesis*, 2010.
59. A. D. McFarland, M. A. Young, J. A. Dieringer and R. P. Van Duyne, *The Journal of Physical Chemistry B*, 2005, **109**, 11279-11285.
60. S. B. Chaney, S. Shanmukh, R. A. Dluhy and Y. P. Zhao, *Applied Physics Letters*, 2005, **87**, 1-3.
61. E. C. Le Ru, E. Blackie, M. Meyer and P. G. Etchegoin, *The Journal of Physical Chemistry C*, 2007, **111**, 13794-13803.
62. P. H. C. Camargo, C. M. Cobley, M. Rycenga and Y. Xia, *Nanotechnology*, 2009, **20**, 1-8.
63. T. A. Laurence, G. B. Braun, N. O. Reich and M. Moskovits, *Nano Letters*, 2012, **12**, 2912-2917.
64. S. Schlucker, *Chemphyschem*, 2009, **10**, 1344-1354.
65. D. Radziuk, A. Skirtach, G. Sukhorukov, D. Shchukin and H. Möhwald, *Macromolecular Rapid Communications*, 2007, **28**, 848-855.
66. Y. J. Kwon, D. H. Son, S. J. Ahn, M. S. Kim and K. Kim, *Journal of Physical Chemistry*, 1994, **98**, 8481-8487.
67. Y. J. Kwon, S. B. Lee, K. Kim and M. S. Kim, *J Mol Struct*, 1994, **318**, 25-35.
68. M. Graff and J. Bukowska, *The Journal of Physical Chemistry B*, 2005, **109**, 9567-9574.
69. H. Chu, H. Yang, S. Huan, G. Shen and R. Yu, *The Journal of Physical Chemistry B*, 2006, **110**, 5490-5497.
70. G. F. S. Andrade and M. L. A. Temperini, *Vibrational Spectroscopy*, 2010, **54**, 148-154.
71. U. Wenning, B. Pettinger and H. Wetzel, *Chemical Physics Letters*, 1980, **70**, 49-54.
72. C. A. Melendres, C. B. Rios, X. Feng and R. McMasters, *The Journal of Physical Chemistry*, 1983, **87**, 3526-3531.

73. C. A. Szafranski, W. Tanner, P. E. Laibinis and R. L. Garrell, *Langmuir*, 1998, **14**, 3570-3579.
74. Y. Peng, Z. Niu, W. Huang, S. Chen and Z. Li, *The Journal of Physical Chemistry B*, 2005, **109**, 10880-10885.
75. R. Mažeikienė, G. Niaura and A. Malinauskas, *Journal of Colloid and Interface Science*, 2009, **336**, 195-199.
76. Y. Kim, K. Cho, K. Lee, J. Choo, M.-s. Gong and S.-W. Joo, *J Mol Struct*, 2008, **878**, 155-161.
77. J.-L. Yao, B. Ren, G.-K. Liu, D.-Y. Wu, R.-A. Gu and Z.-Q. Tian, *J Raman Spectrosc*, 2003, **34**, 221-226.
78. J.-L. Yao, Y.-X. Yuan, X.-M. Fan, B. Ren, R.-A. Gu and Z.-Q. Tian, *Journal of Electroanalytical Chemistry*, 2008, **624**, 129-133.
79. G.-k. Liu, B. Ren, D.-y. Wu, J.-m. Lin, R.-a. Gu and Z.-q. Tian, *Journal of Electroanalytical Chemistry*, 2006, **594**, 73-79.
80. L. Seballos, J. Z. Zhang and R. Sutphen, *Analytical and Bioanalytical Chemistry*, 2005, **383**, 763-767.
81. I. Delfino, A. R. Bizzarri and S. Cannistraro, *Chem Phys*, 2006, **326**, 356-362.
82. Z. Liron, A. Zifman and V. Heleg-Shabtai, *Analytica Chimica Acta*, 2011, **703**, 234-238.
83. N. H. Jang, *Bulletin of the Korean Chemical Society*, 2002, **23**, 1790-1800.
84. A. M. Schwartzberg, C. D. Grant, A. Wolcott, R. Bogomolni and J. Z. Zhang, *Plasmonics: Metallic Nanostructures and Their Optical Properties*, 2003, **5221**, 100-107.
85. C. Ruan, W. Wang and B. Gu, *Analytical Chemistry*, 2006, **78**, 3379-3384.
86. A. R. Bizzarri and S. Cannistraro, *Nanomed-Nanotechnol*, 2007, **3**, 306-310.
87. S. S. R. Dasary, A. K. Singh, D. Senapati, H. Yu and P. C. Ray, *Journal of the American Chemical Society*, 2009, **131**, 13806-13812.
88. Creighton J.A, *Surface Science*, 1986, **173**, 665-672.
89. L.-Y. Chen, J.-S. Yu, T. Fujita and M.-W. Chen, *Adv Funct Mater*, 2009, **19**, 1221-1226.
90. L. Yang, X. Jiang, W. Ruan, B. Zhao, W. Xu and J. R. Lombardi, *J Raman Spectrosc*, 2009, **40**, 2004-2008.

91. D. D. Whitmore, P. Z. El-Khoury, L. Fabris, P. Chu, G. C. Bazan, E. O. Potma and V. A. Apkarian, *The Journal of Physical Chemistry C*, 2011, **115**, 15900-15907.
92. Y. Cui, B. Ren, J.-L. Yao, R.-A. Gu and Z.-Q. Tian, *The Journal of Physical Chemistry B*, 2006, **110**, 4002-4006.
93. S. J. Oldenburg, S. L. Westcott, R. D. Averitt and N. J. Halas, *Journal of Chemical Physics*, 1999, **111**, 4729-4735.
94. W. B. Li, Y. Y. Guo and P. Zhang, *Journal of Physical Chemistry C*, 2010, **114**, 7263-7268.
95. F. Bao, J.-L. Yao and R.-A. Gu, *Langmuir*, 2009, **25**, 10782-10787.
96. Y. Wang, K. Wang, B. Zou, T. Gao, X. Zhang, Z. Du and S. Zhou, *Journal of Materials Chemistry C*, 2013, **1**, 2441-2447.
97. J. D. Driskell, S. Shanmukh, Y. Liu, S. B. Chaney, X. J. Tang, Y. P. Zhao and R. A. Dluhy, *The Journal of Physical Chemistry C*, 2008, **112**, 895-901.
98. Y. Wang, H. Chen and E. Wang, *Nanotechnology*, 2008, **19**, 1-5.
99. T. T. Xu, J. A. Huang, L. F. He, Y. He, S. Su and S. T. Lee, *Applied Physics Letters*, 2011, **99**, 1-3.
100. H. W. Liu, L. Zhang, X. Y. Lang, Y. Yamaguchi, H. S. Iwasaki, Y. S. Inouye, Q. K. Xue and M. W. Chen, *Scientific Reports*, 2011, **1**, 1-5.
101. K. D. Jernshoj, S. Hassing, R. S. Hansen and P. Krohne-Nielsen, *Journal of Chemical Physics*, 2011, **135**, 1-10.
102. Y. Zhu, R. A. Dluhy and Y. Zhao, *Sensors and Actuators B: Chemical*, 2011, **157**, 42-50.
103. J. Du and C. Jing, *The Journal of Physical Chemistry C*, 2011, **115**, 17829-17835.
104. X. Yang, C. Shi, D. Wheeler, R. Newhouse, B. Chen, J. Z. Zhang and C. Gu, *J. Opt. Soc. Am. A-Opt. Image Sci. Vis.*, 2010, **27**, 977-984.
105. A. Gutes, C. Carraro and R. Maboudian, *ACS Applied Materials & Interfaces*, 2009, **1**, 2551-2555.
106. M. Brust, M. Walker, D. Bethell, D. J. Schiffrin and R. Whyman, *Journal of the Chemical Society-Chemical Communications*, 1994, 801-802.
107. M. Brust, J. Fink, D. Bethell, D. J. Schiffrin and C. Kiely, *Journal of the Chemical Society-Chemical Communications*, 1995, 1655-1656.

108. M. J. Hostetler, J. E. Wingate, C.-J. Zhong, J. E. Harris, R. W. Vachet, M. R. Clark, J. D. Londono, S. J. Green, J. J. Stokes, G. D. Wignall, G. L. Glish, M. D. Porter, N. D. Evans and R. W. Murray, *Langmuir*, 1998, **14**, 17-30.

109. J. Turkevich, P. C. Stevenson and J. Hillier, *Discussions of the Faraday Society*, 1951, 55-75.

110. G. Frens, *Nature-Physical Science*, 1973, **241**, 20-22.

111. N. R. Jana, L. Gearheart and C. J. Murphy, *Langmuir*, 2001, **17**, 6782-6786.

112. J. Rodríguez-Fernández, J. Pérez-Juste, F. J. García de Abajo and L. M. Liz-Marzán, *Langmuir*, 2006, **22**, 7007-7010.

113. C. Ziegler and A. Eychmüller, *The Journal of Physical Chemistry C*, 2011, **115**, 4502-4506.

114. B. V. Enustun and J. Turkevich, *Journal of the American Chemical Society*, 1963, **85**, 3317-&.

115. J. Turkevich, *Gold Bulletin*, 1985, **18**, 86-91.

116. M. K. Chow and C. F. Zukoski, *Journal of Colloid and Interface Science*, 1994, **165**, 97-109.

117. J. Kimling, M. Maier, B. Okenve, V. Kotaidis, H. Ballot and A. Plech, *Journal of Physical Chemistry B*, 2006, **110**, 15700-15707.

118. X. H. Ji, X. N. Song, J. Li, Y. B. Bai, W. S. Yang and X. G. Peng, *Journal of the American Chemical Society*, 2007, **129**, 13939-13948.

119. B. Rodriguez-Gonzalez, P. Mulvaney and L. M. Liz-Marzan, *Zeitschrift Fur Physikalische Chemie-International Journal of Research in Physical Chemistry & Chemical Physics*, 2007, **221**, 415-426.

120. J. Polte, T. T. Ahner, F. Delissen, S. Sokolov, F. Emmerling, A. F. Thünemann and R. Kraehnert, *Journal of the American Chemical Society*, 2010, **132**, 1296-1301.

121. I. Ojea-Jiménez and J. M. Campanera, *The Journal of Physical Chemistry C*, 2012, **116**, 23682-23691.

122. C. Engelbrekt, P. S. Jensen, K. H. Sørensen, J. Ulstrup and J. Zhang, *The Journal of Physical Chemistry C*, 2013, **117**, 11818-11828.

123. S. Basu, S. K. Ghosh, S. Kundu, S. Panigrahi, S. Praharaj, S. Pande, S. Jana and T. Pal, *Journal of Colloid and Interface Science*, 2007, **313**, 724-734.

124. K. L. Kelly, E. Coronado, L. L. Zhao and G. C. Schatz, *Journal of Physical Chemistry B*, 2003, **107**, 668-677.

125. G. Mie, *Ann Phys-Leipzig*, 1908, **25**, 377-445.
126. P. K. Jain, K. S. Lee, I. H. El-Sayed and M. A. El-Sayed, *Journal of Physical Chemistry B*, 2006, **110**, 7238-7248.
127. X. H. Huang, P. K. Jain, I. H. El-Sayed and M. A. El-Sayed, *Nanomedicine*, 2007, **2**, 681-693.
128. S. Link and M. A. El-Sayed, *The Journal of Physical Chemistry B*, 1999, **103**, 4212-4217.
129. T. Makiabadi, A. Bouvree, V. Le Nader, H. Terrisse and G. Louarn, *Plasmonics*, 2010, **5**, 21-29.
130. http://nanocomposix.com/kb/gold/optical-properties, Viewed on March 2013.
131. U. Kreibig and L. Genzel, *Surface Science*, 1985, **156, Part 2**, 678-700.
132. N. T. K. Thanh and Z. Rosenzweig, *Analytical Chemistry*, 2002, **74**, 1624-1628.
133. J. C. Love, L. A. Estroff, J. K. Kriebel, R. G. Nuzzo and G. M. Whitesides, *Chemical Reviews*, 2005, **105**, 1103-1169.
134. C. S. Weisbecker, M. V. Merritt and G. M. Whitesides, *Langmuir*, 1996, **12**, 3763-3772.
135. L. A. Porter, D. Ji, S. L. Westcott, M. Graupe, R. S. Czernuszewicz, N. J. Halas and T. R. Lee, *Langmuir*, 1998, **14**, 7378-7386.
136. N. Garg, E. Carrasquillo-Molina and T. R. Lee, *Langmuir*, 2002, **18**, 2717-2726.
137. V. Ganesh, R. R. Pandey, B. D. Malhotra and V. Lakshminarayanan, *Journal of Electroanalytical Chemistry*, 2008, **619**, 87-97.
138. M. S. Fleming and D. R. Walt, *Langmuir*, 2001, **17**, 4836-4843.
139. E. M. S. Azzam, A. M. Badawi, A. R. E. Alawady and A. Soliman, *J Disper Sci Technol*, 2009, **30**, 540-547.
140. E. Sabatani, J. Cohenboulakia, M. Bruening and I. Rubinstein, *Langmuir*, 1993, **9**, 2974-2981.
141. D. Barriet, C. M. Yam, O. E. Shmakova, A. C. Jamison and T. R. Lee, *Langmuir*, 2007, **23**, 8866-8875.
142. K. Rajalingam, L. Hallmann, T. Strunskus, A. Bashir, C. Woll and F. Tuczek, *Phys Chem Chem Phys*, 2010, **12**, 4390-4399.
143. T. Zhu, X. Zhang, J. Wang, X. Fu and Z. Liu, *Thin Solid Films*, 1998, **327–329**, 595-598.
144. A. Gole, C. J. Orendorff and C. J. Murphy, *Langmuir*, 2004, **20**, 7117-7122.

145. C. J. Orendorff, A. Gole, T. K. Sau and C. J. Murphy, *Analytical Chemistry*, 2005, **77**, 3261-3266.
146. M. Fan and A. G. Brolo, *Chemphyschem*, 2008, **9**, 1899-1907.
147. Y. S. Shon, C. Mazzitelli and R. W. Murray, *Langmuir*, 2001, **17**, 7735-7741.
148. H. Takiguchi, K. Sato, T. Ishida, K. Abe, K. Yase and K. Tamada, *Langmuir*, 1999, **16**, 1703-1710.
149. E. Valerio, L. M. Abrantes and A. S. Viana, *Electroanalysis*, 2008, **20**, 2467-2474.
150. A. Mocanu, I. Cernica, G. Tomoaia, L.-D. Bobos, O. Horovitz and M. Tomoaia-Cotisel, *Colloids and Surfaces A: Physicochemical and Engineering Aspects*, 2009, **338**, 93-101.
151. I. A. Darwish, *International journal of biomedical science : IJBS*, 2006, **2**, 217-235.
152. T. Porstmann and S. T. Kiessig, *Journal of Immunological Methods*, 1992, **150**, 5-21.
153. S. D. Lidofsky, T. Imasaka and R. N. Zare, *Analytical Chemistry*, 1979, **51**, 1602-1605.
154. G. Shan, W. Huang, S. J. Gee, B. A. Buchholz, J. S. Vogel and B. D. Hammock, *Proceedings of the National Academy of Sciences of the United States of America*, 2000, **97**, 2445-2449.
155. M. F. Katmeh, G. W. Aherne and D. Stevenson, *Analyst*, 1996, **121**, 329-332.
156. H. Stanker Larry and C. Beier Ross, in *ACS Symposium Series*, American Chemical Society, 1996, pp. 2-16.
157. B. Sun, W. Xie, G. Yi, D. Chen, Y. Zhou and J. Cheng, *Journal of Immunological Methods*, 2001, **249**, 85-89.
158. S. Gupta, S. Huda, P. K. Kilpatrick and O. D. Velev, *Analytical Chemistry*, 2007, **79**, 3810-3820.
159. Y. R. Chemla, H. L. Grossman, Y. Poon, R. McDermott, R. Stevens, M. D. Alper and J. Clarke, *Proceedings of the National Academy of Sciences*, 2000, **97**, 14268-14272.
160. T. L. Paxon, R. S. Duthie, C. Renko, A. A. Burns, M. L. Lesaicherre and F. J. Mondello, in *Photonic Microdevices/Microstructures for Sensing Iii*, 2011, pp. 1-3.
161. J. H. Granger, M. C. Granger, M. A. Firpo, S. J. Mulvihill and M. D. Porter, *Analyst*, 2013, **138**, 410-416.

162. T. E. Rohr, T. Cotton, N. Fan and P. J. Tarcha, *Analytical Biochemistry*, 1989, **182**, 388-398.

163. X. Dou, T. Takama, Y. Yamaguchi, H. Yamamoto and Y. Ozaki, *Analytical Chemistry*, 1997, **69**, 1492-1495.

164. X. Dou, Y. Yamaguchi, H. Yamamoto, S. Doi and Y. Ozaki, *J Raman Spectrosc*, 1998, **29**, 739-742.

165. J. D. Driskell, K. M. Kwarta, R. J. Lipert, M. D. Porter, J. D. Neill and J. F. Ridpath, *Analytical Chemistry*, 2005, **77**, 6147-6154.

166. J. D. Driskell, J. M. Uhlenkamp, R. J. Lipert and M. D. Porter, *Analytical Chemistry*, 2007, **79**, 4141-4148.

167. R. Narayanan, R. J. Lipert and M. D. Porter, *Analytical Chemistry*, 2008, **80**, 2265-2271.

168. M. D. Porter, R. J. Lipert, L. M. Siperko, G. Wang and R. Narayanana, *Chemical Society Reviews*, 2008, **37**, 1001-1011.

169. E. Boisselier and D. Astruc, *Chemical Society Reviews*, 2009, **38**, 1759-1782.

170. S. Pahlow, A. Maerz, B. Seise, K. Hartmann, I. Freitag, E. Kaemmer, R. Boehme, V. Deckert, K. Weber, D. Cialla and J. Popp, *Engineering in Life Sciences*, 2012, **12**, 131-143.

171. T. Li, L. P. Guo and Z. Wang, *Analytical Sciences*, 2008, **24**, 907-910.

172. M. Schutz, D. Steinigeweg, M. Salehi, K. Kompe and S. Schlucker, *Chemical Communications*, 2011, **47**, 4216-4218.

173. G. F. Wang, H. Y. Park and R. J. Lipert, *Analytical Chemistry*, 2009, **81**, 9643-9650.

174. H. Chon, S. Lee, S. W. Son, C. H. Oh and J. Choo, *Analytical Chemistry*, 2009, **81**, 3029-3034.

175. M. Lee, S. Lee, J.-h. Lee, H.-w. Lim, G. H. Seong, E. K. Lee, S.-I. Chang, C. H. Oh and J. Choo, *Biosensors and Bioelectronics*, 2011, **26**, 2135-2141.

176. F. Domenici, A. R. Bizzarri and S. Cannistraro, *International Journal of Nanomedicine*, 2011, **6**, 2033-2042.

177. Y. Cui, B. Ren, J.-L. Yao, R.-A. Gu and Z.-Q. Tian, *J Raman Spectrosc*, 2007, **38**, 896-902.

178. X. Huang, I. H. El-Sayed, W. Qian and M. A. El-Sayed, *Nano Letters*, 2007, **7**, 1591-1597.

179. S. Keren, C. Zavaleta, Z. Cheng, A. de la Zerda, O. Gheysens and S. S. Gambhir, *Proceedings of the National Academy of Sciences of the United States of America*, 2008, **105**, 5844-5849.

180. C. M. MacLaughlin, N. Mullaithilaga, G. Yang, S. Y. Ip, C. Wang and G. C. Walker, *Langmuir*, 2013, **29**, 1908-1919.

181. H. Chon, S. Lee, S.-Y. Yoon, S.-I. Chang, D. W. Lim and J. Choo, *Chemical Communications*, 2011, **47**, 12515-12517.

182. S. Chen, Y. Yuan, J. Yao, S. Han and R. Gu, *Chemical Communications*, 2011, **47**, 4225-4227.

183. R. Arshady, *Colloid & Polymer Science*, 1992, **270**, 717-732.

184. S. Freiberg and X. X. Zhu, *International Journal of Pharmaceutics*, 2004, **282**, 1-18.

185. H. Fenniri, S. Chun, L. H. Ding, Y. Zyrianov and K. Hallenga, *Journal of the American Chemical Society*, 2003, **125**, 10546-10560.

186. K. Saralidze, L. H. Koole and M. L. W. Knetsch, *Materials*, 2010, **3**, 3537-3564.

187. C. E. Reese and S. A. Asher, *Journal of Colloid and Interface Science*, 2002, **248**, 41-46.

188. B. S. Hawkett, D. H. Napper and R. G. Gilbert, *Journal of the Chemical Society-Faraday Transactions I*, 1980, **76**, 1323-1343.

189. S. E. Shim, Y. J. Cha, J. M. Byun and S. Choe, *Journal of Applied Polymer Science*, 1999, **71**, 2259-2269.

190. D. Mouran, J. Reimers and F. J. Schork, *J Polym Sci Pol Chem*, 1996, **34**, 1073-1081.

191. C. S. Chern and T. J. Chen, *Colloid Polym Sci*, 1997, **275**, 546-554.

192. S. S. Atik and J. K. Thomas, *Journal of the American Chemical Society*, 1981, **103**, 4279-4280.

193. J. S. Guo, M. S. Elaasser and J. W. Vanderhoff, *J Polym Sci Pol Chem*, 1989, **27**, 691-710.

194. C. Bunyakan and D. Hunkeler, *Polymer*, 1999, **40**, 6213-6224.

195. H. S. Mickley, A. S. Michales, A. S. Michaels and A. L. Moore, *Journal of Polymer Science*, 1962, **60**, 121-140.

196. T. J. Romack, E. E. Maury and J. M. Desimone, *Macromolecules*, 1995, **28**, 912-915.

197. J. S. Downey, R. S. Frank, W.-H. Li and H. D. H. Stöver, *Macromolecules*, 1999, **32**, 2838-2844.
198. J. M. Jin, J. M. Lee, M. H. Ha, K. Lee and S. Choe, *Polymer*, 2007, **48**, 3107-3115.
199. S. Kawaguchi and K. Ito, in *Polymer Particles*, ed. M. Okubo, 2005, pp. 299-328.
200. D. Horák, *Acta Polymerica*, 1996, **47**, 20-28.
201. J. S. Song, F. Tronc and M. A. Winnik, *Journal of the American Chemical Society*, 2004, **126**, 6562-6563.
202. J.-S. Song and M. A. Winnik, *Macromolecules*, 2005, **38**, 8300-8307.
203. K. C. Lee and S. Y. Lee, *Macromolecular Research*, 2007, **15**, 244-255.
204. K. C. Lee and S. Y. Lee, *Macromolecular Research*, 2008, **16**, 293-302.
205. K. P. Lok and C. K. Ober, *Canadian Journal of Chemistry*, 1985, **63**, 209-216.
206. J. S. Song, L. Chagal and M. A. Winnik, *Macromolecules*, 2006, **39**, 5729-5737.
207. J. H. Hughes, A. V. Tuomari, D. R. Mann and V. V. Hamparian, *Journal of Clinical Microbiology*, 1984, **20**, 441-447.
208. N. I. Prokopov, I. A. Gritskova, V. R. Cherkasov and A. E. Chalykh, *Russian Chemical Reviews*, 1996, **65**, 167-180.
209. D. Holmes, J. K. She, P. L. Roach and H. Morgan, *Lab on a Chip*, 2007, **7**, 1048-1056.
210. H.-L. Lee, Y.-P. Weng, W.-Y. Ku and L. L. H. Huang, *Journal of the Taiwan Institute of Chemical Engineers*, 2012, **43**, 9-14.
211. K. L. Kellar, R. R. Kalwar, K. A. Dubois, D. Crouse, W. D. Chafin and B.-E. Kane, *Cytometry*, 2001, **45**, 27-36.
212. K. L. Kellar and M. A. Iannone, *Experimental Hematology*, 2002, **30**, 1227-1237.
213. K. L. Kellar and J. P. Douglass, *Journal of Immunological Methods*, 2003, **279**, 277-285.
214. W. Deng, K. Drozdowicz-Tomsia, D. Jin and E. M. Goldys, *Analytical Chemistry*, 2009, **81**, 7248-7255.
215. Z. Zhang, Y. Long, J. Pan and X. Yan, *J Mater Chem*, 2010, **20**, 1179-1185.
216. M. Y. Han, X. H. Gao, J. Z. Su and S. Nie, *Nature Biotechnology*, 2001, **19**, 631-635.
217. J. Riegler, O. Ehlert and T. Nann, *Analytical and Bioanalytical Chemistry*, 2006, **384**, 645-650.
218. Q. Yang, Y. Li, T. Song and J. Chang, *J Mater Chem*, 2012, **22**, 7043-7049.

219. T. Song, Q. Zhang, C. Lu, X. Gong, Q. Yang, Y. Li, J. Liu and J. Chang, *J Mater Chem*, 2011, **21**, 2169-2177.

220. G. Wang, Y. Leng, H. Dou, L. Wang, W. Li, X. Wang, K. Sun, L. Shen, X. Yuan, J. Li, K. Sun, J. Han, H. Xiao and Y. Li, *ACS Nano*, 2012, **7**, 471-481.

221. Y.-H. Li, T. Song, J.-Q. Liu, S.-J. Zhu and J. Chang, *J Mater Chem*, 2011, **21**, 12520-12528.

222. D. R. Blais, R. A. Alvarez-Puebla, J. P. Bravo-Vasquez, H. Fenniri and J. P. Pezacki, *Biotechnology Journal*, 2008, **3**, 948-953.

223. A. A. Farah, R. A. Alvarez-Puebla and H. Fenniri, *Journal of Colloid and Interface Science*, 2008, **319**, 572-576.

224. A. F. McCabe, C. Eliasson, R. A. Prasath, A. Hernandez-Santana, L. Stevenson, I. Apple, P. A. G. Cormack, D. Graham, W. E. Smith, P. Corish, S. J. Lipscomb, E. R. Holland and P. D. Prince, *Faraday Discuss*, 2006, **132**, 303-308.

225. R. J. Stokes, A. Hernandez-Santana, A. Macaskill, P. A. G. Cormack, W. E. Smith and D. Graham, *Micro & Nano Letters*, 2006, **1**, 57-61.

226. B. H. Jun, J. H. Kim, H. Park, J. S. Kim, K. N. Yu, S. M. Lee, H. Choi, S. Y. Kwak, Y. K. Kim, D. H. Jeong, M. H. Cho and Y. S. Lee, *Journal of Combinatorial Chemistry*, 2007, **9**, 237-244.

227. V. Amendola and M. Meneghetti, *The Journal of Physical Chemistry C*, 2009, **113**, 4277-4285.

228. S. I. Stoeva, J. S. Lee, C. S. Thaxton and C. A. Mirkin, *Angewandte Chemie-International Edition*, 2006, **45**, 3303-3306.

229. K. Faulds, F. McKenzie, W. E. Smith and D. Graham, *Angewandte Chemie-International Edition*, 2007, **46**, 1829-1831.

230. X. Wu, H. Liu, J. Liu, K. N. Haley, J. A. Treadway, J. P. Larson, N. Ge, F. Peale and M. P. Bruchez, *Nat Biotech*, 2003, **21**, 41-46.

231. W. C. W. Chan and S. M. Nie, *Science*, 1998, **281**, 2016-2018.

232. Y. Li, Y. T. H. Cu and D. Luo, *Nature Biotechnology*, 2005, **23**, 885-889.

233. C. Radhakumary and K. Sreenivasan, *Analytical Chemistry*, 2011, **83**, 2829-2833.

234. K. Sokolov, M. Follen, J. Aaron, I. Pavlova, A. Malpica, R. Lotan and R. Richards-Kortum, *Cancer Research*, 2003, **63**, 1999-2004.

235. X. H. Huang, I. H. El-Sayed, W. Qian and M. A. El-Sayed, *Journal of the American Chemical Society*, 2006, **128**, 2115-2120.

236. C. M. McIntosh, E. A. Esposito, A. K. Boal, J. M. Simard, C. T. Martin and V. M. Rotello, *Journal of the American Chemical Society*, 2001, **123**, 7626-7629.

237. J. S. Suh and M. Moskovits, *Journal of the American Chemical Society*, 1986, **108**, 4711-4718.

238. K. M. Mayer, S. Lee, H. Liao, B. C. Rostro, A. Fuentes, P. T. Scully, C. L. Nehl and J. H. Hafner, *Acs Nano*, 2008, **2**, 687-692.

239. B. Guven, N. Basaran-Akgul, E. Temur, U. Tamer and I. H. Boyaci, *Analyst*, 2011, **136**, 740-748.

240. G. T. Hermanson, *Amsterdam: Boston* 2008.

241. B. Vercelli, G. Zotti and A. Berlin, *Chemistry of Materials*, 2007, **19**, 443-452.

242. Y. L. Hung, T. M. Hsiung, Y. Y. Chen, Y. F. Huang and C. C. Huang, *Journal of Physical Chemistry C*, 2010, **114**, 16329-16334.

243. A. Michota and J. Bukowska, *J Raman Spectrosc*, 2003, **34**, 21-25.

244. H. Park, S. B. Lee, K. Kim and M. S. Kim, *The Journal of Physical Chemistry*, 1990, **94**, 7576-7580.

245. C. A. Mirkin, R. L. Letsinger, R. C. Mucic and J. J. Storhoff, *Nature*, 1996, **382**, 607-609.

246. K. Cho, Y. Lee, C. H. Lee, K. Lee, Y. Kim, H. Choi, P. D. Ryu, S. Y. Lee and S. W. Joo, *Journal of Physical Chemistry C*, 2008, **112**, 8629-8633.

247. A. I. Abdelrahman, O. Ornatsky, D. Bandura, V. Baranov, R. Kinach, S. Dai, S. C. Thickett, S. Tanner and M. A. Winnik, *Journal of Analytical Atomic Spectrometry*, 2010, **25**, 260-268.

248. A. I. Abdelrahman, S. Dai, S. C. Thickett, O. Ornatsky, D. Bandura, V. Baranov and M. A. Winnik, *Journal of the American Chemical Society*, 2009, **131**, 15276-15283.

249. C. Y. Liang and S. Krimm, *Journal of Polymer Science*, 1958, **27**, 241-254.

250. L. Sun, C. Yu and J. Irudayaraj, *Analytical Chemistry*, 2007, **79**, 3981-3988.

251. K. K. Maiti, A. Samanta, M. Vendrell, K.-S. Soh, M. Olivo and Y.-T. Chang, *Chemical Communications*, 2011, **47**, 3514-3516.

252. K. Kim, H. B. Lee, H. K. Park and K. S. Shin, *Journal of Colloid and Interface Science*, 2008, **318**, 195-201.

253. S. L. Westcott, S. J. Oldenburg, T. R. Lee and N. J. Halas, *Langmuir*, 1998, **14**, 5396-5401.

254. S. J. Oldenburg, R. D. Averitt, S. L. Westcott and N. J. Halas, *Chemical Physics Letters*, 1998, **288**, 243-247.

255. Q. Wu, Z. Wang, X. Kong, X. Gu and G. Xue, *Langmuir*, 2008, **24**, 7778-7784.

256. J.-H. Lee, D. O. Kim, G.-S. Song, Y. Lee, S.-B. Jung and J.-D. Nam, *Macromolecular Rapid Communications*, 2007, **28**, 634-640.

257. Y. Lu, Y. Yin, Z.-Y. Li and Y. Xia, *Nano Letters*, 2002, **2**, 785-788.

258. E. Mine, A. Yamada, Y. Kobayashi, M. Konno and L. M. Liz-Marzán, *Journal of Colloid and Interface Science*, 2003, **264**, 385-390.

259. O. Niitsoo and A. Couzis, *Journal of Colloid and Interface Science*, 2011, **354**, 887-890.

260. X. J. Cheng, S. C. Tiong, Q. Zhao and R. K. Y. Li, *J Polym Sci Pol Chem*, 2009, **47**, 4547-4554.

261. Y. X. Li, Y. F. Pan, L. L. Zhu, Z. Q. Wang, D. M. Su and G. Xue, *Macromolecular Rapid Communications*, 2011, **32**, 1741-1747.

262. Z. Wang, S. Zong, H. Chen, H. Wu and Y. Cui, *Talanta*, 2011, **86**, 170-177.

263. J.-M. Li, W.-F. Ma, C. Wei, L.-J. You, J. Guo, J. Hu and C.-C. Wang, *Langmuir*, 2011, **27**, 14539-14544.

264. J.-M. Li, W.-F. Ma, C. Wei, J. Guo, J. Hu and C.-C. Wang, *J Mater Chem*, 2011, **21**, 5992-5998.

265. J.-M. Li, C. Wei, W.-F. Ma, Q. An, J. Guo, J. Hu and C.-C. Wang, *J Mater Chem*, 2012, **22**, 12100-12106.

266. U. Kreibig and M. Vollmer, *Springer: Berlin*, 1995.

267. S. Link and M. A. El-Sayed, *Journal of Physical Chemistry B*, 1999, **103**, 8410-8426.

268. Y.-C. Cao, Z. Wang, X. Jin, X.-F. Hua, M.-X. Liu and Y.-D. Zhao, *Colloids and Surfaces A: Physicochemical and Engineering Aspects*, 2009, **334**, 53-58.

269. H. M. Lee, M. S. Kim and K. Kim, *Vibrational Spectroscopy*, 1994, **6**, 205-214.

270. M. A. Correa-Duarte, M. Giersig and L. M. Liz-Marzán, *Chemical Physics Letters*, 1998, **286**, 497-501.

271. F. Caruso, M. Spasova, V. Saigueirino-Maceira and L. M. Liz-Marzan, *Advanced Materials*, 2001, **13**, 1090-1094.

272. C.-W. Lu, Y. Hung, J.-K. Hsiao, M. Yao, T.-H. Chung, Y.-S. Lin, S.-H. Wu, S.-C. Hsu, H.-M. Liu, C.-Y. Mou, C.-S. Yang, D.-M. Huang and Y.-C. Chen, *Nano Letters*, 2006, **7**, 149-154.

273. V. Salgueirino-Maceira, M. A. Correa-Duarte, M. Spasova, L. M. Liz-Marzan and M. Farle, *Adv Funct Mater*, 2006, **16**, 509-514.

274. N. R. Jana, C. Earhart and J. Y. Ying, *Chemistry of Materials*, 2007, **19**, 5074-5082.

275. A. Guerrero-Martínez, J. Pérez-Juste and L. M. Liz-Marzán, *Advanced Materials*, 2010, **22**, 1182-1195.

276. W. Stober, A. Fink and E. Bohn, *Journal of Colloid and Interface Science*, 1968, **26**, 62-69.

277. L. M. Liz-Marzán, M. Giersig and P. Mulvaney, *Langmuir*, 1996, **12**, 4329-4335.

278. T. Ung, L. M. Liz-Marzán and P. Mulvaney, *Langmuir*, 1998, **14**, 3740-3748.

279. Y. Kobayashi, H. Katakami, E. Mine, D. Nagao, M. Konno and L. M. Liz-Marzán, *Journal of Colloid and Interface Science*, 2005, **283**, 392-396.

280. Y.-H. Deng, C.-C. Wang, J.-H. Hu, W.-L. Yang and S.-K. Fu, *Colloids and Surfaces A: Physicochemical and Engineering Aspects*, 2005, **262**, 87-93.

281. D. Gerion, F. Pinaud, S. C. Williams, W. J. Parak, D. Zanchet, S. Weiss and A. P. Alivisatos, *The Journal of Physical Chemistry B*, 2001, **105**, 8861-8871.

282. Y. Lu, J. McLellan and Y. Xia, *Langmuir*, 2004, **20**, 3464-3470.

283. Y. Kobayashi, K. Misawa, M. Kobayashi, M. Takeda, M. Konno, M. Satake, Y. Kawazoe, N. Ohuchi and A. Kasuya, *Colloids and Surfaces a-Physicochemical and Engineering Aspects*, 2004, **242**, 47-52.

284. C. Graf, D. L. J. Vossen, A. Imhof and A. van Blaaderen, *Langmuir*, 2003, **19**, 6693-6700.

285. J. Hong, J. Lee, Y.-M. Rhym, D.-H. Kim and S. E. Shim, *Journal of Colloid and Interface Science*, 2010, **344**, 410-416.

286. A. B. D. Nandiyanto, T. Iwaki, T. Ogi and K. Okuyama, *Journal of Colloid and Interface Science*, 2013, **389**, 134-146.

287. L. Zhang, H. Wang, Z. Zhang, F. Qin, W. Liu and Z. Song, *Applied Surface Science*, 2011, **258**, 1217-1224.

288. Y. An, M. Chen, Q. Xue and W. Liu, *Journal of Colloid and Interface Science*, 2007, **311**, 507-513.

289. H. Giesche, *Journal of the European Ceramic Society*, 1994, **14**, 189-204.

290. K. Lee, J.-L. Look, M. T. Harris and A. V. McCormick, *Journal of Colloid and Interface Science*, 1997, **194**, 78-88.

291. J. A. Balmer, S. P. Armes, P. W. Fowler, T. Tarnai, Z. Gáspár, K. A. Murray and N. S. J. Williams, *Langmuir*, 2009, **25**, 5339-5347.

292. J. A. Balmer, O. O. Mykhaylyk, S. P. Armes, J. P. A. Fairclough, A. J. Ryan, J. Gummel, M. W. Murray, K. A. Murray and N. S. J. Williams, *Journal of the American Chemical Society*, 2010, **133**, 826-837.

293. G. H. Bogush and C. F. Zukoski Iv, *Journal of Colloid and Interface Science*, 1991, **142**, 19-34.

294. V. M. Masalov, N. S. Sukhinina, E. A. Kudrenko and G. A. Emelchenko, *Nanotechnology*, 2011, **22**, 1-9.

295. A. M. Bernard, A. Vyskocil and R. R. Lauwerys, *Clinical Chemistry*, 1981, **27**, 832-837.

296. N. Vudac, A. Chekkor, H. Parra, P. Duthilleul and J. C. Fruchart, *Journal of Lipid Research*, 1985, **26**, 267-269.

297. A. Abe, Y. Yoshimura, T. Sekine, S. Maeda, S. Yamashita and A. Noma, *Clinica Chimica Acta*, 1994, **225**, 105-113.

298. S. V. Vaidya, M. L. Gilchrist, C. Maldarelli and A. Couzis, *Analytical Chemistry*, 2007, **79**, 8520-8530.

299. Q. Zhang, Y. Han, W.-C. Wang, L. Zhang and J. Chang, *Eur Polym J*, 2009, **45**, 550-556.

300. H. Fenniri, O. Terreau, S. Chun, S. J. Oh, W. F. Finney and M. D. Morris, *Journal of Combinatorial Chemistry*, 2006, **8**, 192-198.

301. K. Otto, *Plos Biology*, 2008, **6**, 1392-1394.

302. A. Tuncel, R. Kahraman and E. Piskin, *Journal of Applied Polymer Science*, 1993, **50**, 303-319.

303. H. Han, C. K. Hong, J. Hong, D. W. Park and S. E. Shim, *Journal of Applied Polymer Science*, 2009, **111**, 2900-2907.

304. J. Lee, J. U. Ha, S. Choe, C.-S. Lee and S. E. Shim, *Journal of Colloid and Interface Science*, 2006, **298**, 663-671.

305. P. K. Horan and L. L. Wheeless, *Science*, 1977, **198**, 149-157.

306. T. Oonishi and N. Uyesaka, *Journal of Immunological Methods*, 1985, **84**, 143-154.

307. X. Gao and S. Nie, *Analytical Chemistry*, 2004, **76**, 2406-2410.

308. E. Morgan, R. Varro, H. Sepulveda, J. A. Ember, J. Apgar, J. Wilson, L. Lowe, R. Chen, L. Shivraj, A. Agadir, R. Campos, D. Ernst and A. Gaur, *Clinical Immunology*, 2004, **110**, 252-266.

309. G. Goddard, J. C. Martin, M. Naivar, P. M. Goodwin, S. W. Graves, R. Habbersett, J. P. Nolan and J. H. Jett, *Cytometry Part A*, 2006, **69A**, 842-851.

310. D. A. Watson, L. O. Brown, D. R. Gaskill, M. Naivar, S. W. Graves, S. K. Doorn and J. P. Nolan, *Cytometry Part A*, 2008, **73A**, 119-128.

311. J. H. Jett, *Cytometry Part A*, 2008, **73A**, 109-110.

312. D. A. Watson, D. F. Gaskill, L. O. Brown, S. K. Doorn and J. P. Nolan, *Cytometry Part A*, 2009, **75A**, 460-464.

313. J. P. Nolan and D. S. Sebba, in *Recent Advances in Cytometry, Part A: Instrumentation, Methods, Fifth Edition*, 2011, pp. 515-532.

314. D. S. Sebba, D. A. Watson and J. P. Nolan, *Acs Nano*, 2009, **3**, 1477-1484.

315. G. Goddard, L. O. Brown, R. Habbersett, C. I. Brady, J. C. Martin, S. W. Graves, J. P. Freyer and S. K. Doorn, *Journal of the American Chemical Society*, 2010, **132**, 6081-6090.

316. M. P. Cecchini, M. A. Stapountzi, D. W. McComb, T. Albrecht and J. B. Edel, *Analytical Chemistry*, 2011, **83**, 1418-1424.

317. S. Kawaguchi, A. Yekta and M. A. Winnik, *Journal of Colloid and Interface Science*, 1995, **176**, 362-369.

Appendix

L. Wei, B. Jin and S. Dai, Polymer Microbead-Based Surface Enhanced Raman Scattering Immunoassays, *The Journal of Physical Chemistry C* 2012, 116:17174-17081.

Wei, L., Jin, B. & Dai, S. (2012) Polymer microbead-based surface enhanced raman scattering immunoassays.
Journal of Physical Chemistry C, v. 116(32), pp. 17174-17181